Simulation of Euler transonic flows by means of explicit finite element type schemas

F. Angrand, Alain Dervieux, L. Loth, G. Vijayasundaram

INRIA
CENTRE DE ROCQUENCOURT

Institut National
de Recherche
en Informatique
et en Automatique

Domaine de Voluceau
Rocquencourt
B.P 105
78153 Le Chesnay Cedex
France
Tél. (3) 954 90 20

Rapports de Recherche

N° 250

SIMULATION OF EULER TRANSONIC FLOWS BY MEANS OF EXPLICIT FINITE ELEMENT-TYPE SCHEMES

Françoise ANGRAND
Alain DERVIEUX
Laurent LOTH
Ganesan VIJAYASUNDARAM

Octobre 1983

SIMULATION OF EULER TRANSONIC FLOWS BY MEANS OF EXPLICIT FINITE ELEMENT-TYPE SCHEMES

Françoise ANGRAND*, Alain DERVIEUX*
Laurent LOTH*, Ganesan VIJAYASUNDARAM**

* INRIA - Domaine de Voluceau
Rocquencourt, B.P. 105
78153 LE CHESNAY CEDEX - France

** Tata Institute of Fundamental Research,
Indian Institute of Science, BANGALORE 560012
India

SUMMARY :

Several explicit schemes are presented for triangular P_o (constant by triangle), P_1 (linear by triangle) and P_2 (quadratical) Finite Volume or Finite Element methods, to solve the Euler first order hyperbolic system.
A first order accurate upwind P_o scheme is compared to a FLIC type method. A characteristic upwind method is presented. A second order accurate Richtmyer scheme is constructed. A Runge-Kutta method is implemented with P_1 and P_2 elements. Applications are given for the Euler system of conservation laws in 2-dimensional case.

RESUME :

On présente plusieurs schémas explicites en volumes ou éléments finis P_o (constants par triangle) P_1 (continus, linéaires par triangles, et P_2 (quadratiques) pour résoudre des systèmes hyperboliques du premier ordre. On compare un schéma P_o à un pas à une méthode de type FLIC. On présente aussi une méthode de décentrage reposant sur les directions caractéristiques. On construit un schéma du second ordre (de type Richtmyer). Un schéma de Runge-Kutta est aussi expérimenté avec des éléments P_1 et P_2. Tous ces schémas sont testés sur la simulation d'écoulements bidimensionnels régis par les équations d'Euler.

0. INTRODUCTION

In the past few years, several methods have been developed for solving systems of nonlinear hyperbolic laws which admit discontinuities of shock type with finite differences. Our purpose is to study numerical simulation by Finite Element Methods of Euler steady transonic flows.
In this paper we deal mainly with several explicit and low-order accurate unsteady methods ; such a choice is convenient if the geometry is complex so that many points of discretization are needed. However experiments with quadratic elements will be also presented.

P_o convective upwinding :

A P_o approximation (constant by triangle) with upwinding of the convective terms have been experimented ; the comparison of the number of degrees of freedom with the cost of computation is particularly favourable to this choice. Unfortunately a general stability analysis seems non trivial.

Caracteristic upwinding :

A second way to introduce upwinding is to consider the eigenvalues of matrixes obtained by linearization of the fluxes ; the characteristic upwinding presented uses a fully two-dimensional flux splitting and is coherent - although very simplified - with the corresponding Rieman problems.

Richtmyer scheme :

To obtain second order accuracy, a P_1 (continuous, linear by triangles) approximation is used to construct a two-dimensional Richtmyer scheme.

Runge-Kutta experiments :

Finally, P_1 and P_2 Finite Elements/explicit Runge-Kutta schemes are presented and compared with the preceeding schemes.

The plan is the following

1. UPWIND METHODS FOR P_o F.E.M.

1.1. The Flic method

1.2. A one-step method

1.3. Numerical results

2. A CHARACTERISTIC UPWIND METHOD FOR A P_1 F.E.M.

2.1. Scalar case

2.2. Extension to the two-dimensional case

2.3. Numerical results.

3. A RICHTMYER SCHEME

3.1. The linear scalar case

3.2. Extension to nonlinear systems

3.3. Transonic experiments

4. A RUNGE-KUTTA SCHEME

4.1. Spatial Variational discretization

4.2. Boundary conditions

4.3. Time stepping

4.4. Linear Elements

4.5. Quadratic Elements.

5. CONCLUSION

1. UPWIND METHODS FOR P_0 F.E.M.

1.1. The Flic method

It is mainly NAGAYAMA and ADACHI's method [15].

1.1.1. The equations

The basic equations for two-dimensional inviscid compressible flows are described as follows

$$(1.1) \qquad \frac{\partial W}{\partial t} + \frac{\partial}{\partial x} F(W) + \frac{\partial}{\partial y} G(W) = 0$$

where

$$(1.2)_1 \qquad W = \begin{pmatrix} \rho \\ \rho u \\ \rho v \\ e \end{pmatrix} , \quad F(W) = \begin{pmatrix} \rho u \\ \rho u^2+p \\ \rho uv \\ (e+p)u \end{pmatrix} , \quad G(W) = \begin{pmatrix} \rho v \\ \rho uv \\ \rho v^2+p \\ (e+p)v \end{pmatrix}$$

and with

$$(1.2)_2 \qquad p = 0.4 \left[e - \frac{1}{2} \rho (u^2 + v^2) \right] \quad ;$$

ρ is the density, p is the pressure, e is the total energy, u and v are the components of the velocity $\vec{V}$.

We may write (1.1) and $(1.2)_1$ as

$$(1.3) \qquad \frac{\partial W}{\partial t} + \operatorname{div}[H(W)\vec{V}] = - \frac{\partial}{\partial x} F_1(W) - \frac{\partial}{\partial y} G_1(W)$$

where

$$(1.4)\qquad H(W) = \begin{pmatrix} \rho \\ \rho u \\ \rho v \\ e \end{pmatrix} \quad , \; F_1(W) = \begin{pmatrix} o \\ p \\ o \\ pu \end{pmatrix} \quad , \; G_1(W) = \begin{pmatrix} o \\ o \\ p \\ pv \end{pmatrix}$$

1.1.2. Definition of the scheme

As usual we consider a triangulation $\mathcal{C}_h$ of a polygon Ω_h which approximates the domain Ω of integration of (1.1) (see for example ZIENKIEWICZ [24]). From $\mathcal{C}_h$ we derive a space V_h of functions which are constant on each triangle ; the set $\{\pi_T\}_{T\in\mathcal{C}_h}$ is a basis of V_h :

$$(1.5)\qquad \pi_T(x) = \begin{cases} 1 \text{ if } x \in T \\ 0 \text{ elsewhere.} \end{cases}$$

Multiplying (1.3) by π_T and integrating by parts we get, for each triangle T

$$(1.6)\qquad \begin{cases} \displaystyle\iint_T \frac{\partial W}{\partial t}\, dxdy + \int_{\partial T} H(W)\, \vec{V}.\vec{n}\, d\sigma = \\ \qquad\qquad - \displaystyle\int_{\partial T} [F_1(W)\, n_x + G_1(W)\, n_y]\, d\sigma \end{cases}$$

where ∂T and $\vec{n} = (n_x, n_y)$ denote respectively the boundary of element T and the (outward pointing) normal vector.

We can now define the scheme as a two-steps advancing one for time differencing (we follow [15]) :

Step 1 : Intermediate values $\tilde{W}^n(T)$ are computed from equation (1.6) by neglecting the divergence terms

$$(1.7)\quad \begin{cases} \tilde{W}^n(T) = W^n(T) \\ \\ - \dfrac{\Delta t}{\text{area}(T)} \displaystyle\sum_{c_{ij}}{}' \left\{ \dfrac{F_1[W^n(T_{ij})] + F_1[W^n(T)]}{2}\, n_x^{ij,T}\, \text{length}(c_{ij}) \right. \\ \left. \qquad + \dfrac{G_1[W^n(T_{ij})] + G_1[W^n(T)]}{2}\, n_y^{ij,T}\, \text{length}(c_{ij}) \right\} \end{cases}$$

where the superscript n indicates the time level $t = n\Delta t$ (Δt is the time increment),

the sum Σ' is taken over the three sides c_{ij} of T,

T_{ij} denotes the neighbour triangle of T along side c_{ij}

$\vec{n}^{ij,T} = (n_x^{ij,T}, n_y^{ij,T})$ is the normal vector to side c_{ij} outward from T.

Step 2 : New values $W^{n+1}(T)$ are computed by applying the divergence part to the intermediate values of (1.7) :

$$(1.8)\quad \begin{cases} W^{n+1}(T) = \tilde{W}^n(T) \\ \\ - \dfrac{\Delta t}{\text{area}(T)} \displaystyle\sum_{c_{ij}}{}' \left[\chi_{ij}^n\, \tilde{W}^n(T_{ij}) + (1 - \chi_{ij}^n)\, \tilde{W}^n(T)\right] \vec{V}_{ij}^n \cdot \vec{n}^{ij,T}\, \text{length}(c_{ij}) \end{cases}$$

where

$$(1.9)_1 \qquad \vec{V}_{ij}^n = \frac{1}{2}\left[\vec{V}^n(T_{ij}) + \vec{V}^n(T)\right]$$

$$(1.9)_2 \quad \begin{cases} \chi_{ij}^n = 1 \quad \text{if } \vec{V}_{ij}^n \cdot \vec{n}^{ij,T} < 0 \\ \\ = 0 \quad \text{otherwise.} \end{cases}$$

The upwinding coefficient χ_{ij}^n indicates the one which, between T and T_{ij} is upstream

Wall (or profile) boundary conditions are simply implemented by computing boundary fluxes with only the pressure terms (using the vanishing of normal velocity) ; consistent P_o interpolation is used for the pressure boundary values.

Inflow and outflow boundary conditions are taken into account by imposing all the values at infinity to variables along the boundaries ; because of the upwinding, this means that the complete four conditions are imposed at inflow, and only the pressure at outflow.

1.2. A one-step method

One of our aims is to compute steady states solutions ; now, when we look at the corresponding steady equation, e + p appears as the variable in the energy equation. So, considering an upwind integration for the variables ρ, ρu, ρv, e + p, we note that only pressure terms appearing in ρu and ρv equations should have a centered integration.

More precisely we write (1.1) as follows

$$(1.10)_1 \quad \frac{\partial W}{\partial t} + \operatorname{div} K(W)\vec{V} = -\frac{\partial}{\partial x} F_2(W) - \frac{\partial}{\partial y} G_2(W)$$

with

$$(1.10)_2 \quad K(W) = \begin{pmatrix} \rho \\ \rho u \\ \rho v \\ e + p \end{pmatrix} \qquad F_2(W) = \begin{pmatrix} o \\ p \\ o \\ o \end{pmatrix} \qquad G_2(W) = \begin{pmatrix} o \\ o \\ p \\ o \end{pmatrix} .$$

Using the same P_o discretization as in Section 1.1, we get (similarly to (1.6)) :

$$(1.11) \quad \left\{ \begin{array}{l} \displaystyle\iint_T \frac{\partial W}{\partial t}\, dxdy + \int_{\partial T} K(W)\vec{V}\cdot\vec{n}\, d\sigma = \\ \qquad \displaystyle - \int_{\partial T} [F_2(W)n_x + G_2(W)n_y]\, d\sigma \end{array} \right.$$

and we define $W^{n+1}(T)$ as follows

$$W^{n+1}(T) = W^n(T) - \frac{\Delta t}{\text{area}(T)} \sum_{c_{ij}}{}' \{[\chi_{ij}^n K(W^n(T_{ij})) + (1-\chi_{ij}^n)K(W^n(T))]$$

$$\times \vec{V}_{ij}^n \cdot n^{ij}\, \text{length}(c_{ij}) + \frac{F_2(W^n(T_{ij})) + F_2(W^n(T))}{2} n_x^{ij,T}\, \text{length}(c_{ij})$$

$$+ \frac{G_2(W^n(T_{ij})) + G_2(W^n(T))}{2} n_y^{ij,T} \text{length}(c_{ij})\}$$

with the same notations as in (1.7) ; the upwinding is similar to the FLIC methods, only the variables upon which it is applied are different.

Boundary conditions are dealt with as in Section 1.1.

1.3. Numerical results

First we compare the two above methods with the shock tube problem described by SOD [19] with initial conditions

$$\rho_1 = 1. \quad , \; p_1 = 1. \; , \quad u_1 = 0. \quad , \quad v_1 = 0.$$
$$\rho_2 = .125 \; , \; p_2 = .1 \; , \quad u_2 = 0. \quad , \quad v_2 = 0.$$

The triangulation is regular, comparable to a 101 × 3 finite difference mesh (the size of sides parallel to x axis is 0.01).

The results at time t = 0.16 are presented in Figures 1.1 and 1.2. Compared with the so-called "upwind scheme" presented by SOD [19], the two above schemes are much more efficient, without any spurious shock.

Our second test is the calculation of the steady-state of a channel transonic flow past a circular bump : we chose a test problem proposed at the GAMM workshop held in 1979 at Stockholm [17] ; this problem has also be tested by BORREL and MORICE [4] ; the bump is a 4,2 % thick circular arc with length 1. and the canal is of height 2.073. Free stream values correspond to a Mach number of .85.

For consistency with the GAMM test, we use a triangulation with 72 × 21 vertices, which gives 2840 triangles (= degrees of freedom). For the NACA0012 we have a triangulation with the same caractéristics. The Mach at infinity is .8.

Consistent (not local) time stepping is used, without any artificial damping, to obtain the steady state ; convergence is measured from root mean square value of $\frac{\partial \rho}{\partial t}$.

For the FLIC simulation, 5600 iterations corresponding to time T = 11.5 sec (u = 1 at infinity) correspond to RMS $\frac{\partial \rho}{\partial t} = 0.6\ 12^{-2}$.

For the one-step method, 5600 iterations corresponding to time T = 11.6 sec correspond to RMS $\frac{\partial \rho}{\partial t} = 0.38\ 10^{-4}$.

We observed that the one-step method is slightly cheaper for each iteration and needs less iterations to converge.

Conservely, at the sight of the results (Figures 1.3 to 1.22) the FLIC scheme seems less diffusive.

Some P_1 variant (VIJAYASUNDARAM ; not published) of the two schemes have been proved to be as expensive with the same number of triangles and much more diffusive.

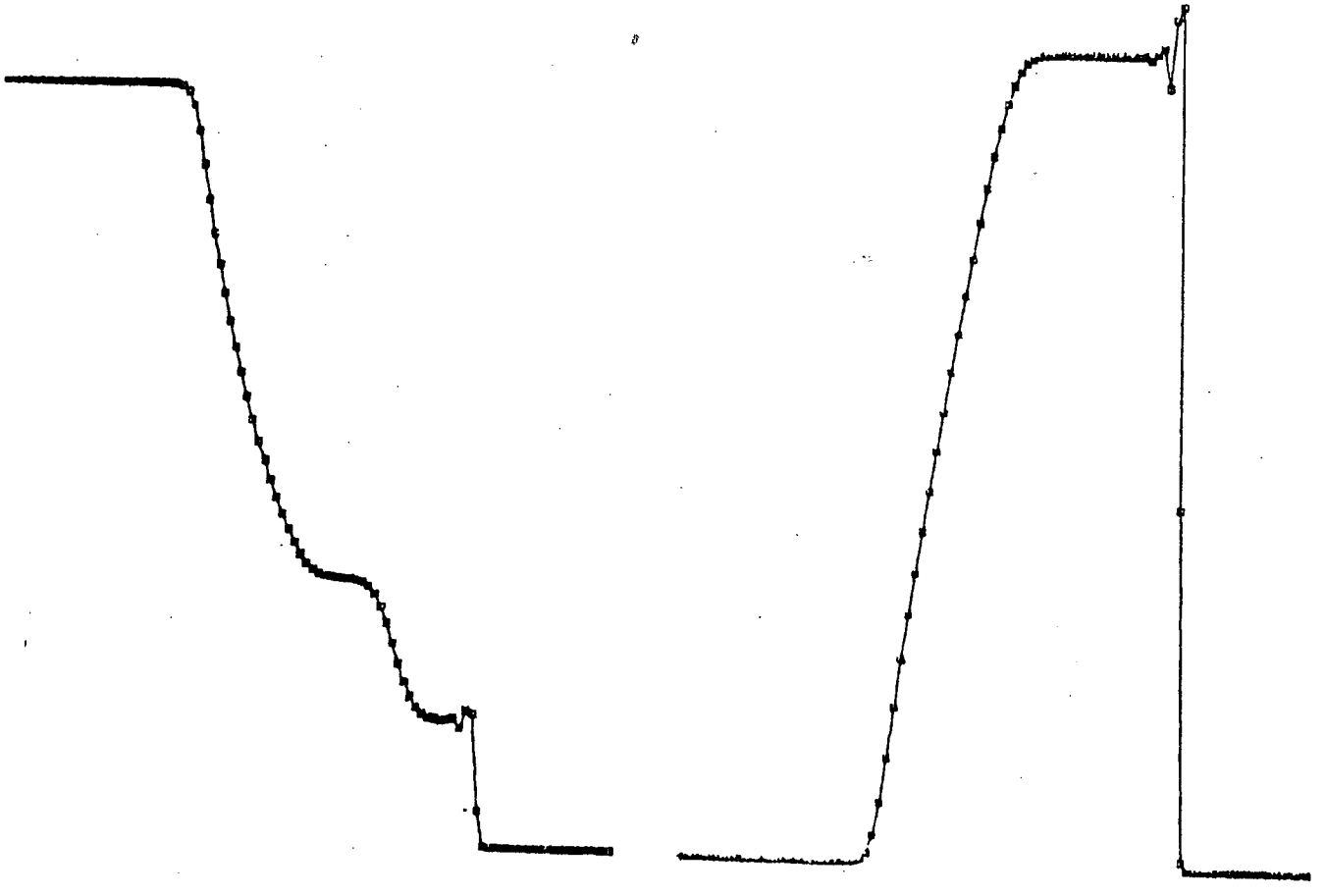

density

velocity

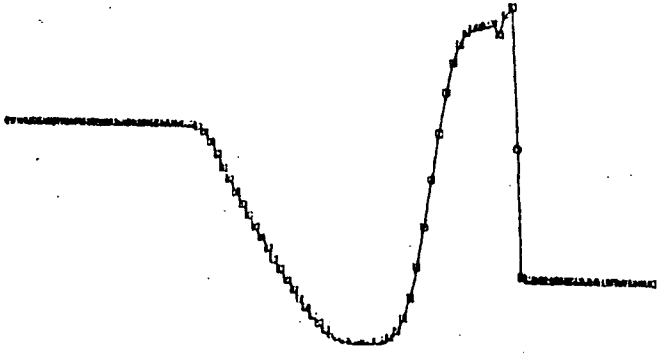

temperature

Figure 1.1 : Shock tube (Flic method)

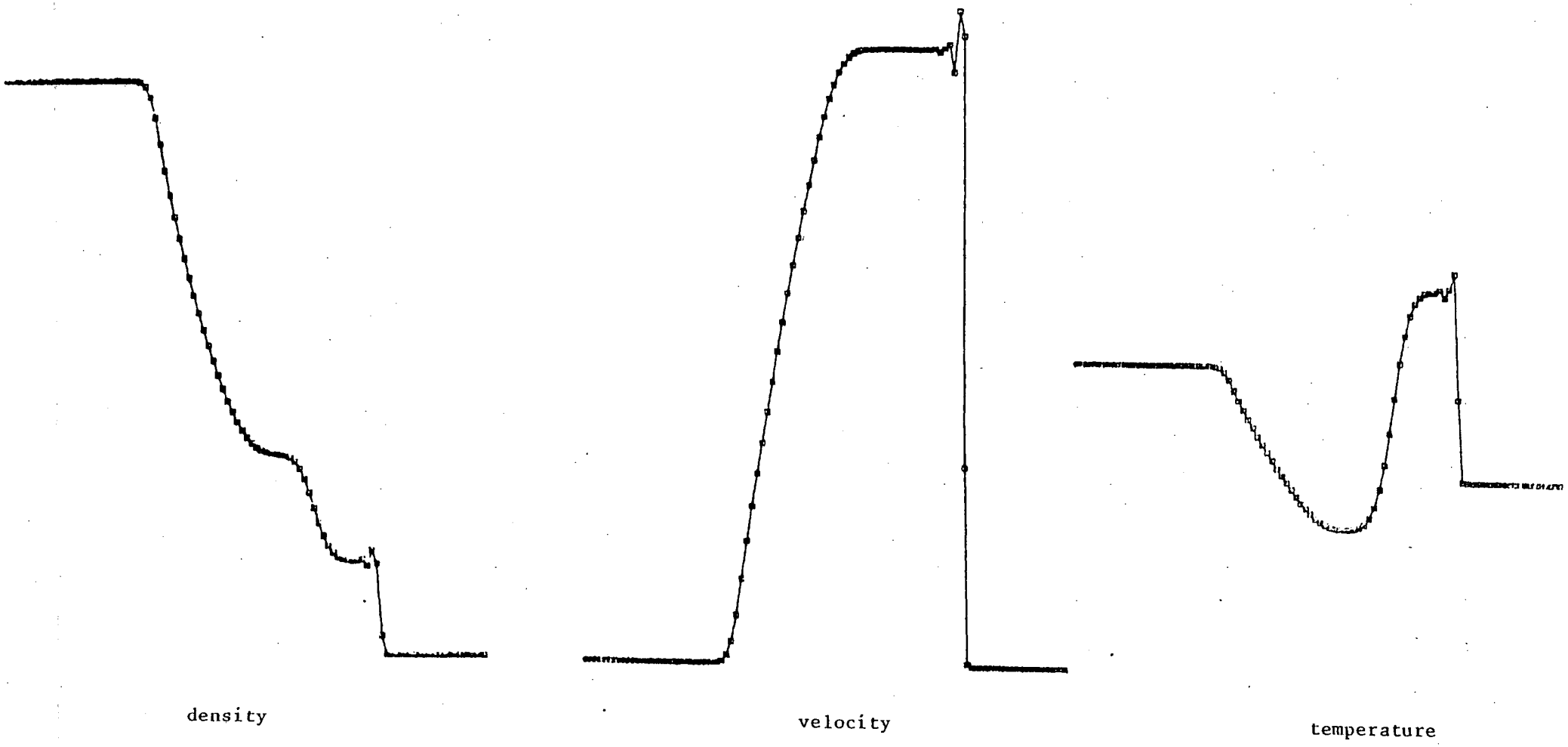

Figure 1.2 : Shock tube (one step upwind method)

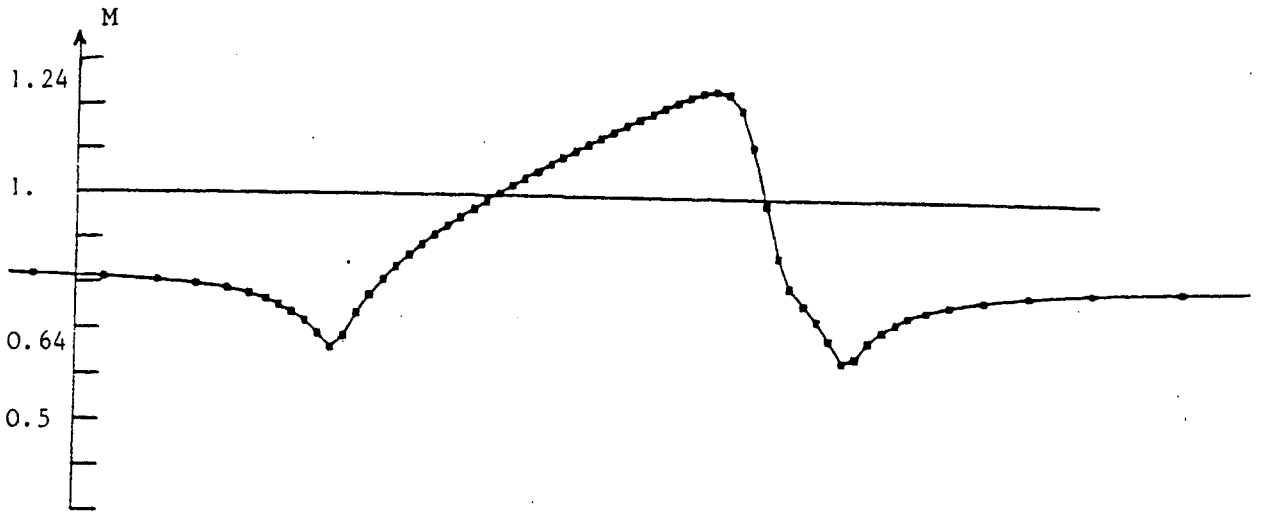

Figure 1.3 : GAMM channel with circular bump ; Mach distribution on the bottom (Flic method)

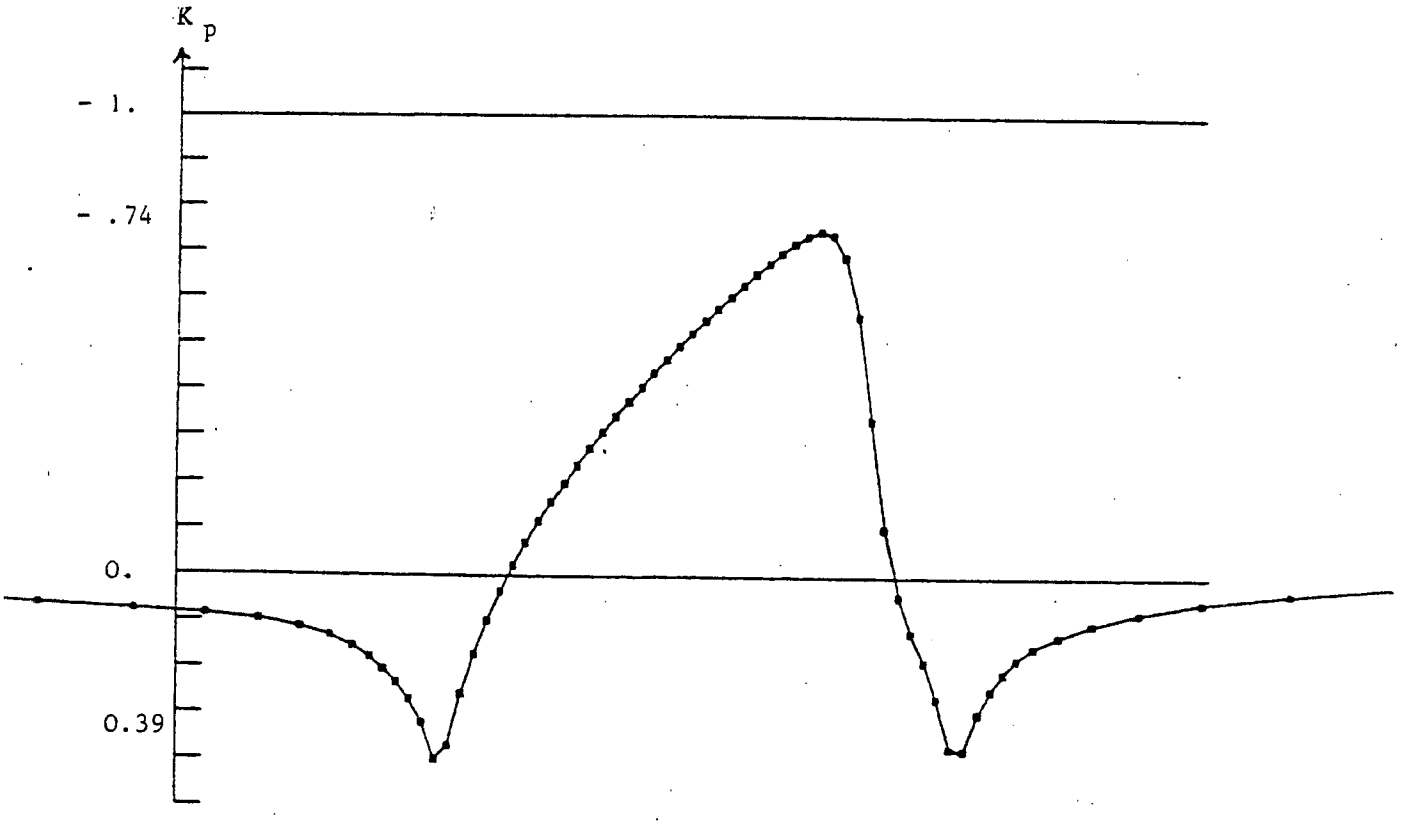

Figure 1.4 : GAMM channel with circular bump ; K_p distribution on the bottom (Flic method)

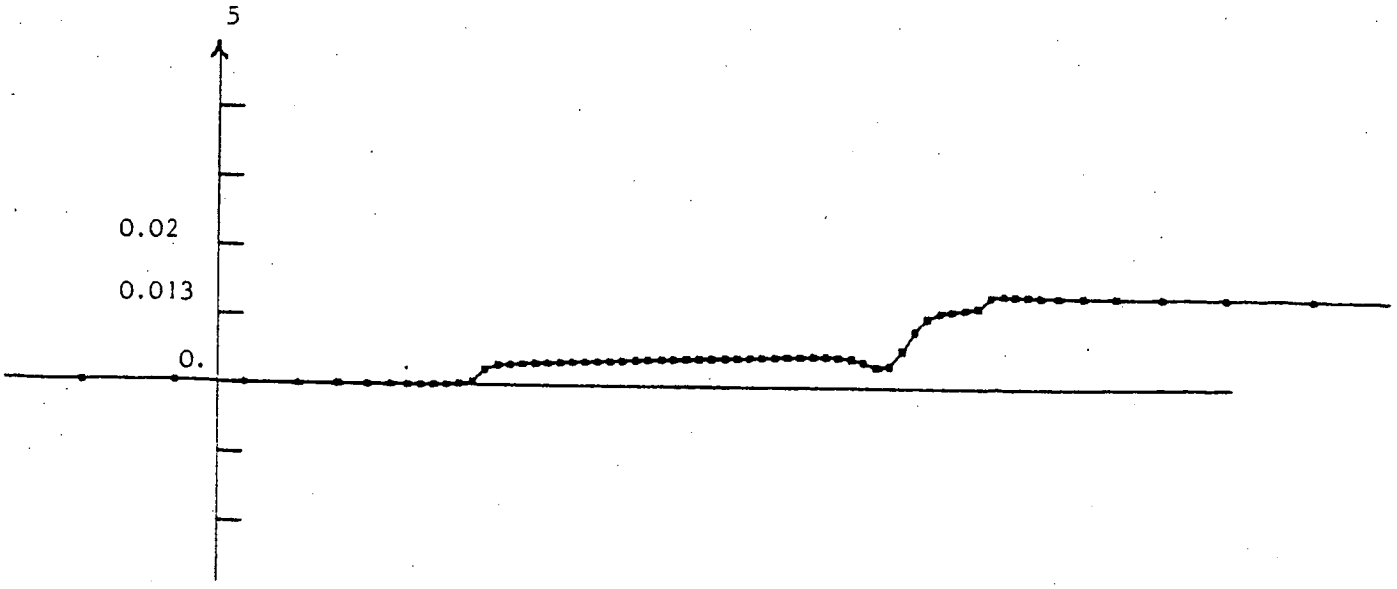

Figure 1.5 : GAMM channel with circular bump ; distribution on the bottom of deviation entropy . $S = (\frac{P}{P\infty})/(\frac{\rho}{\rho\infty})^{\gamma} - 1$ (Flic method)

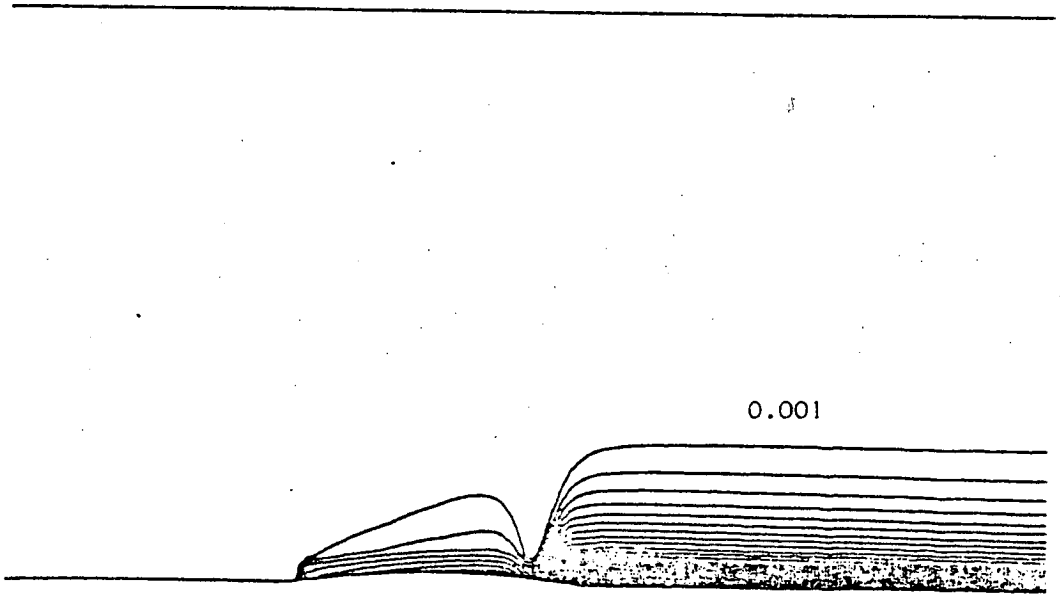

Figure 1.6 : GAMM channel with circular bump ; isentropic lines (increment $\Delta S = 0.001$) (Flic method)

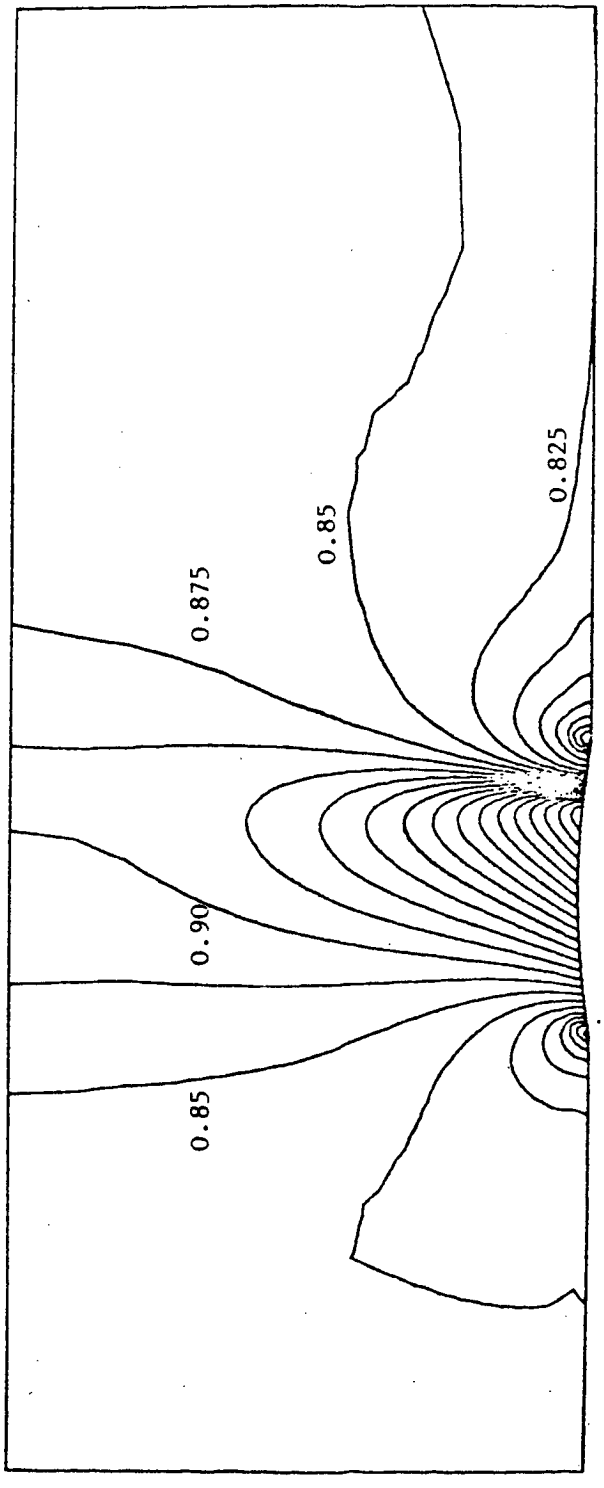

Figure 1.7 : GAMM channel with circular bump ; isomach lines (Flic method)

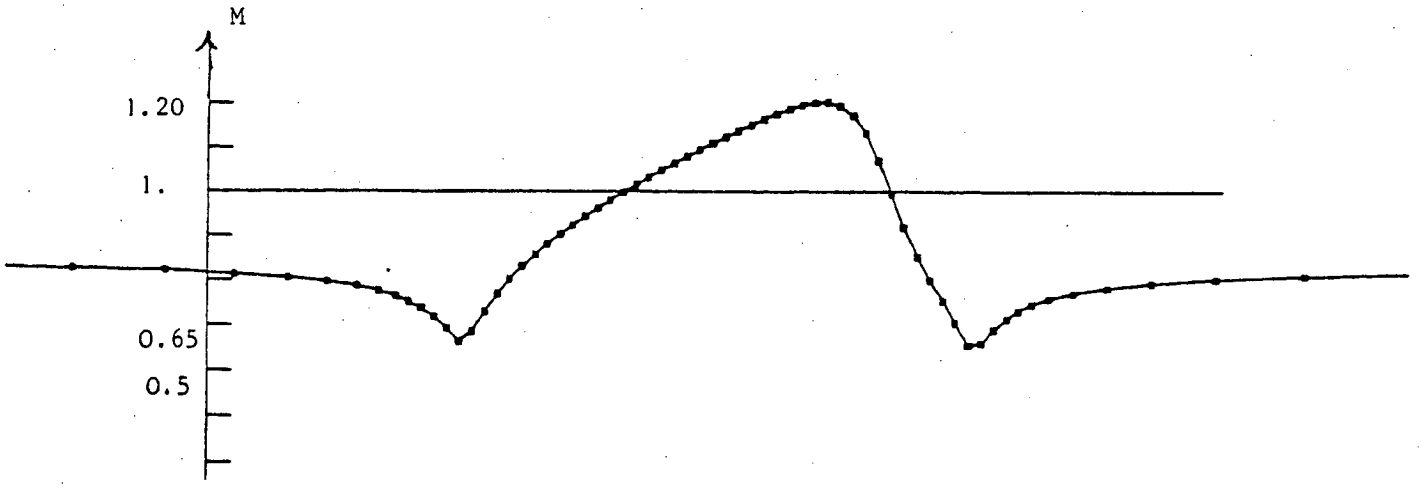

Figure 1.8 : GAMM channel with circular bump ; Mach distribution on the bottom (one step upwind method)

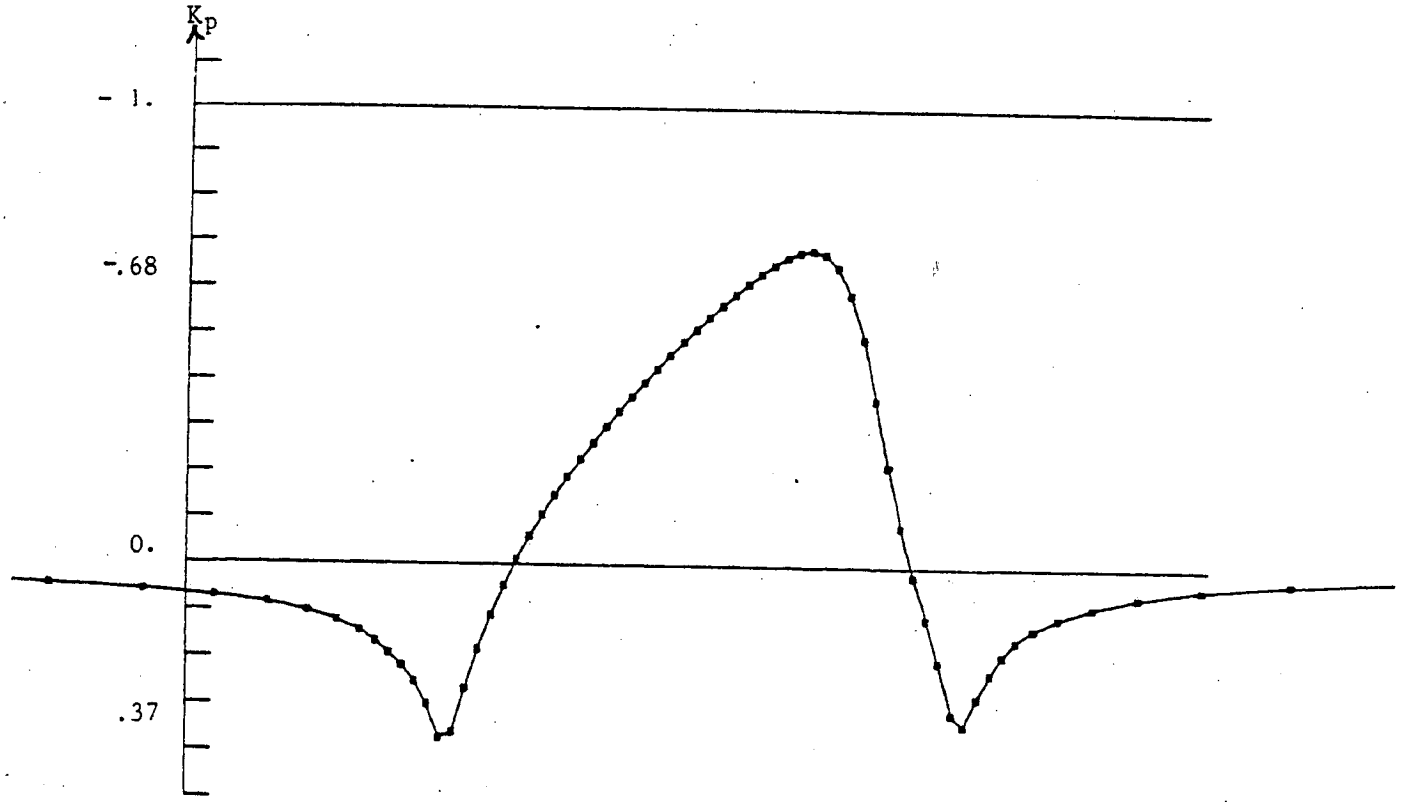

Figure 1.9 : GAMM channel with circular bump ; K_p distribution on the bottom - (one step upwind method)

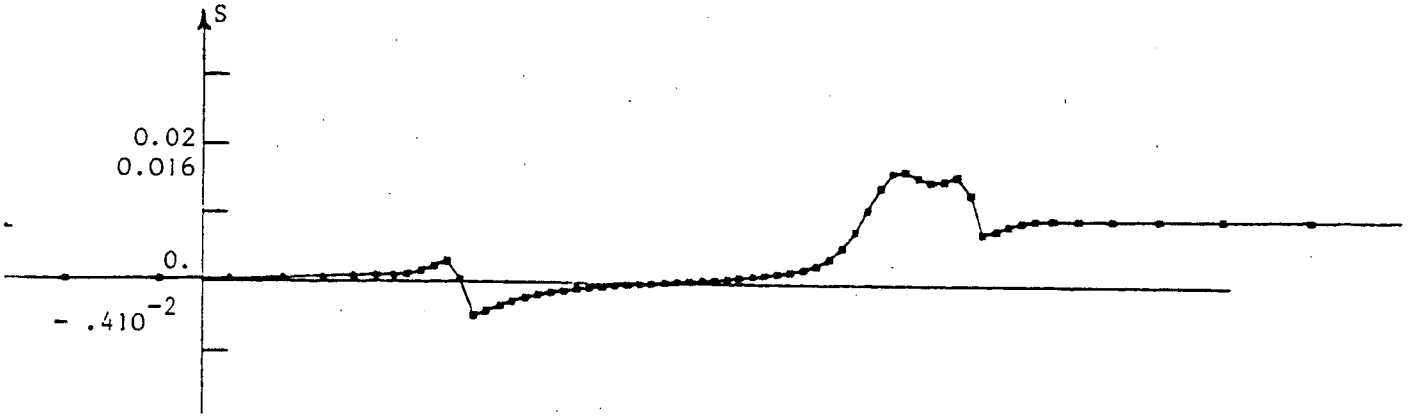

Figure 1.10 : GAMM channel with circular bump ; entropy distribution on the bottom (one step upwind method)

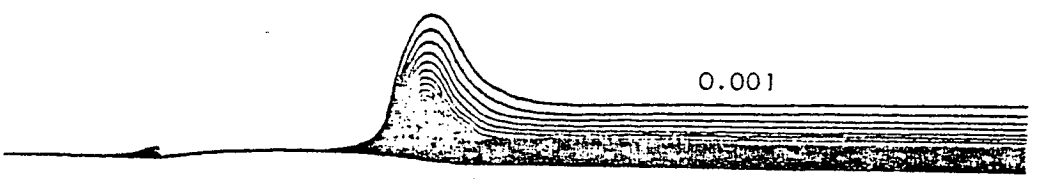

Figure 1.11 : GAMM channel with circular bump ; isentropic lines (increment $\Delta S = 0.001$) (one step upwind method)

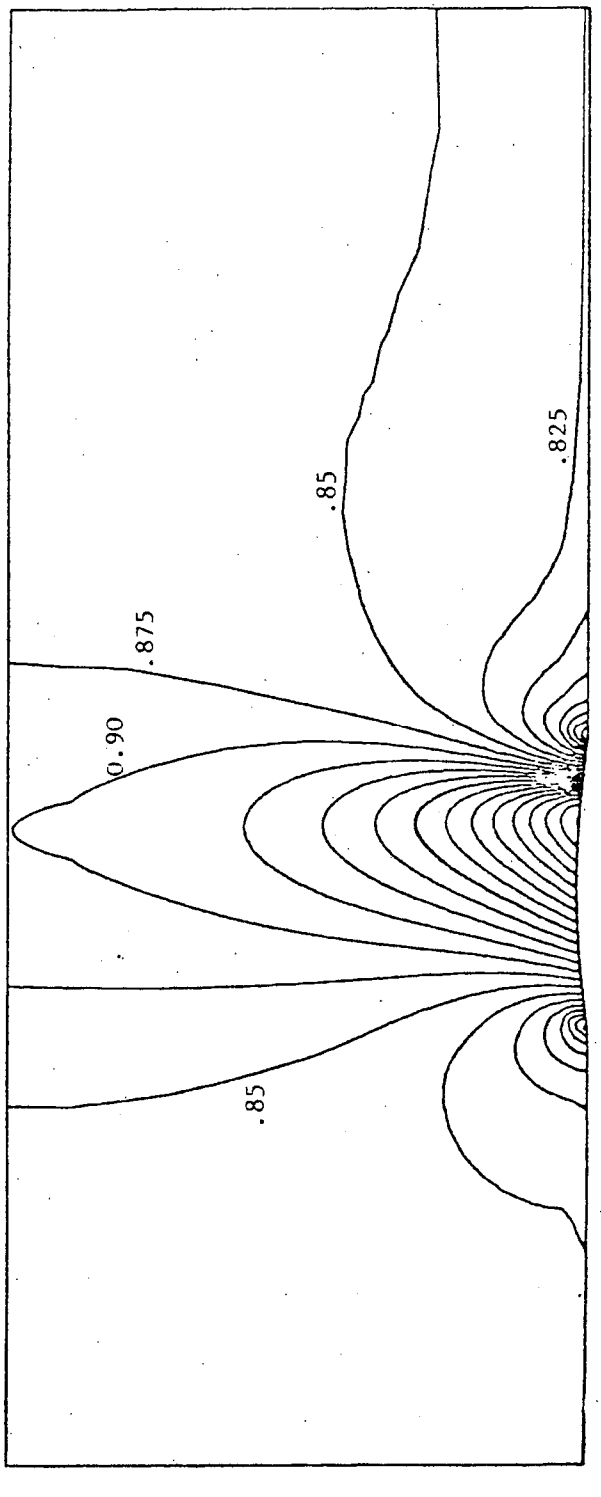

Figure 1.12 : GAMM channel with circular bump ; isomach lines. (one step upwind method)

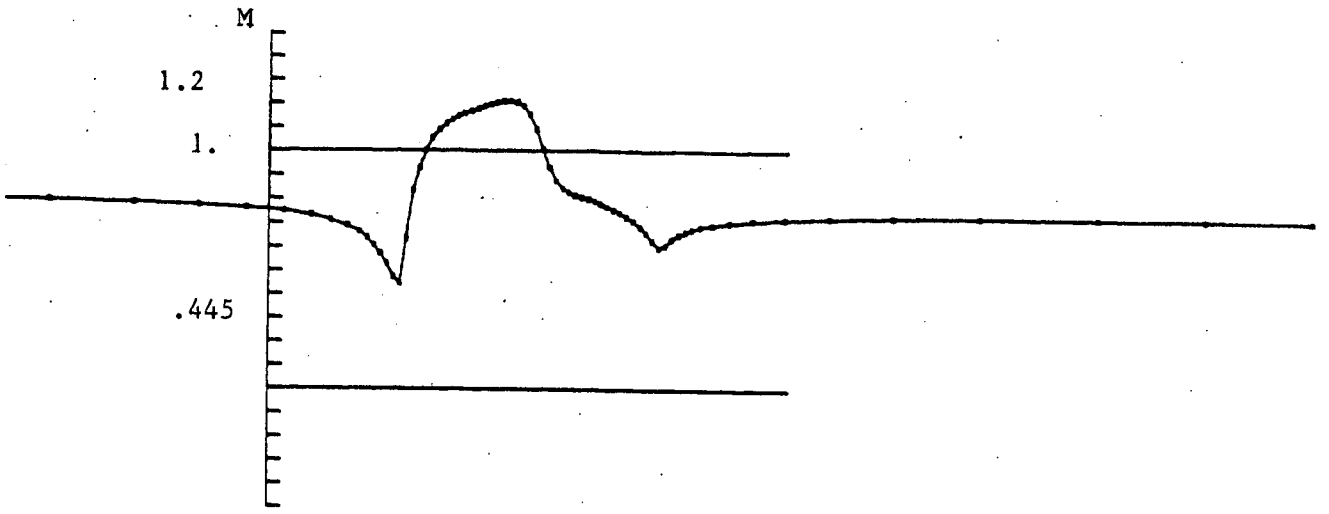

Figure 1.13 : 1/2 NACA0012 in a channel ; Mach distribution around the profile (FLIC Method)

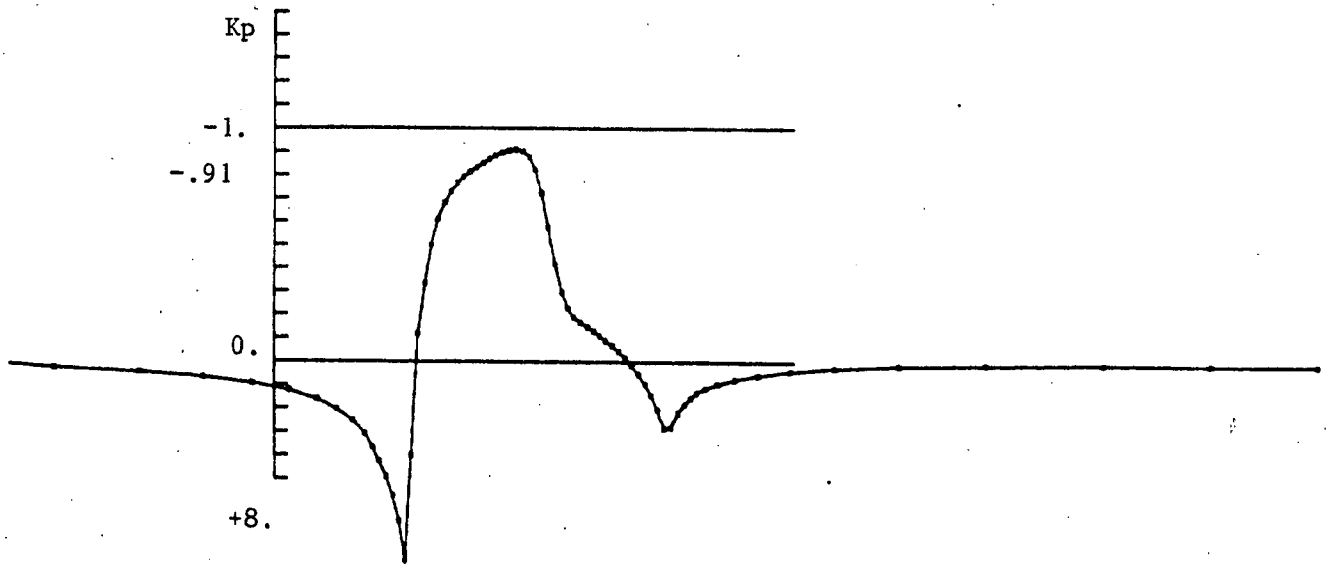

Figure 1.14 : 1/2 NACA0012 in a channel ; Kp distribution around the profile (FLIC method).

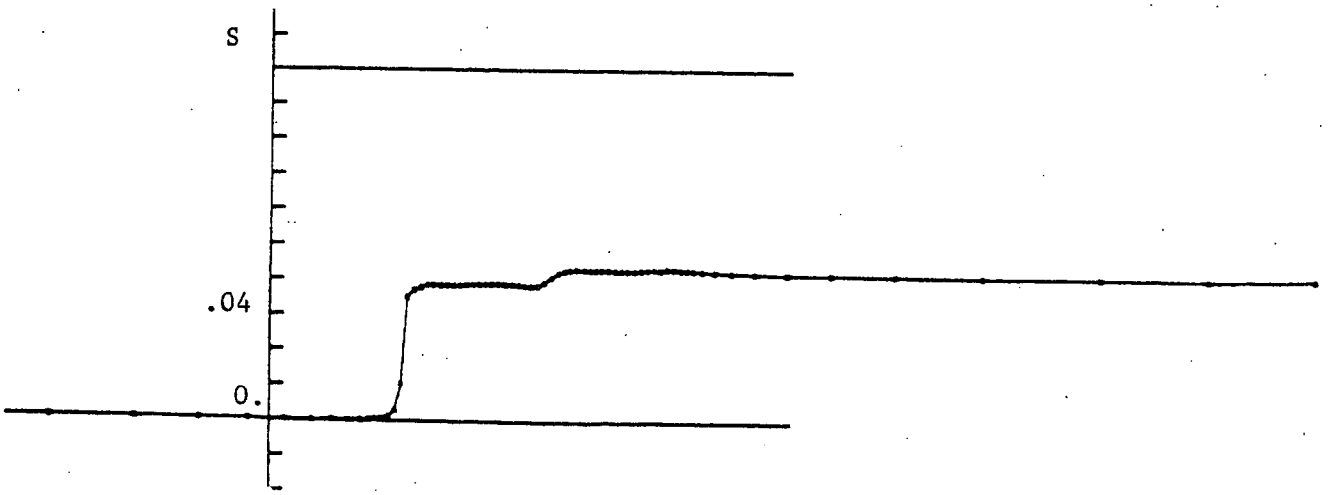

Figure 1.15 : 1/2 NACA0012 in a channel ; distribution on the profile of deviation entropy (FLIC method)

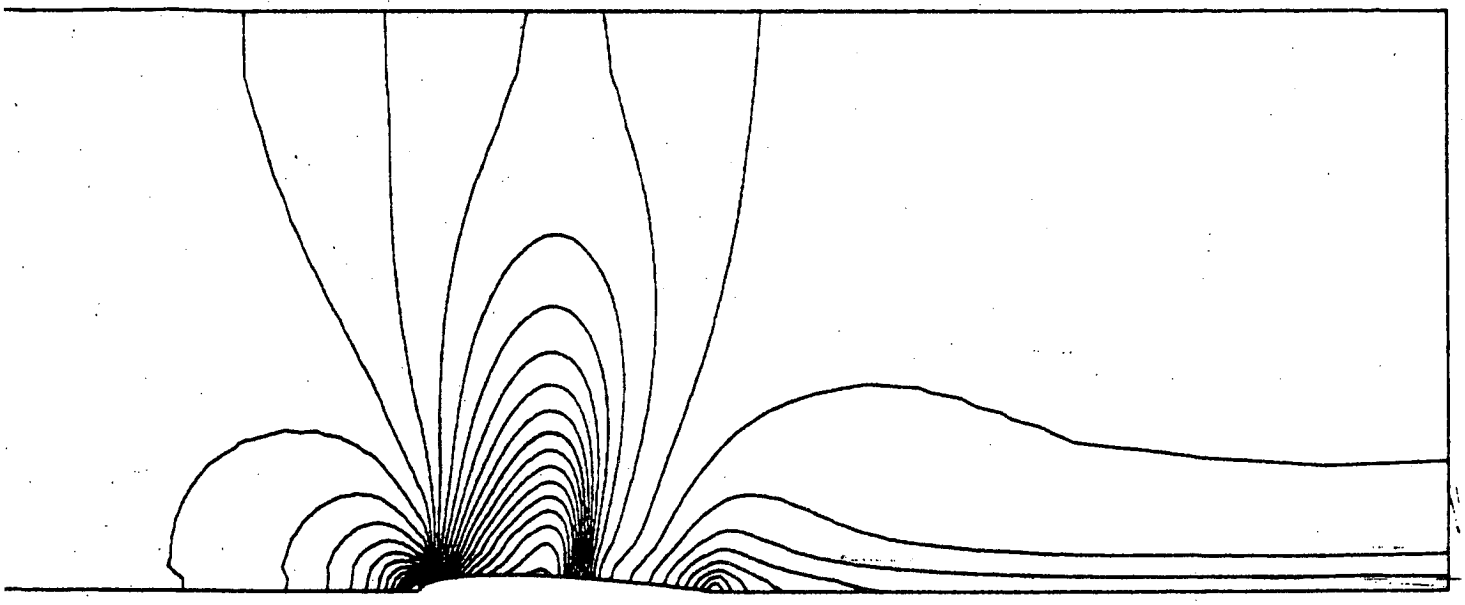

Figure 1.16. : 1/2 NACA0012 in a channel
isomach lines (FLIC method)

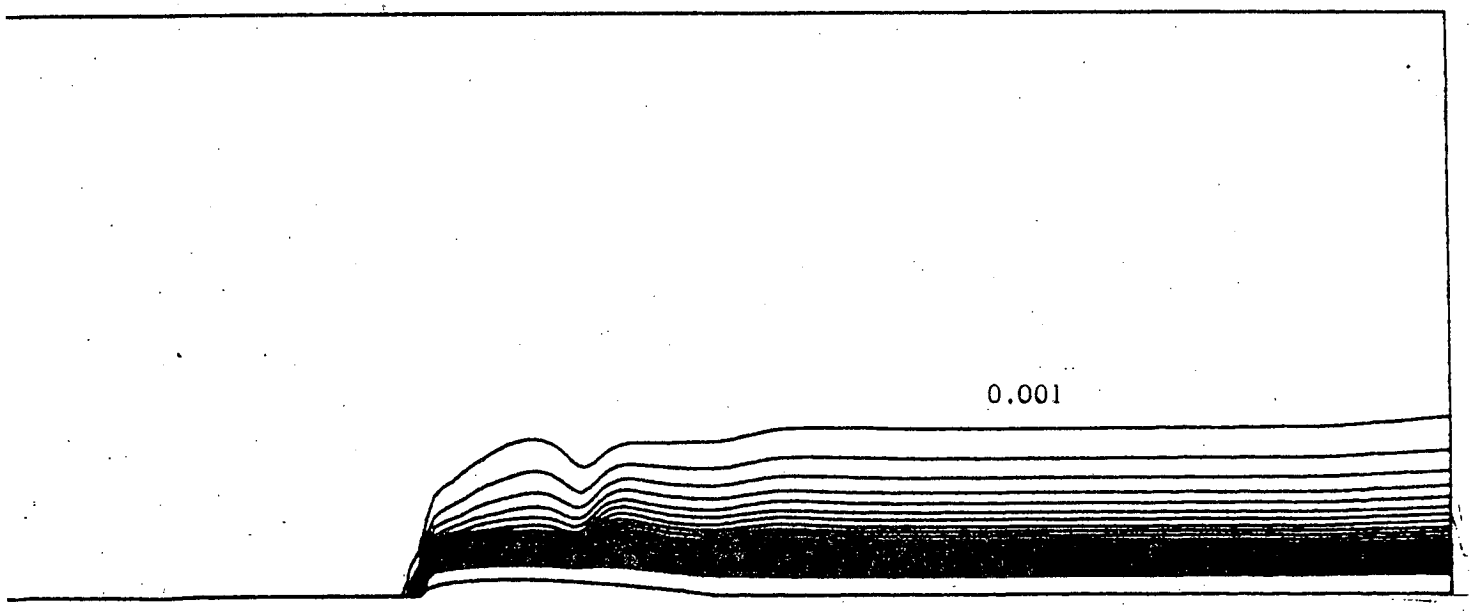

Figure 1.17. : 1/2 NACA0012 in a channel ; isentropic lines
(increment $\Delta S = 0.001$) (FLIC Method).

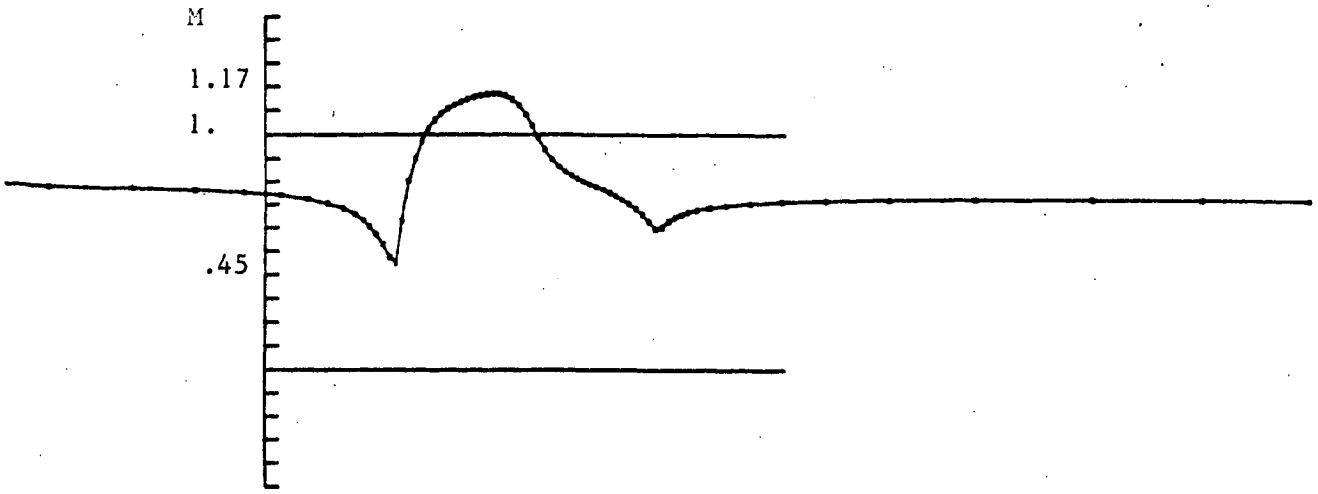

Figure 1.18 : 1/2 NACA0012 in a channel ; Mach distribution on the profile (one step upwind method)

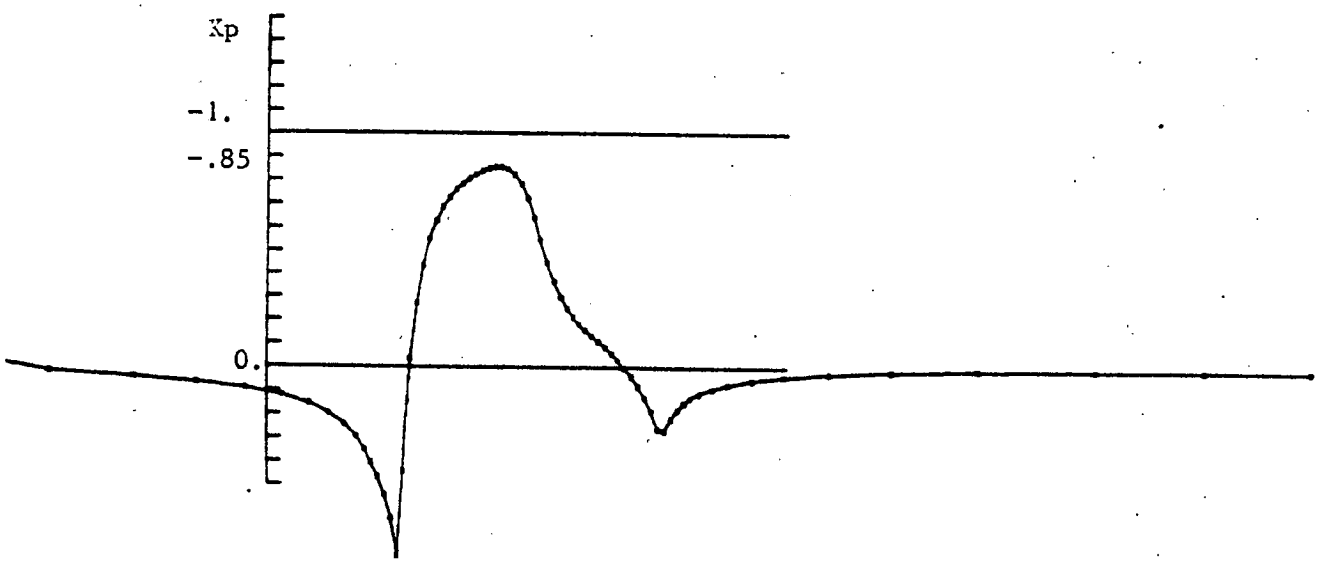

Figure 1.19 : 1/2 NACA0012 in a channel ; Kp distribution on the profile (one step upwinding method)

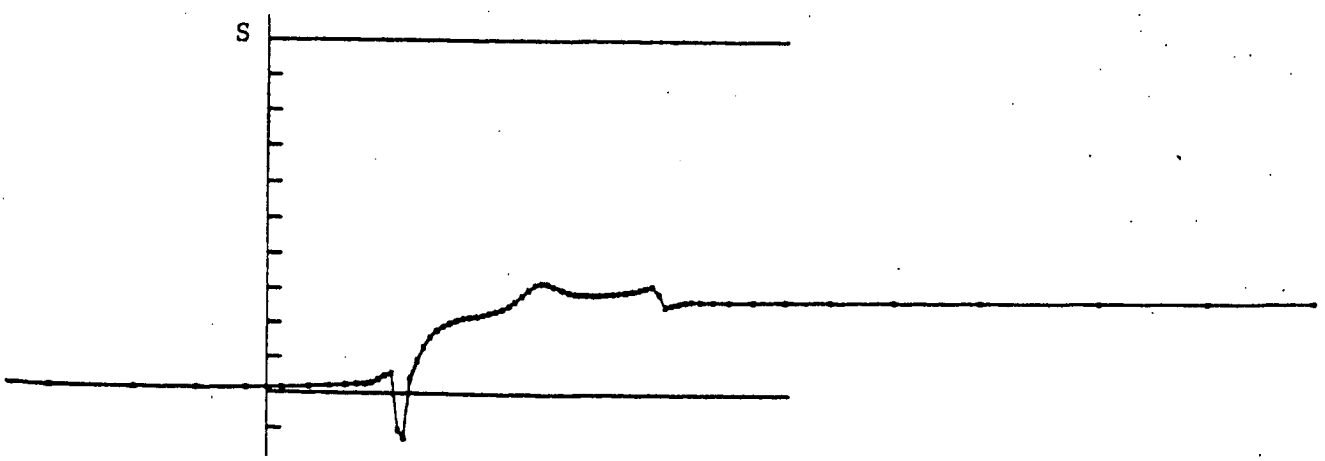

Figure 1.20 : 1/2 NACA0012 in a channel ; distribution of entropy deviation on the profile (one step upwind method).

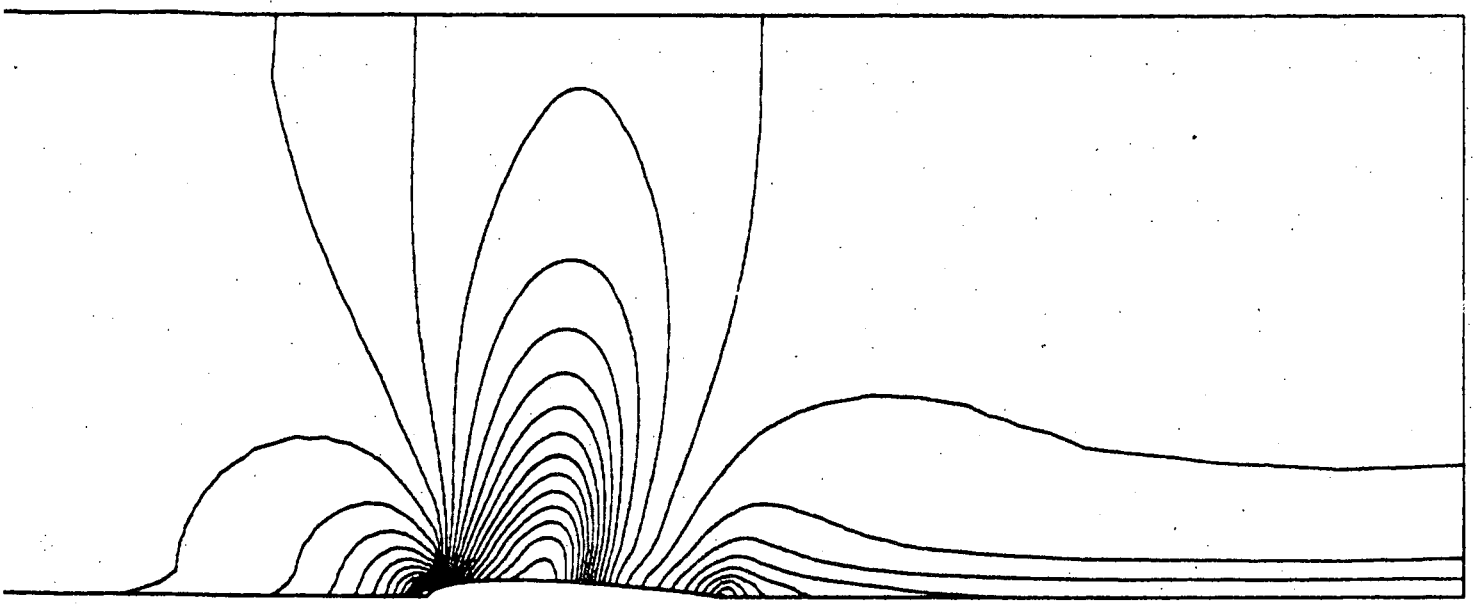

Figure 1.21 : 1/2 NACA0012 in a channel ; isomach lines (one step upwind method).

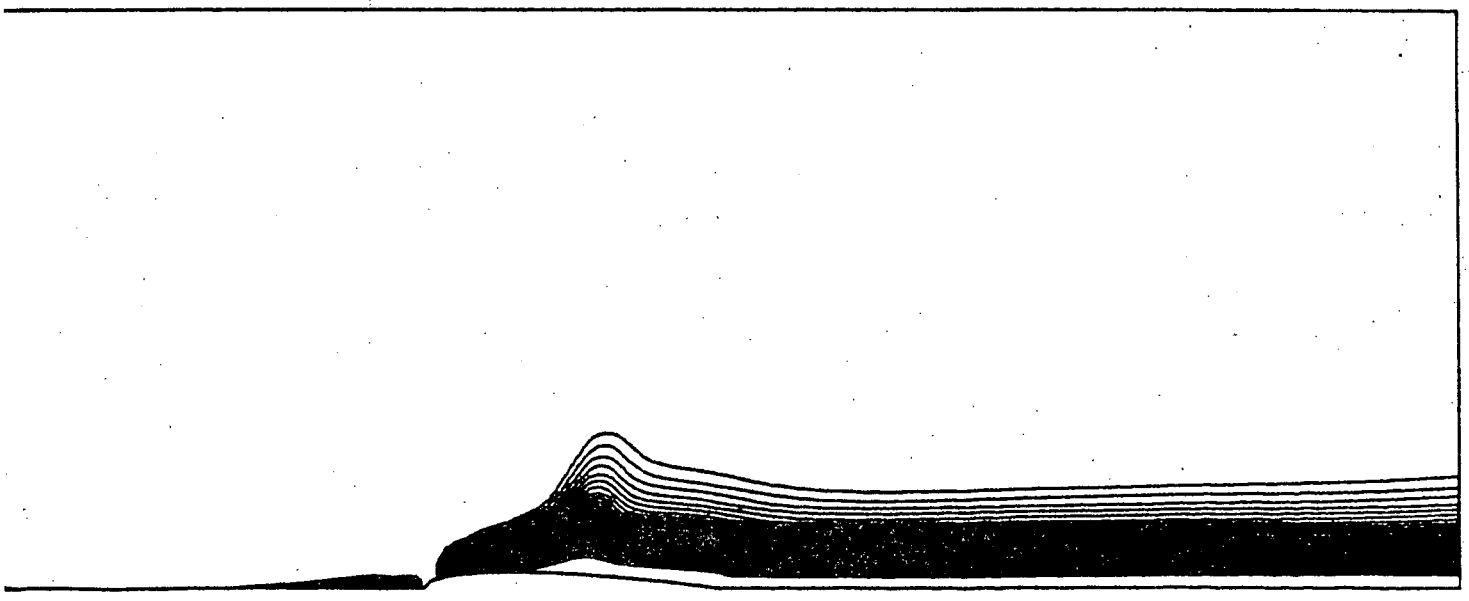

Figure 1.22 : 1/2 NACA0012 in a channel ; isentropic lines (increment $\Delta S = 0.001$) (one step upwind method).

2. A CARACTERISTIC GODUNOV TYPE UPWIND SCHEME FOR P_1 F.E.M.

2.1. The scalar case

The conservation law

$$W_t + F(W)_x \tag{2.1}$$

is assumed to be homogenous, i.e.

$$F(\lambda W) = \lambda F(W) \quad \forall \lambda \in \mathbb{R}, \quad W \in \mathbb{R}^d \ ; \tag{2.2}$$

from Euler's theorem we derive

$$F(W) = F'(W)W \ , \tag{2.3}$$

and the conservative

$$W_t + (F'(W)W)_x = 0 \tag{2.4}$$

and non conservative

$$W_t + F'(W)W_x = 0 \tag{2.5}$$

variants. Now we assume also that $F'(W)$ is (uniformly) diagonalisable

$$\begin{cases} F'(W) = T(W)\ \Lambda(W)\ T^{-1}(W) \\ \\ \Lambda(W) = \text{diag}\ \{\lambda_1(W), \ldots, \lambda_d(W)\} \end{cases} \tag{2.6}$$

and (2.5) gives the caracteristic variant

$$T^{-1}(W)W_t + \Lambda(W)\ T^{-1}(W)W_x = 0 \ , \tag{2.7}$$

it can be written also as

$$\begin{cases} \sum_{k=1}^{d} T^{-1}_{jk}(W)\left(\frac{\partial}{\partial t} + \lambda_j(W)\ \frac{\partial}{\partial x}\right)W_k = 0 \quad 1 \le j \le d \\ \\ T^{-1} = (T^{-1}_{jk}) \end{cases} \tag{2.8}$$

In the jth equation of (2.8) each W_k, $1 \le k \le d$ is differentiated along the jth caracteristic direction by the operator $\frac{\partial}{\partial t} + \lambda_j(W)\frac{\partial}{\partial x}$. This suggests the construction of an upwind approximation for $\frac{\partial W_k}{\partial x}$ together with centered approximations for $\lambda_j(W)$ and $T^{-1}_{jk}(W)$. Returning to the (2.4)-formulation, we derive a conservative caracteristic upwind scheme :

(2.9)
$$\frac{W_i^{n+1} - W_i^n}{\Delta t}\,\Delta x + \Phi^n_{i+\frac{1}{2}} - \Phi^n_{i-\frac{1}{2}} = 0$$

$$\Phi^n_{i+\frac{1}{2}} = [T\,\Lambda](W^n_{i+\frac{1}{2}})\Big(\sum_{k=1}^{d} T^{-1}_{jk}\,(W^n_{i+\frac{1}{2}})\,W^n_{k,(\alpha j)^n_{i+\frac{1}{2}}}\Big)_{j=1}^{d}$$

$$(\alpha j)^n_{i+\frac{1}{2}} = \begin{cases} i & \text{if } \lambda_j(W^n_{i+\frac{1}{2}}) > 0 \\ i+1 & \text{else} \end{cases}$$

$$W^n_{i+\frac{1}{2}} = \frac{1}{2}(W^n_i + W^n_{i+1})$$

Scheme (2.9) is roughly the homogeneous case of GODUNOV-VAN LEER's scheme (see VAN LEER [22]) :

(2.10)
$$\frac{W_i^{n+1} - W_i^n}{\Delta t}\,\Delta x + \Phi^n_{i+\frac{1}{2}} - \Phi^n_{i-\frac{1}{2}} = 0$$

$$\Phi^n_{i+\frac{1}{2}} = (A^+)^n_{i+\frac{1}{2}}\,W^n_i + (A^-)^n_{i+\frac{1}{2}}\,W^n_{i+1}$$

$$(A^{\pm})^n_{i+\frac{1}{2}} = T(W^n_{i+\frac{1}{2}})\,(\Lambda^{\pm})^n_{i+\frac{1}{2}}\,T^{-1}(W^n_{i+\frac{1}{2}})$$

$$(\Lambda^{\pm})^n_{i+\frac{1}{2}} = \text{diag}\,\{[\lambda_k(W^n_{i+\frac{1}{2}})]^{\pm}\}$$

2.2. Extension to the two-dimensional case

2.2.1. The continuous system

The two-dimensional extension of (2.1) is

(2.11)
$$W_t + F(W)_x + G(W)_y = 0 .$$

System (2.14) is assumed to be hyperbolic, i.e. the matrix

$$H = H(\eta_1,\eta_2,W) = \eta_1 F'(W) + \eta_2 G'(W)$$

has all its eigenvalues real for any (η_1,η_2) in $\mathbb{R}^2$ and W in $\mathbb{R}^d$. Moreover, matrix H is assumed to be uniformly diagonalizable, i.e. there exists a matrix $T_{\eta_1\eta_2}(W)$ satisfying

$$(2.12) \qquad H = T_{\eta_1\eta_2}(W)\ \Lambda_{\eta_1\eta_2}(W)\ T^{-1}_{\eta_1\eta_2}(W)$$

where $\Lambda_{\eta_1\eta_2}(W)$ is a diagonal matrix with eigenvalues of H.

We assume at last that F and G are homogeneous functions with order one :

$$(2.13) \qquad F(\lambda W) = \lambda F(W)\ ;\ G(\lambda W) = \lambda G(W),\ \forall\lambda \in \mathbb{R},\ W \in \mathbb{R}^d$$

so that

$$(2.14) \qquad F(W) = F'(W)W,\ G(W) = G'(W)W\ ,\quad \forall W \in \mathbb{R}^d$$

System (2.11) can be written as follows

$$(2.15) \qquad W_t + F'(W)\ W_x + G'(W)W_y = 0$$

$$(2.16) \qquad W_t + (F'(W)W)_x + (G'(W)W)_y = 0$$

Systems (2.11) and (2.16) are in conservative form but (2.15) is not. For the present two-dimensional case, we cannot write system (2.11) in a caracteristic form analogous to (2.8) without discretizing the space derivative and considering control "volumes" and fluxes along segments.

2.2.2. Space discretization

Let $\mathcal{C}_h$ be a triangulation of $\mathbb{R}^2$. Let a_i a node of $\mathcal{C}_h$ and K_{ij}, $1 \le j \le q_i$ the triangles having a_i as a vertex with a numerotation corresponding to the direct rotation around a_i ; l_{ij} for $1 \le j \le q_i$ is the common side of K_{ij} and K_{ij+1}, with the convention $K_{iq_i+1} = K_{i1}$;

G_{ij} denotes the centroid of triangle K_{ij}, I_{ij} the middle point of l_{ij}, and a_{ij} the extremity of side l_{ij} which is not a_i.
We define the integration zone $\hat{a}_i$ of a_i as the bounded region limited by segments $G_{i1}\,I_{i1}$, $I_{i1}\,G_{i2}$,..., $G_{iq_i}I_{iq_i}$, $I_{iq_i}G_{i1}$ (Figure 2.1)

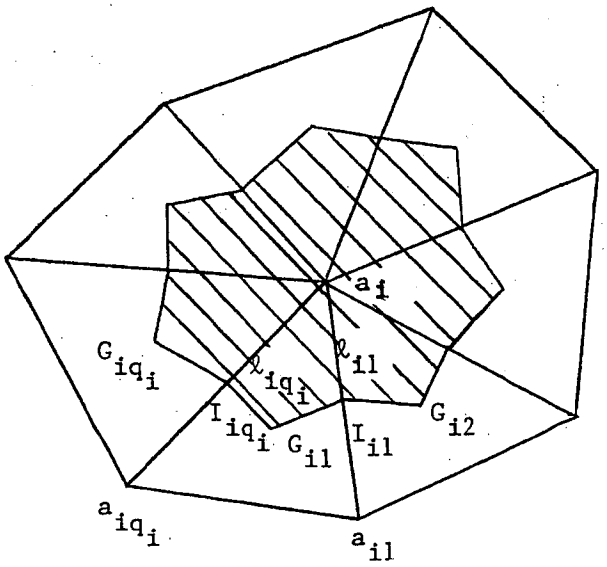

Figure 2.1. Integration zone $\hat{a}_i$ of vertex a_i.

We introduce the following approximate space

$$V_h = \{v_h \in L^2(\mathbb{R}^2) \cap L^\infty(\mathbb{R}^2),\ v_{h|\hat{a}_i} = \text{const.} = v_{h_i} \quad \forall\, a_i \text{ vertex of } \mathcal{C}_h\}\ , \tag{2.17}$$

a basis of which is

$$\chi_i(x,y) = \begin{cases} 1 & \text{if } (x,y) \in \hat{a}_i \\ 0 & \text{elsewhere.} \end{cases}$$

Formally, an approximate solution in V_h of system (2.11) should be a function W_h :

$$W_h : [0, \infty[\to (V_h)^d$$

such that, for v_h belonging $(V_h)^d$.

$$(2.18) \qquad \iint_{\mathbb{R}^2} (W_h)_t \, v_h \, dxdy + \iint_{\mathbb{R}^2} \{F(W_h)_x + G(W_h)_y \, v_h \, dxdy = 0.$$

Integration by parts gives

$$(2.19) \qquad \begin{cases} \sum_{a_i \in \mathcal{C}_h} (W_{hi})_t \, v_{hi} \;\; \text{area } (\hat{a}_i) + \\ \sum_{a_i \in \mathcal{C}_h} \int_{\partial \hat{a}_i} [F(W_h)\nu_x + G(W_h)\nu_y] \, v_h \, d\sigma = 0. \end{cases}$$

Since W_h and v_h are discontinuous along the $\partial \hat{a}_i$, the second integral cannot be defined exactly ; to every approximation of this integral corresponds a scheme for the semi-discrete problem. Before choosing such an approximation we need to discretize the time derivative : an explicit Euler forward approximation is constructed with first order accuracy :

$$(2.20) \qquad (W_{hi})_t \Big|_{t=t^n} \simeq \frac{W_{h_i}^{h+1} - W_{h_i}^n}{\Delta t} + O(\Delta t) \;\; ;$$

taking $v_h = \chi_i$ in (2.19), it becomes

$$(2.21) \qquad \begin{cases} \dfrac{W_{h_i}^{n+1} - W_{h_i}^n}{\Delta t} \;\; \text{area } (\hat{a}_i) + \\ \sum_{j=1}^{q_i} \left[\int_{G_{ij} I_{ij}} + \int_{I_{ij} G_{ij+1}} \right] [F(W_h)\nu_x + G(W_h)\nu_y] \, d\sigma = 0. \;\; \square \end{cases}$$

Let us now precise the approximation of the boundary integral along $\partial \hat{a}_i$; we need the notations (see figure 2.2)

$\nu^1_{ij} = (\nu^1_{xij}, \nu^1_{yij})$ unitary vector, normal to $G_{ij}\ I_{ij}$, pointing outward from $\hat{a}_i$,

$\nu^2_{ij} = (\nu^2_{xij}, \nu_{yij})$ unitary vector, normal to $I_{ij}\ G_{ij+1}$, pointing outward from $\hat{a}_i$,

$$\eta_{xij} = \nu^1_{xij}\ \text{length}(G_{ij}I_{ij}) + \nu^2_{xij}\ \text{length}(I_{ij}G_{ij+1})$$

$$\eta_{yij} = \nu^1_{yij}\ \text{length}(G_{ij}I_{ij}) + \nu^2_{yij}\ \text{length}(I_{ij}G_{ij+1})\ ;$$

henceforward index h is omitted.

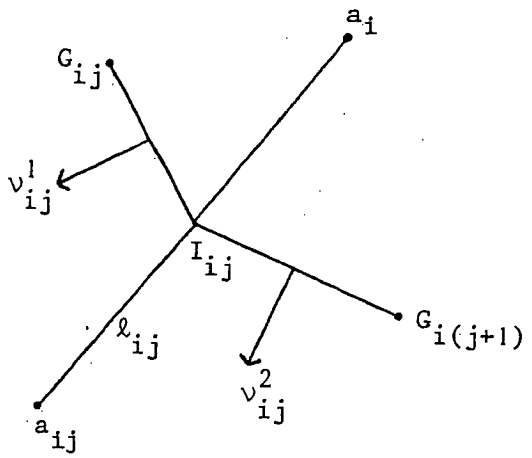

Figure 2.2.

System (2.21) takes the simplified form

$$(2.22)_1 \qquad \frac{W_i^{n+1} - W_i^n}{\Delta t}\ \text{area}(\hat{a}_i) + \sum_{j=1}^{q_i} H^n_{ij} = 0$$

where

$$(2.22)_2 \qquad H^n_{ij} = [\eta_{xij}F + \eta_{yij}G]\ (W_i^n, W_{ij}^n)$$

remains to be precised.

2.2.3. Upwinding

Thanks to the flux splitting (2.22), we are able to transpose the above one dimensional upwind scheme ; introducing

$$(2.23)\quad \begin{cases} P_{ij}(.) = [\eta_{xij} F' + \eta_{yij} G'](.) , \\ P_{ij} = T_{ij}\ \Lambda_{ij}\ T_{ij}^{-1} \quad , \quad P_{ij}^{\pm} = T_{ij}\ \Lambda_{ij}^{\pm}\ T_{ij}^{-1} , \\ (P^{\pm})^{n}_{\frac{ij}{2}} = P_{ij}\left(\frac{W_i^n + W_{ij}^n}{2}\right) , \end{cases}$$

we take in (2.22) :

$$(2.24)\quad H_{ij}^n = (P^+)^{n}_{\frac{ij}{2}}\ W_i^n + (P^-)^{n}_{\frac{ij}{2}}\ W_{ij}^n \quad .$$

Summing up, we may write the scheme proposed as follows

$$(2.25)\quad \boxed{\begin{aligned} W_i^{n+1} = W_i^n &- \frac{\Delta t}{\text{area}(\hat{a}_i)} \sum_{j=1}^{q_i} (P^+)^{n}_{\frac{ij}{2}}\ W_i^n \\ &+ \frac{\Delta t}{\text{area}(\hat{a}_i)} \sum_{j=1}^{q_i} (-P^-)^{n}_{ij}\ W_{ij}^n \\ &(P^{\pm})^{n}_{\frac{ij}{2}} \quad \text{defined by (2.23).} \end{aligned}}$$

For a linear stability analysis, we refer to G. VIJAYASUNDARAM [23] .

2.3. Application to Euler simulations

The above scheme is applied to the two dimensional Euler system. Wall (or profile) boundary conditions are implemented via a boundary integral of pressure terms ; because the nodes are on the boundary, no extrapolation is needed.

Outflow and inflow infinity conditions are constructed as in the first section by imposing the infinity values at the boundary nodes : adequate inflow and outflow characteristic datas are selectioned by the upwind scheme.

The shock tube problem :

The problem and the triangulation are described in Section 1.3. ; results at time t = 0.16 are presented in Figure 2.3.

Channel with a circular bump :

See also Section 1.3 for formulation and triangulation : the number of unknowns in now only 1512 per component (number of vertices).

With 8900 iterations RMS $\frac{\partial p}{\partial t}$ is less than 10^{-6}. With this quite fine triangulation, the diffusion introduced by the first order upwinding is not neatly apparent ; the shock is not at all smeared and we observe a slight overshoot. Globally the result is comparable to second order simulations.

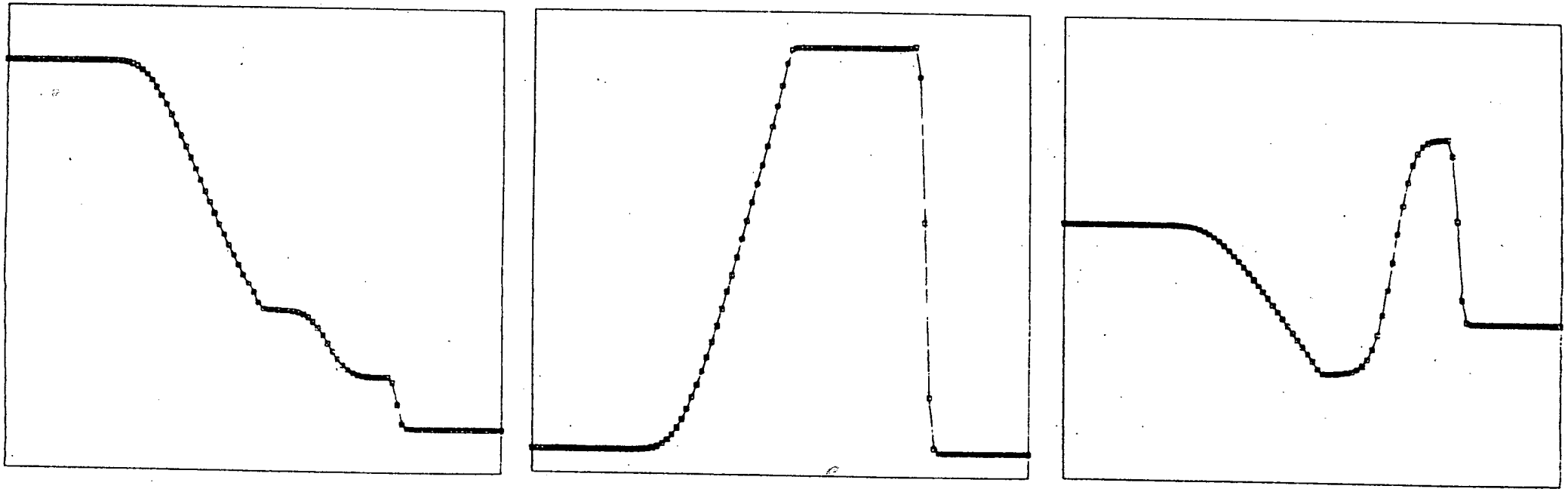

density velocity temperature

Figure 2.3. : The shock tube test for the 2-D Godunov scheme
(time = 0.16)

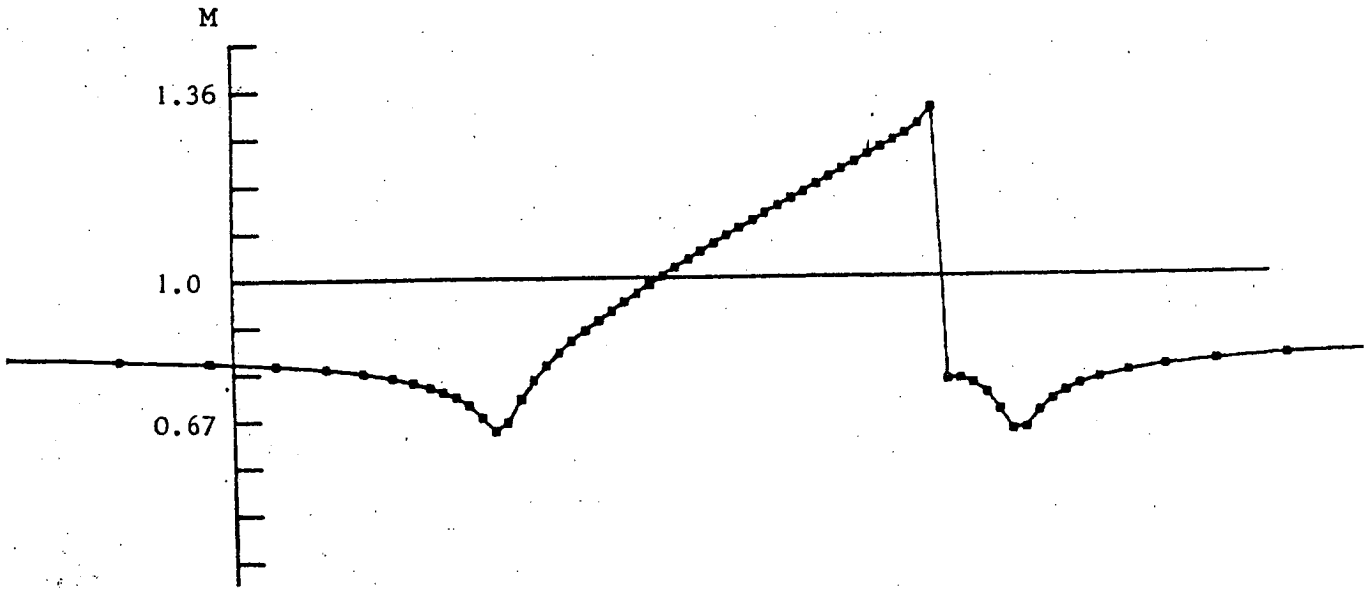

Figure 2.4. : GAMM channel with circular bump ; Mach distribution on the bottom.

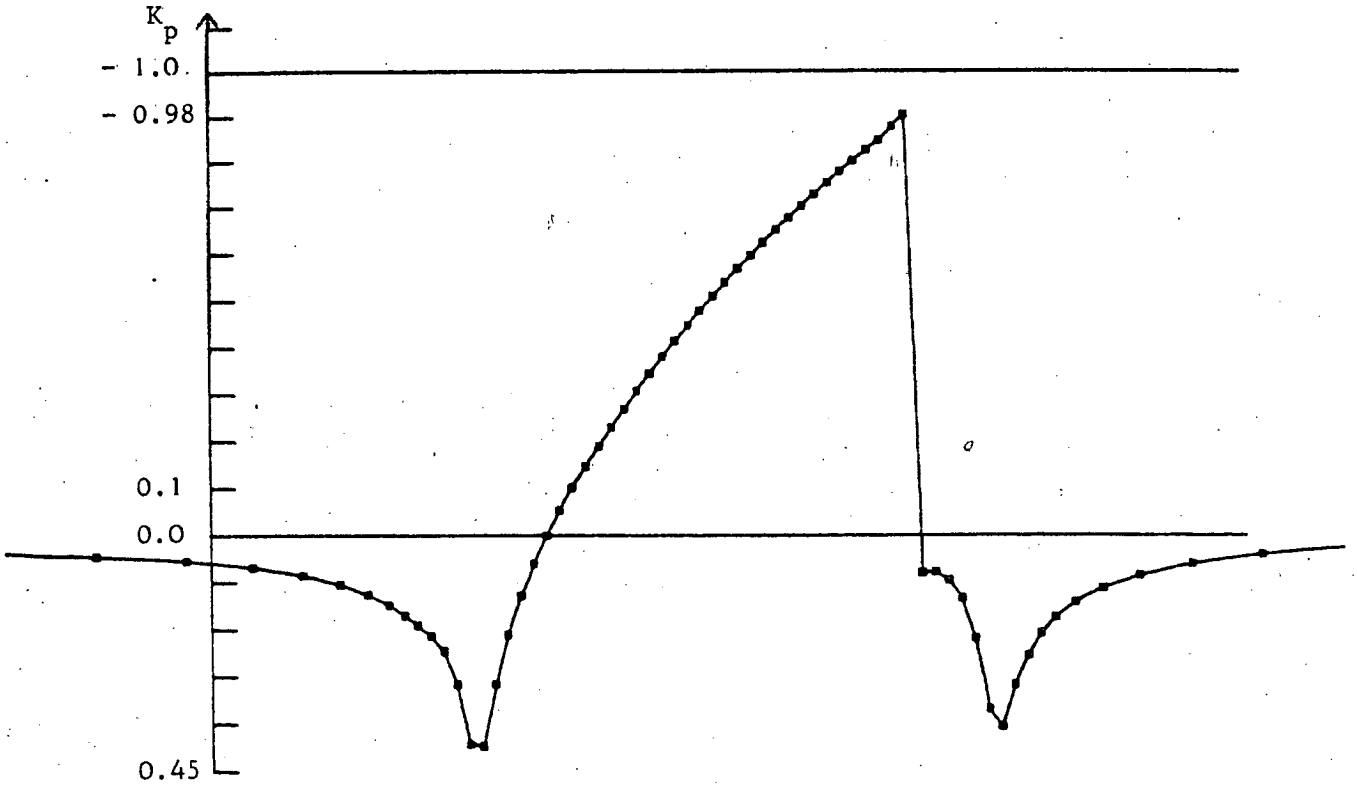

Figure 2.5. : GAMM channel with circular bump ; K_p distribution on the bottom.

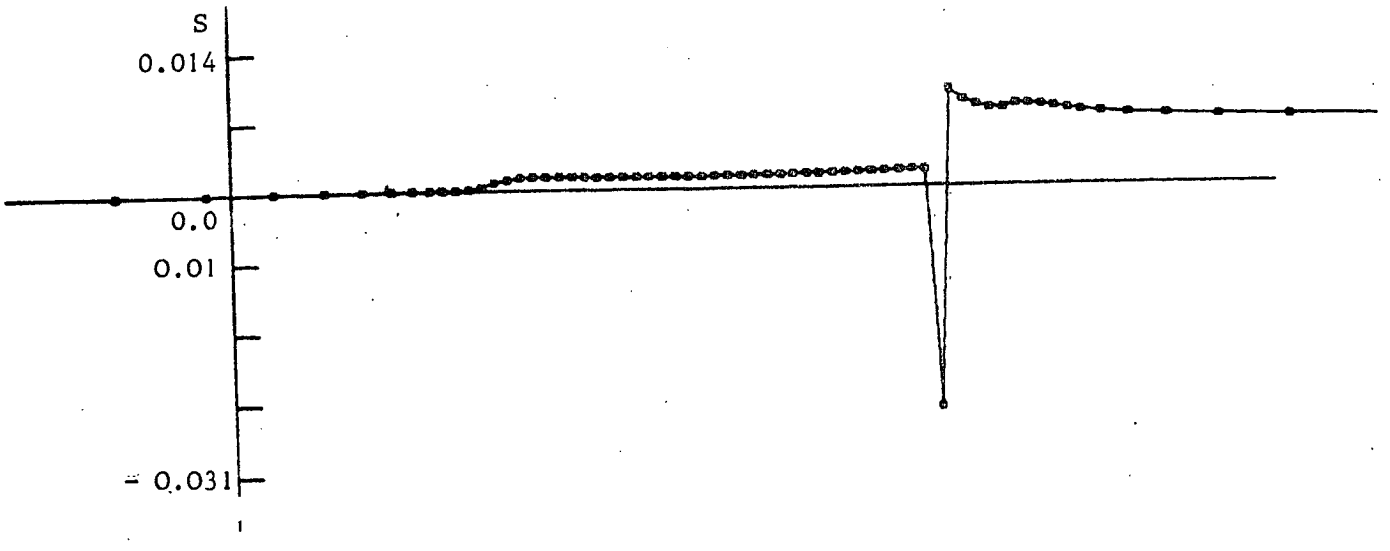

Figure 2.6. : GAMM channel with circular bump ; distribution on the bottom of deviation entropy.

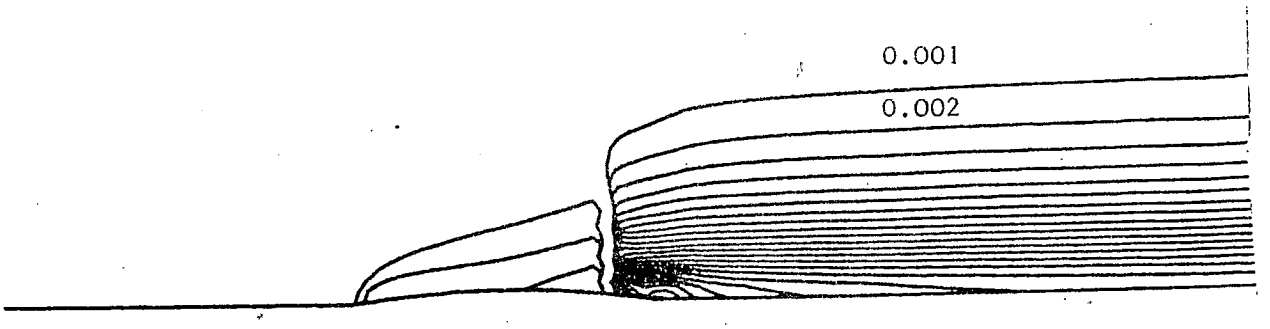

Figure 2.7. : GAMM channel with circular bump ; isentropic lines (increment $\Delta S = 0.001$).

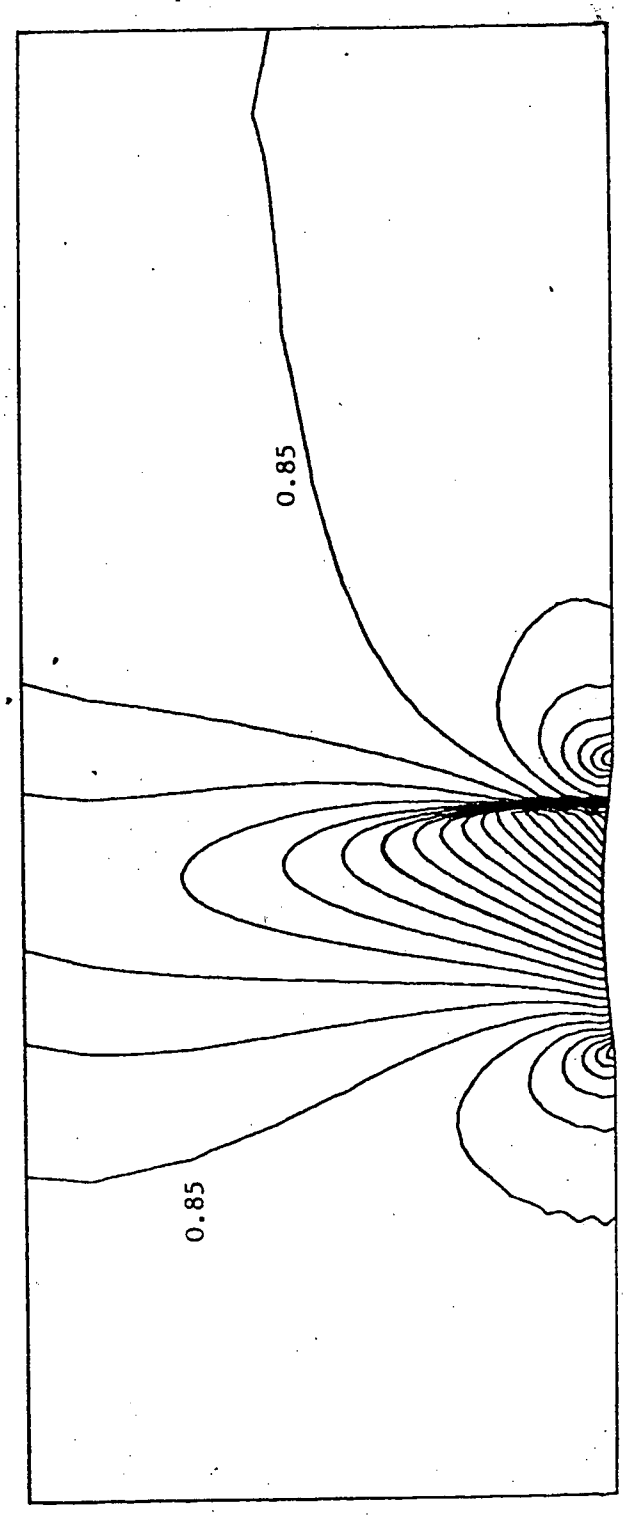

Figure 2.8. : GAMM channel with circular bump ; isomach lines.

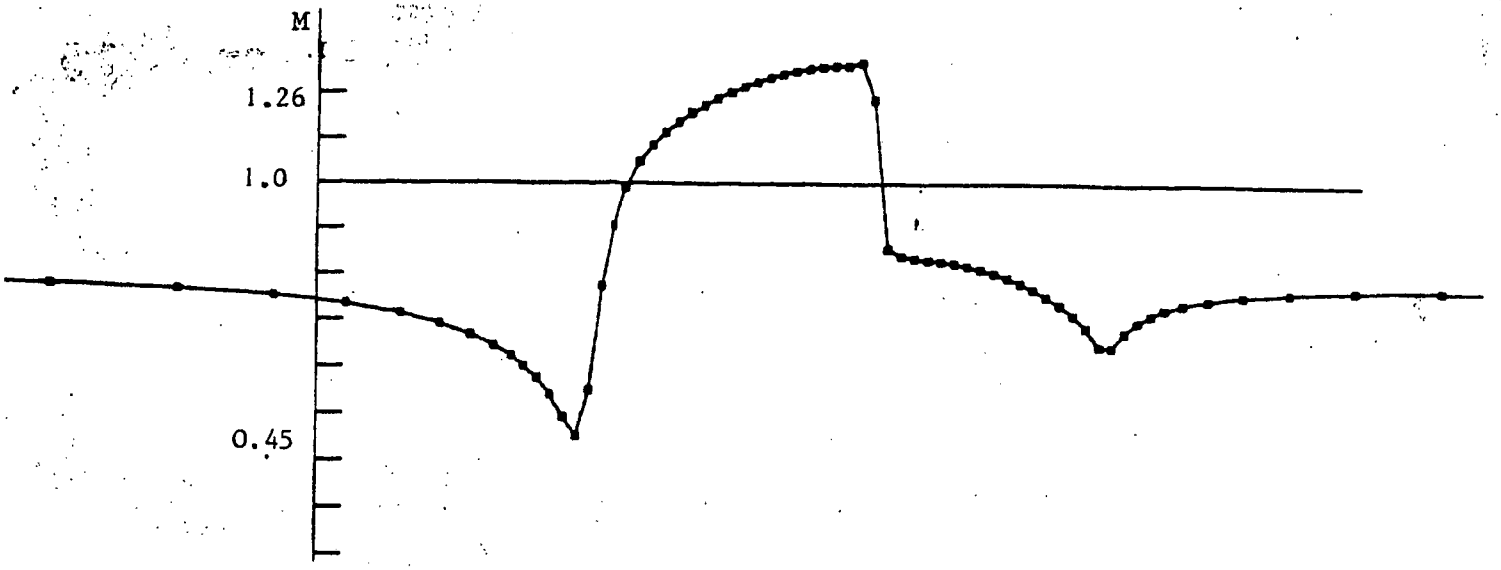

Figure 2.9. : Half NACA 0012 in a channel ; Mach distribution on the profile $M_\infty = 0.8$; $\alpha = 0.0$

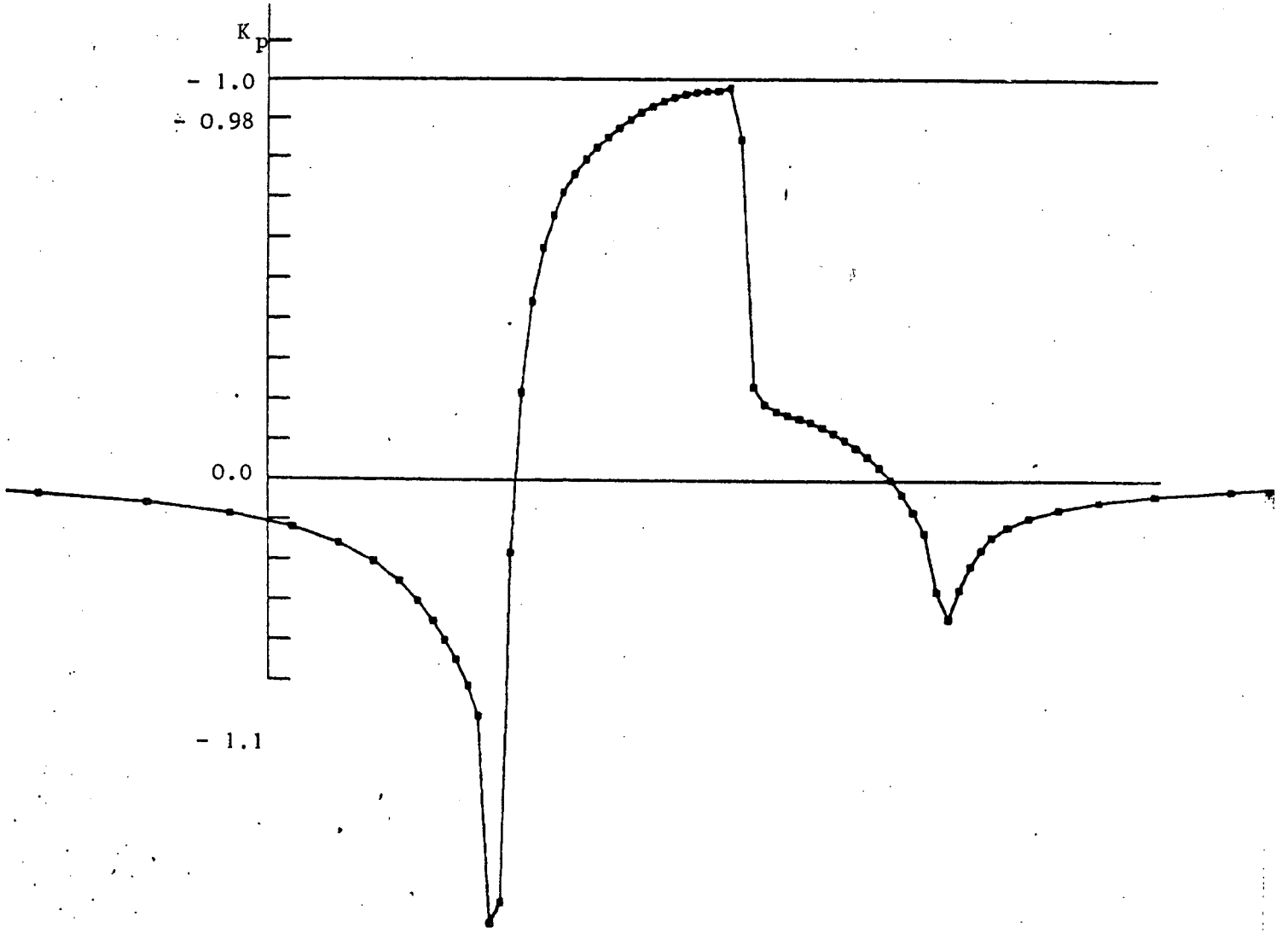

Figure 2.10. : 1/2 NACA 0012 in a channel K_p distribution on the profile.

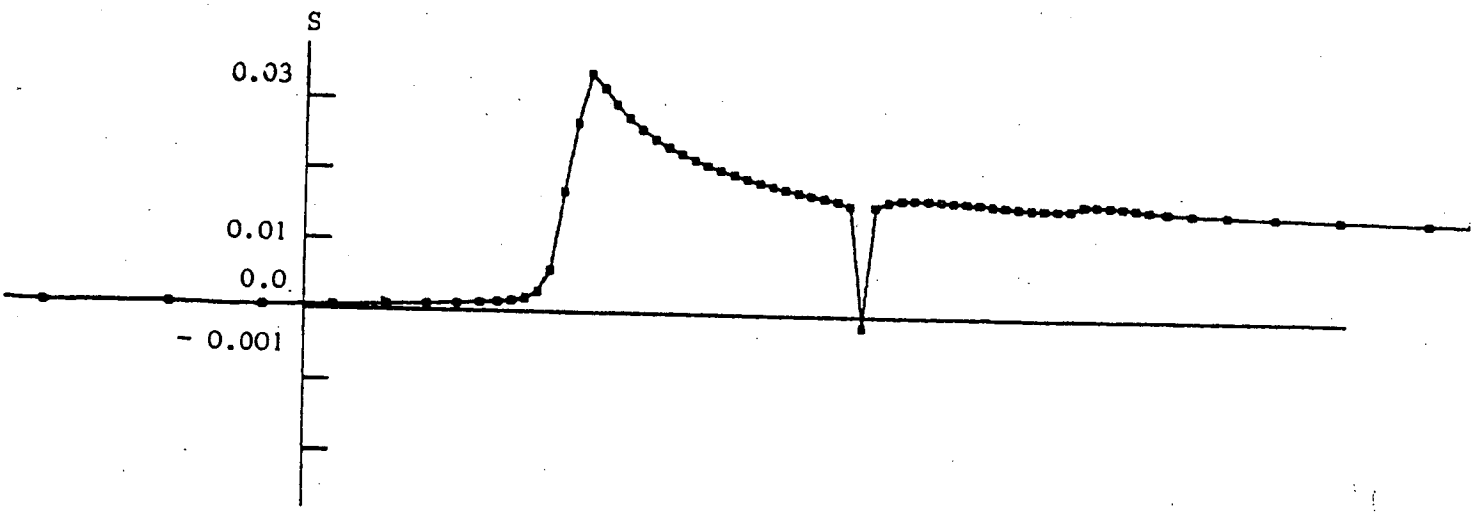

Figure 2.11. : 1/2 NACA 0012 in a channel, distribution of deviation entropy on the profile.

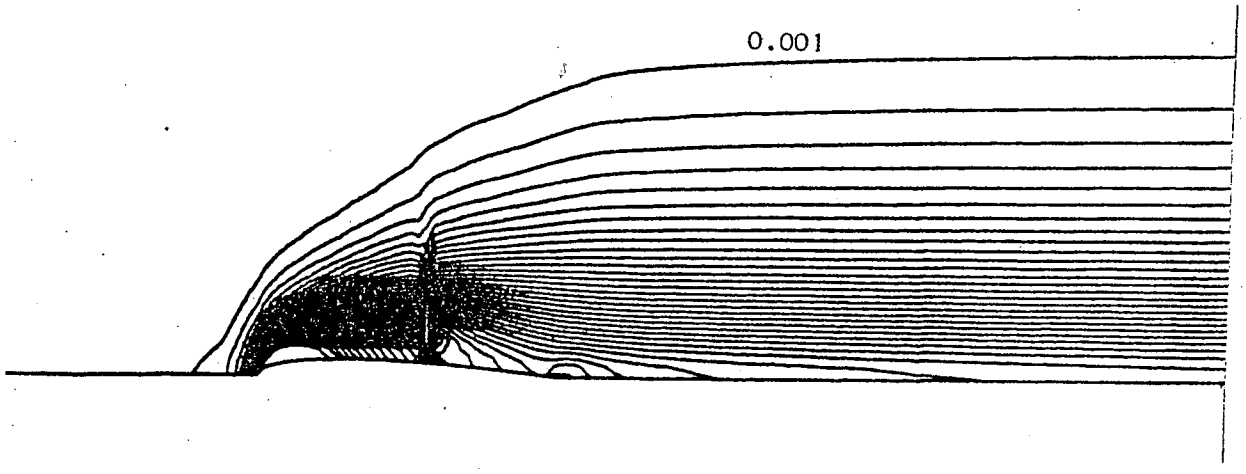

Figure 2.12. : 1/2 NACA 0012 in a channel isentropic lines (increment $\Delta S = 0.001$)

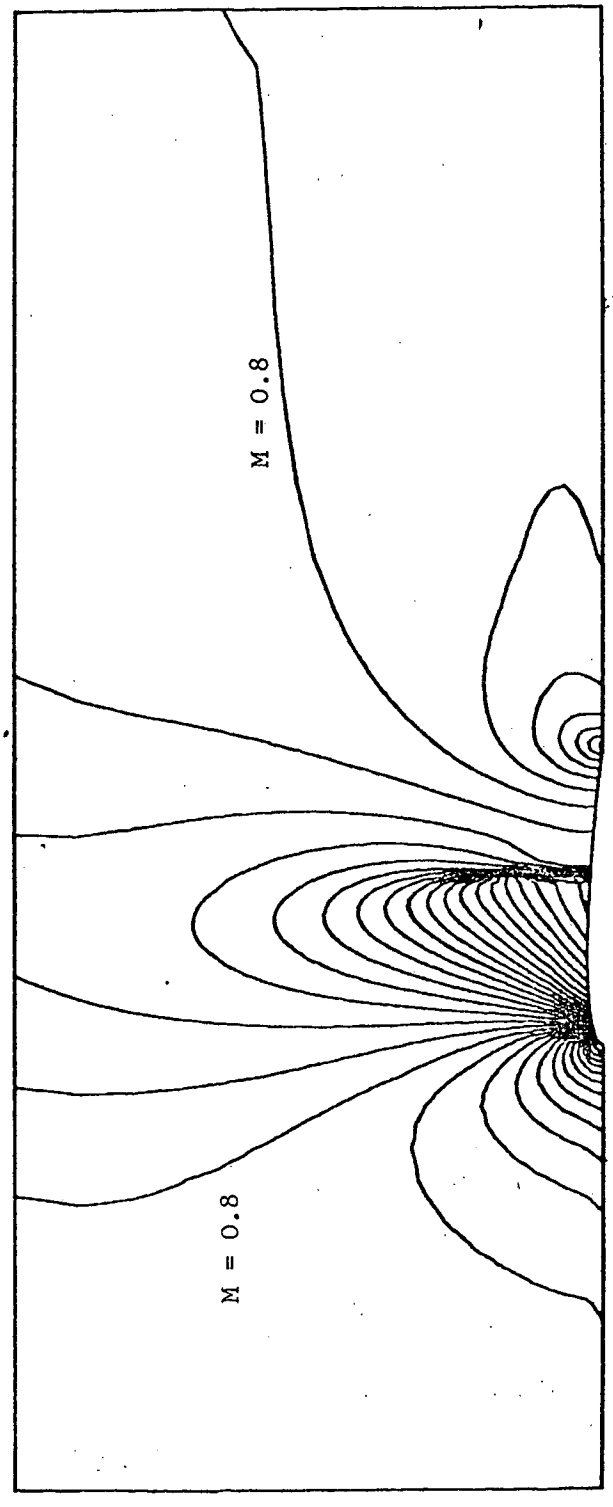

Figure 2.13. : 1/2 NACA0012 in a channel ; isomach lines.

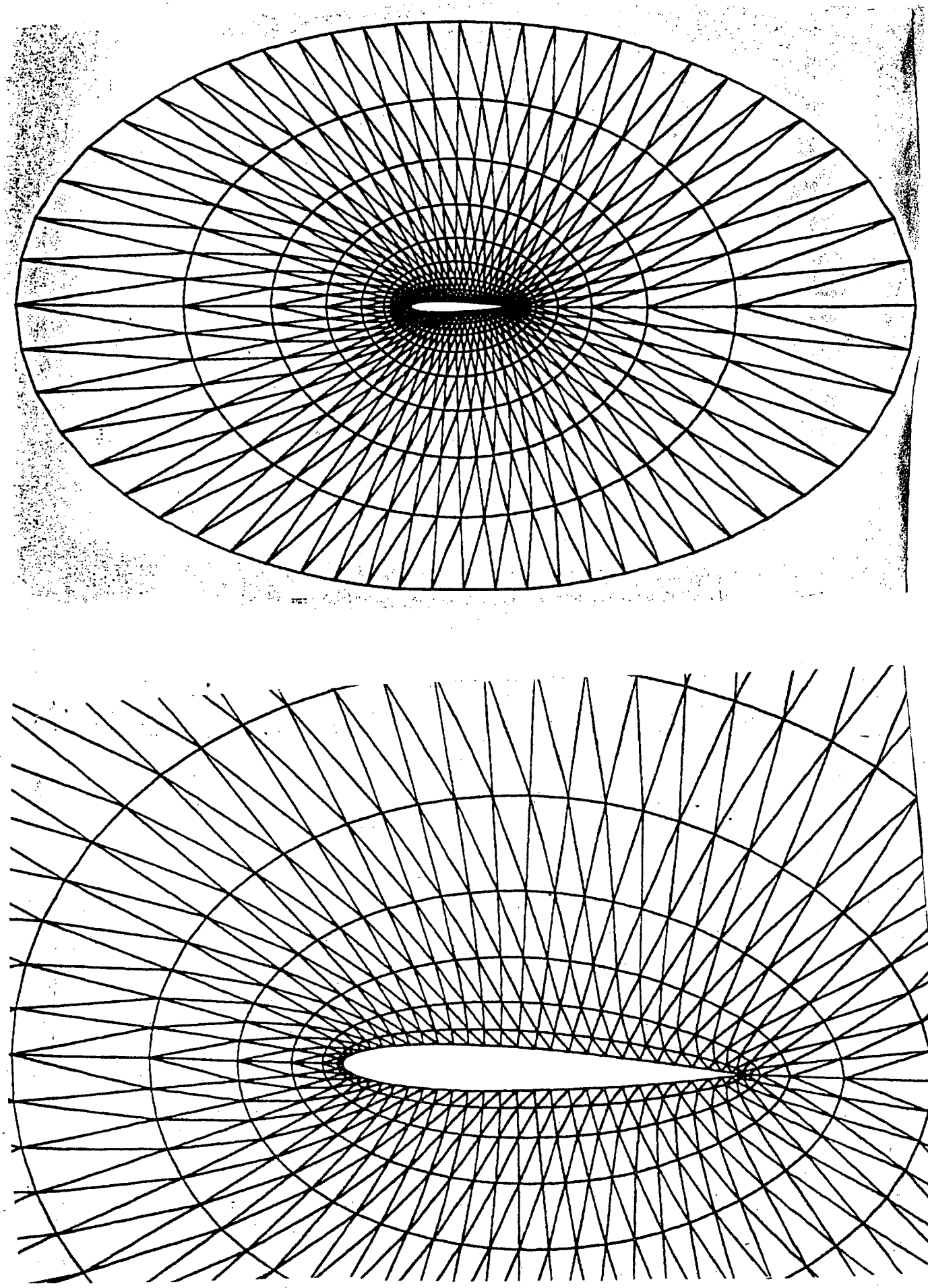

Figure 2.14. : Triangulation around NACA 0012 profile.

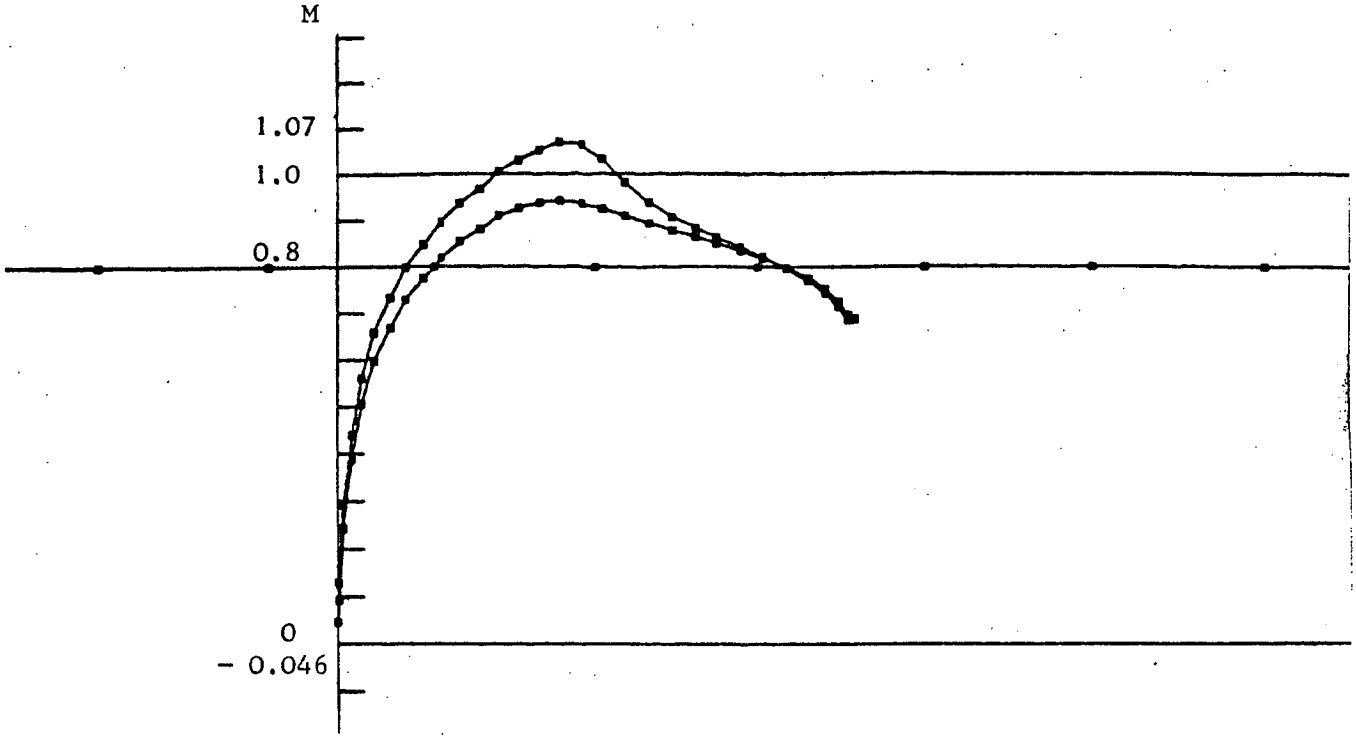

Figure 2.15. : NACA 0012 in incidence. Mach distribution on the profile $M_\infty = .8$, $\alpha = 1.25°$

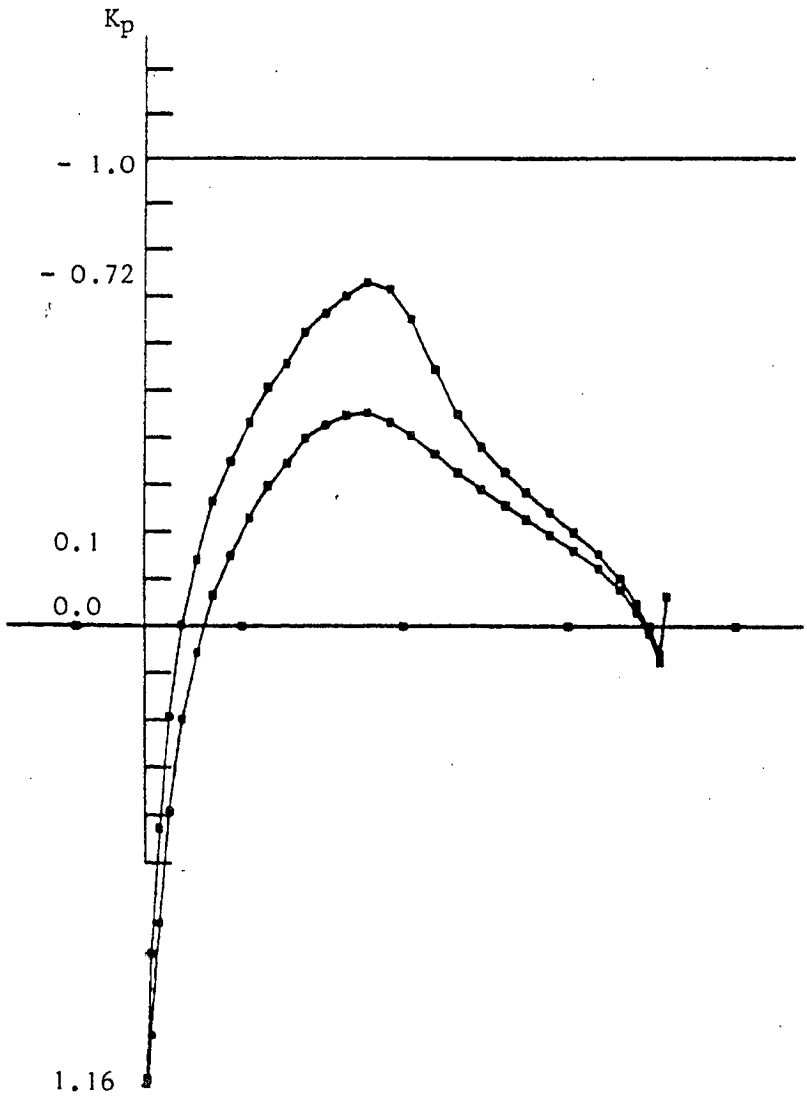

Figure 2.16. : NACA 0012 in incidence. K_p distribution on the profile.

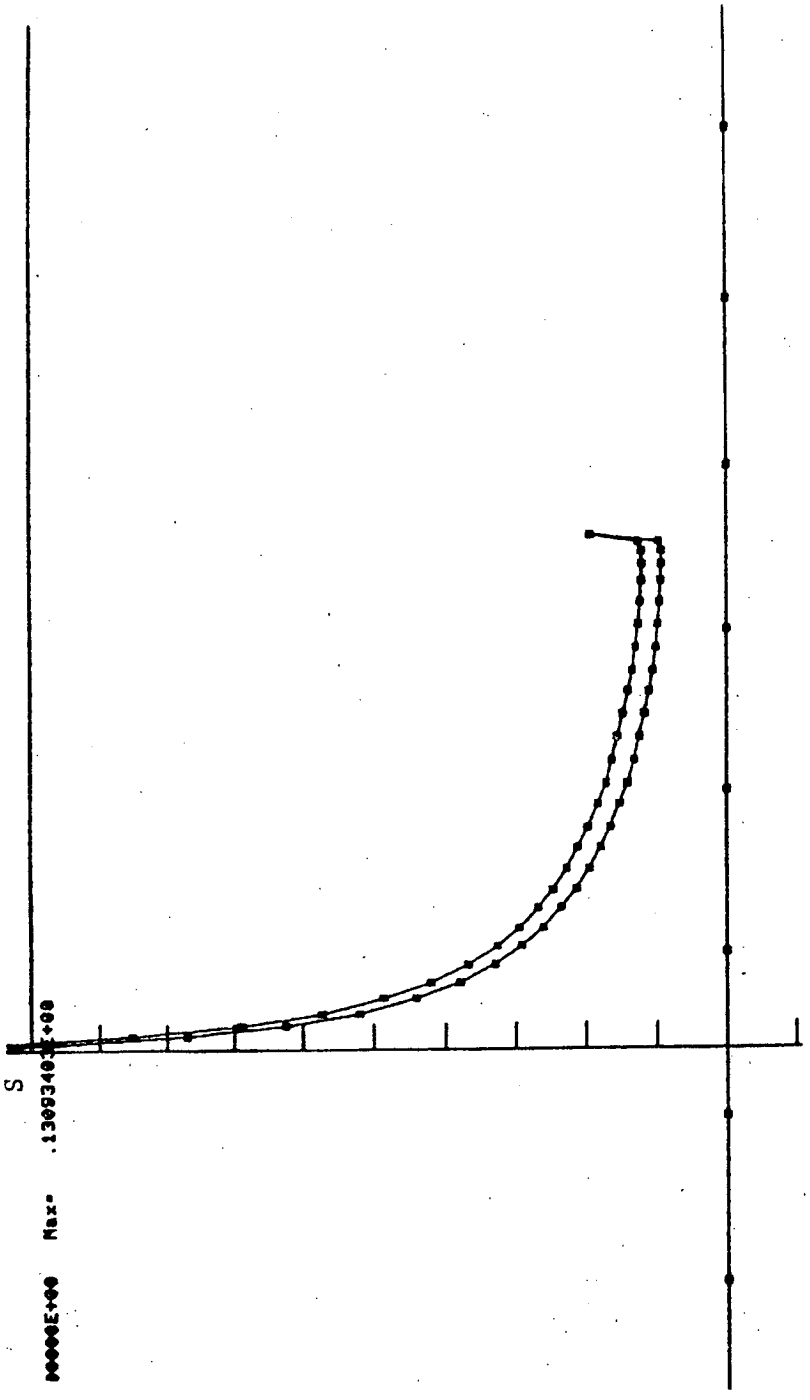

Figure 2.17. : NACA 0012 in incidence distribution of deviation entropy on the profile.

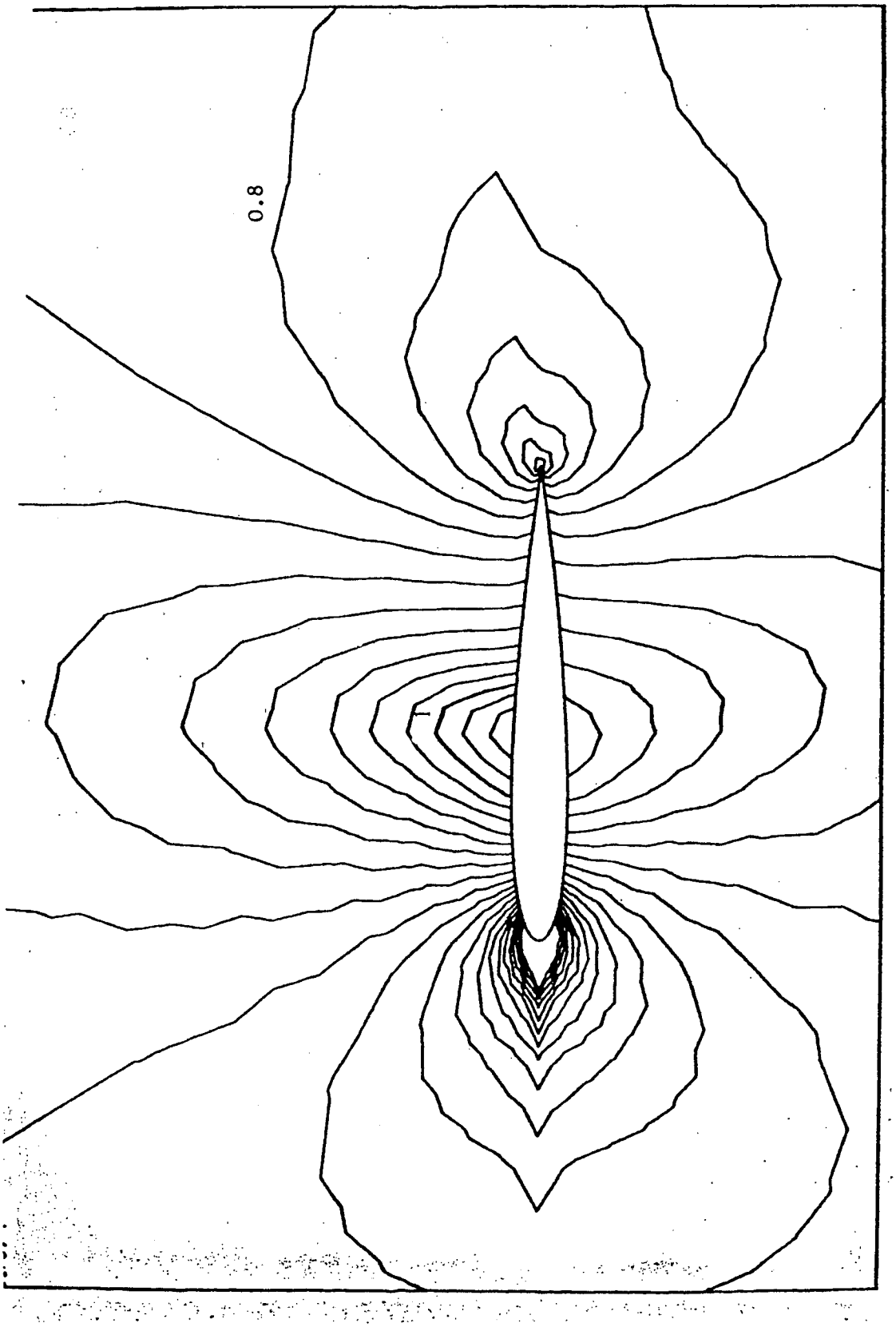

Figure 2.18. : NACA 0012 in incidence.isomach lines.

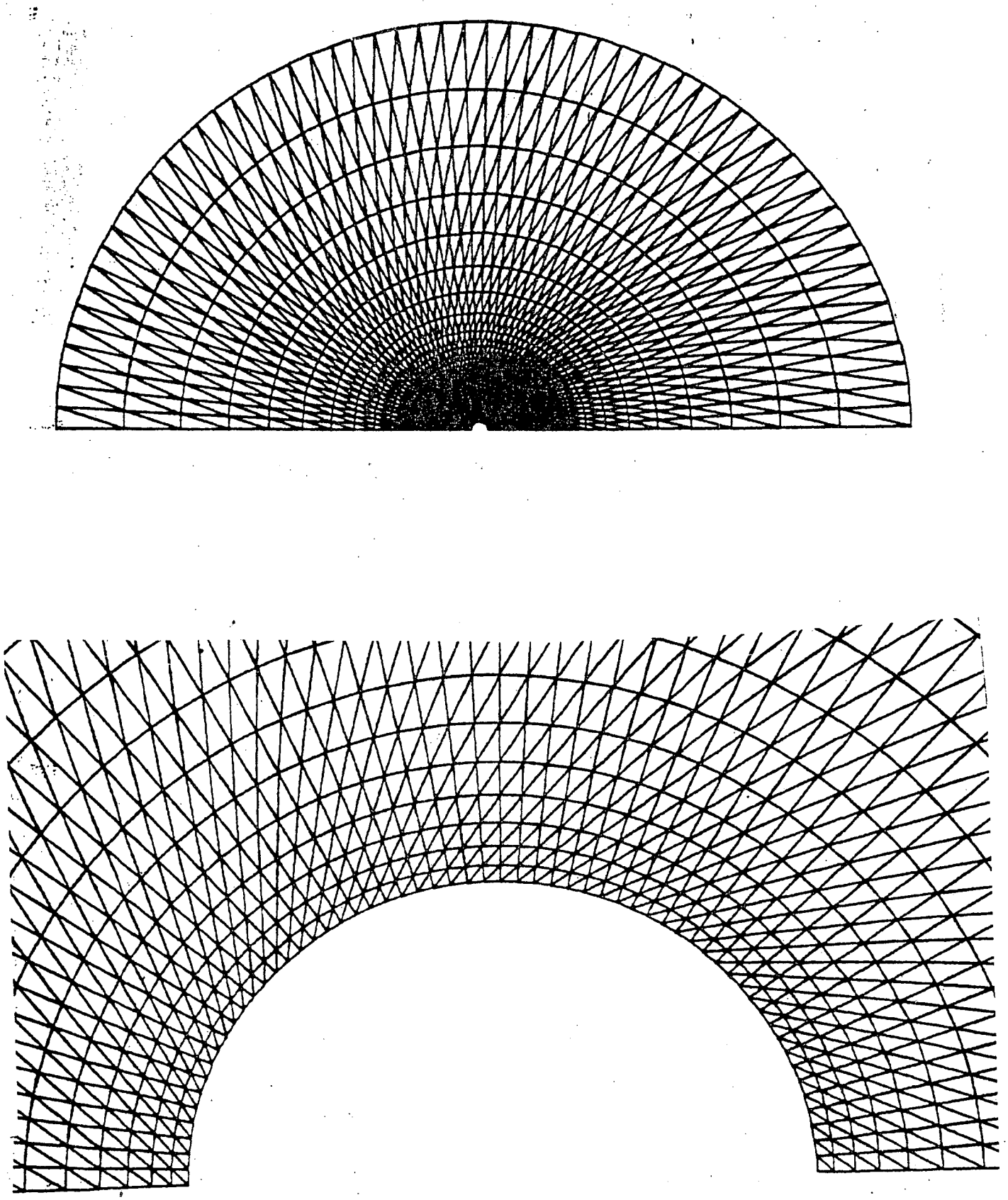

Figure 2.19.: Triangulation around a 1/2 cylinder.

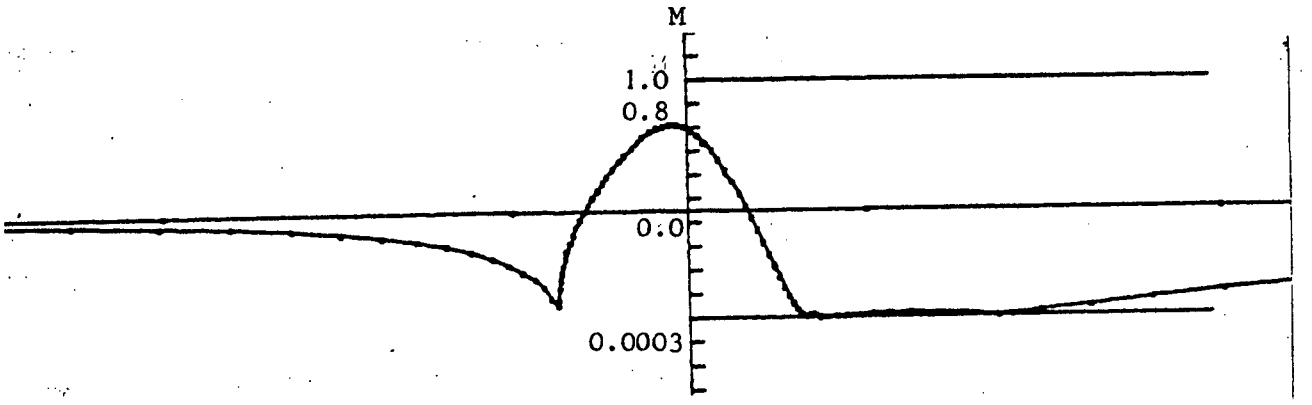

Figure 2.20. : 1/2 cylinder, Mach distribution

$M_\infty = 0.45 \quad \alpha = 0.0$

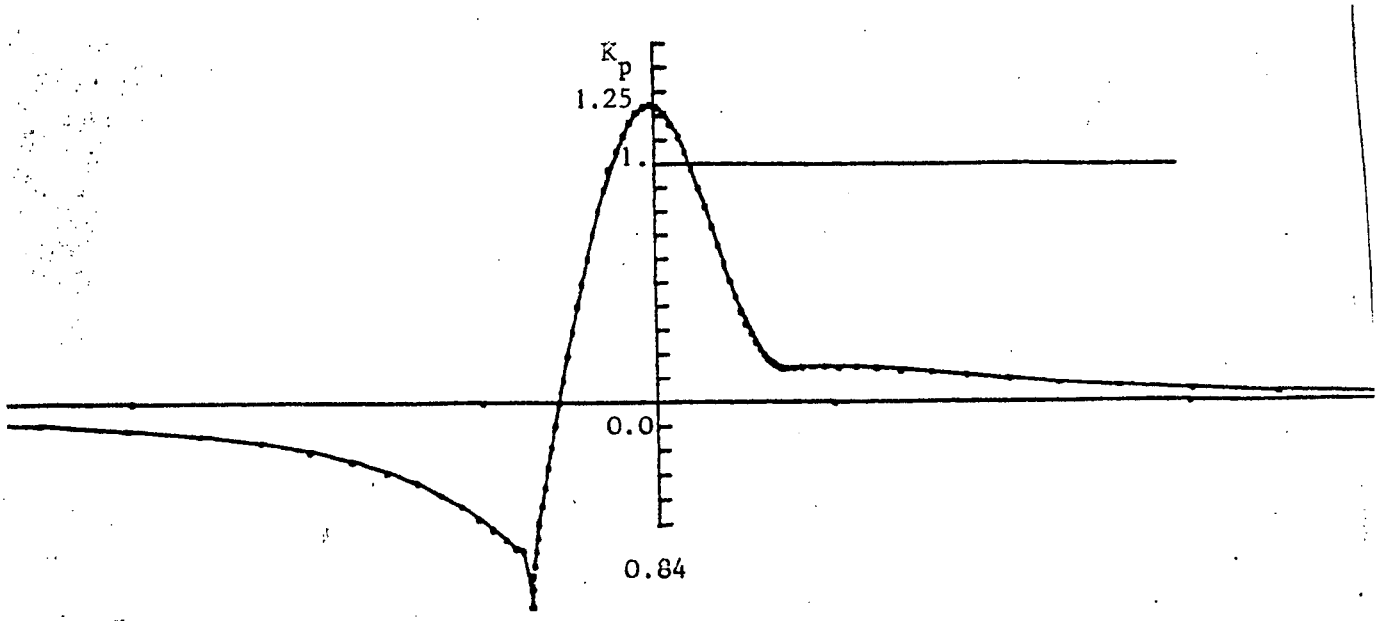

Figure 2.21. : 1/2 cylinder, K_p distribution.

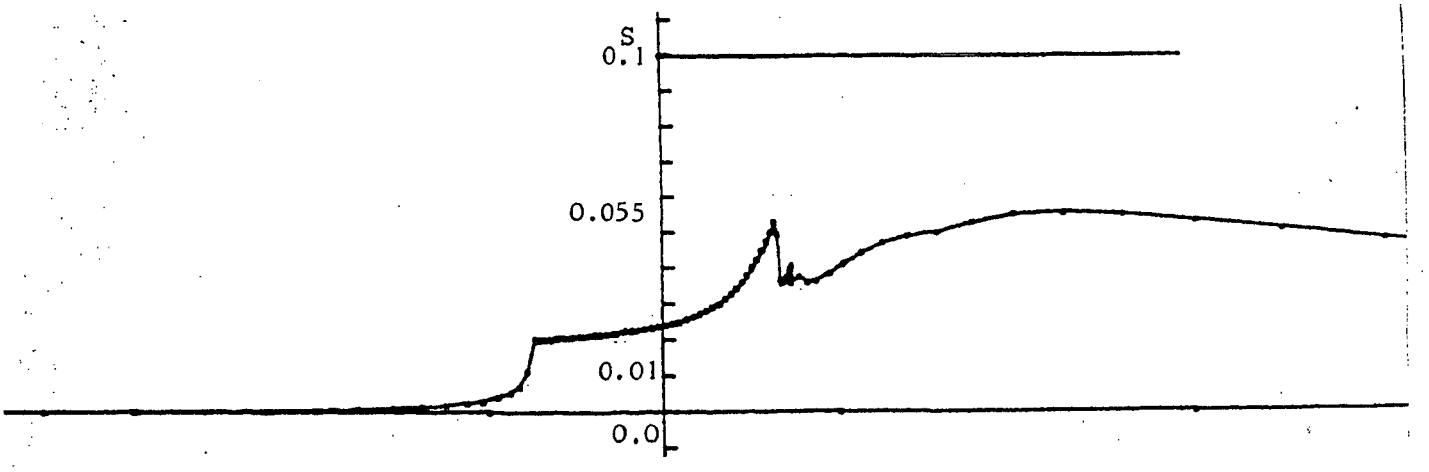

Figure 2.22. : 1/2 cylinder ; distribution of deviation of entropy.

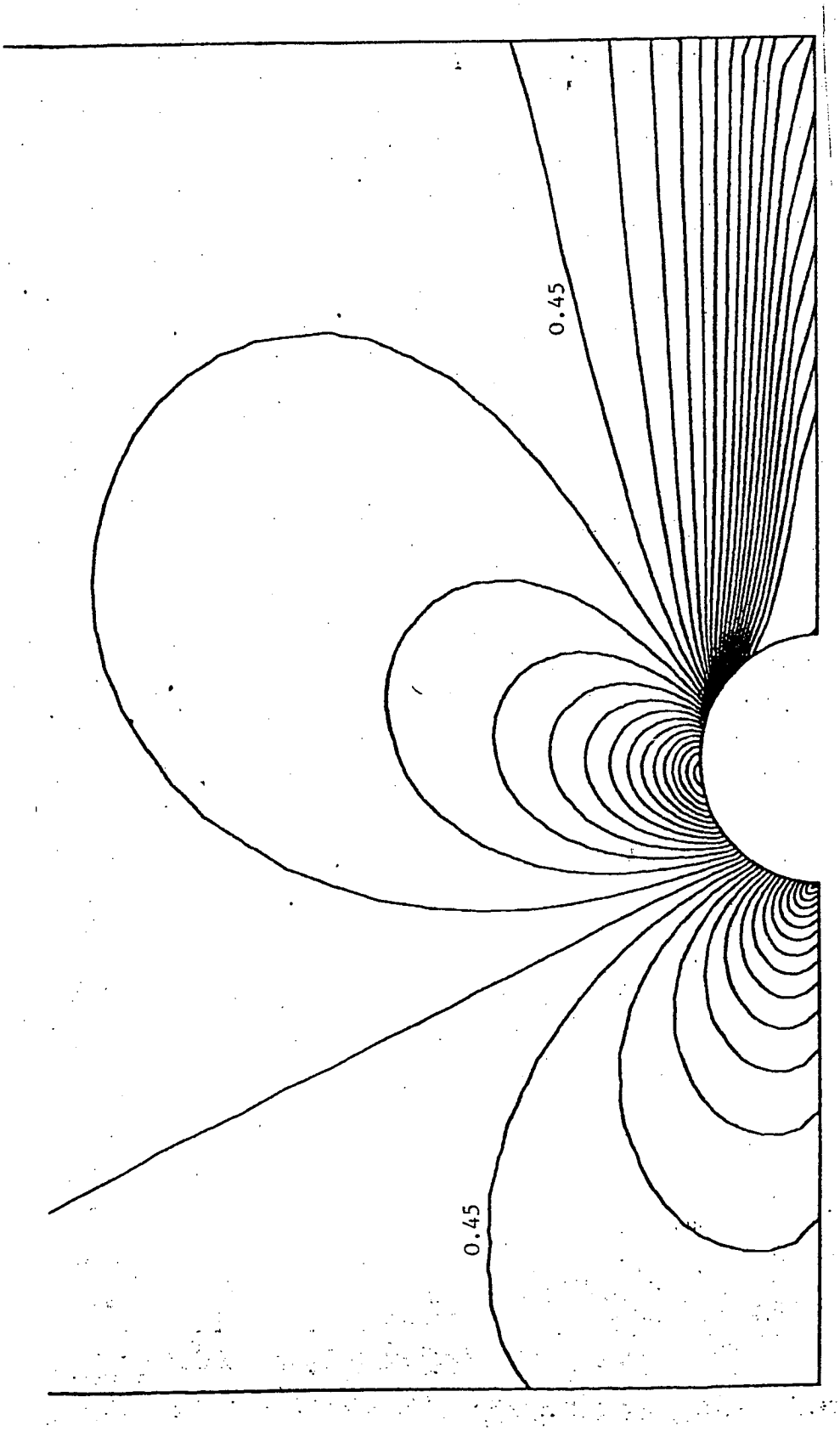

Figure 2.23. : 1/2 cylinder, isomach lines.

3. A RICHTMYER SCHEME

3.1. The scalar linear case

3.1.1. Presentation of the scheme

We want to solve the following system

$$(3.1)\quad \begin{cases} \dfrac{\partial W}{\partial t} + V_1 \dfrac{\partial W}{\partial x} + V_2 \dfrac{\partial W}{\partial y} = 0 \quad \text{in } \mathbb{R}^2 \\ \\ W(x,0) = W_o(x) \end{cases}$$

where $\vec{V} = (V_1, V_2)$ is a constant given velocity.

A classical explicit second-order two-level time discretization is the following

$$(3.2)\quad \begin{cases} W^{n+1}(x) = W^n(x) - \Delta t(V_1 W_x^n + V_2 W_y^n) \\ \qquad + \dfrac{\Delta t^2}{2} \left[V_1 (V_1 W_x^n + V_2 W_y^n)_x + V_2 (V_1 W_x^n + V_2 W_y^n)_y \right] . \end{cases}$$

Let $\mathcal{H}$ be a set of strictly positive parameters with zero in its closure and let $(\mathcal{C}_h)_{h \in \mathcal{H}}$ be a family of triangulations such that h is the length of the largest segment of $\mathcal{C}_h$. We consider the following spaces

$$H_h = \{ v \in L^2(\mathbb{R}^2) \ ; \ v \text{ is continuous} \ ; \ v \text{ is linear on every triangle T of } \mathcal{C}_h \} \ ;$$

$$V_h = \{v \in H_h \cap H^1(\mathbb{R}^2)\} \quad .$$

Then a Galerkin-type variational P_1 space discretization of (3.2) is

$$(3.3)\begin{cases} W_h^{n+1} \in V_h \ , \text{ and } \forall v \in V_h \\ \iint (W_h^{n+1} - W_h^n) v \, dxdy = \\ \qquad - \Delta t \iint v (V_1 \frac{\partial W_h^n}{\partial x} + V_2 \frac{\partial W_h^n}{\partial y}) \, dxdy \\ \qquad + \frac{\Delta t^2}{2} \iint (V_1 \frac{\partial W_h^n}{\partial x} + V_2 \frac{\partial W_h^n}{\partial y})(V_1 \frac{\partial v}{\partial x} + V_2 \frac{\partial v}{\partial y}) \, dxdy \end{cases}$$

where the sums $\iint$ are taken on $\mathbb{R}^2$.

Since the consistent mass matrix of this discretization is not diagonal, system (3.3) is expensive to solve in a bounded domain (and impossible to solve in this $\mathbb{R}^2$ case). Following, among others, USHIJIMA [21], BABA and TABATA [3], we construct the mass-lumped variant of (3.3) by introducing the following notations (h is fixed) :

- For any vertex A of $\mathcal{C}_h$, the integration zone $\hat{A}$ is defined by dividing the neighbour triangles into six sub-triangles with median lines ; then the integration zone $\hat{A}$ is the union of those sub-triangles which have A as a vertex (Figure 3.1).

- S_o is the approximation space of functions which are constant on each $\hat{A}$:

$$S_o = \{v \in L^2(\mathbb{R}^2),\ v_{|\hat{A}} = \text{const.},\ \forall A \text{ vertex of } \mathcal{C}_h\}$$

- $\mathcal{S}_o$ is the trivial projection from H_h to S_o :

$$(3.4)\quad \begin{cases} \forall v \in H_h\ ,\ \mathcal{S}_o v \in S_o \text{ and} \\ \mathcal{S}_o v_{|\hat{A}} = v(A)\ ,\ \forall A \text{ vertex of } \mathcal{C}_h. \end{cases}$$

Then the mass-lumped variant is

$$(3.5)\quad \begin{cases} W_h^{n+1} \in V_h\ ,\ \text{and } \forall v \in V_h \\ \iint \mathcal{S}_o(W_h^{n+1} - W_h^n)\ \mathcal{S}_o v\ dxdy = \\ \quad - \Delta t \iint v(V_1 \frac{\partial W_h^n}{\partial x} + V_2 \frac{\partial W_h^n}{\partial y})\ dxdy \\ \quad + \frac{\Delta t^2}{2} \iint (V_1 \frac{\partial W_h^n}{\partial x} + V_2 \frac{\partial W_h^n}{\partial y})(V_1 \frac{\partial v}{\partial x} + V_2 \frac{\partial v}{\partial y})\ dxdy\ . \end{cases}$$

From the classical results of Finite Elements Methods, the right-hand side is second order occurate ; because of the mass-lumping, the left-hand side is only first-order accurate, except for very special regular meshes ; see USHIJIMA [21] for a discussion of this point with a parabolic context.

However, for nearly or strictly steady simulations (like transonic ones), the weaker accuracy of the time derivative approximation has less importance.

3.1.2. Stability

Fourier analysis for the scalar case gives, for a regular triangulation

$$\|\vec{V}\| \frac{\Delta t}{\Delta l} \leq 1 \tag{3.6}$$

where Δl is the smallest altitude from a given vertex in a neighbour triangle ("local" Courant condition).

For a non regular triangulation, (3.6) is only a necessary condition ; in [2] we use an energy argument to get a sufficient stability condition.

3.2. Extension to nonlinear systems

The extension to systems is done by a two-step process of RICHTMYER type ; a choice is made between nonlinearly different variants ; boundary conditions will be treated either with boundary integrals, or via a different scheme.

The system to be solved is written as

$$\begin{cases} W_t + F(W)_x + G(W)_y = 0 \\ \\ + \text{ boundary conditions} \end{cases} \tag{3.7}$$

where $W(x,y,t)$ is a vector of $\mathbb{R}^d$.

A natural adaptation of RICHTMYER's method is to consider a P_o (constant by triangle) predictor ; similarly to Section 1, we use a control volume formulation for this LAX-FRIEDRICHS's type first step.

According to LERAT and PEYRET's study [12], it is interesting to introduce the length of the first step as a parameter.

Then the scheme is the following :

Step 1 ; Predictor :

$$(3.8)_1 \begin{cases} \forall T \in \mathcal{C}_h \text{ , and for } k = 1, 2, \dots d \text{ ,} \\ \\ \tilde{W}_k(T) = \dfrac{1}{\text{area}(T)} \left\{ \iint_T W_k^n \, dxdy \right. \\ \\ \qquad \left. - \alpha\Delta t \int_{\partial T} [F_k(W^n) n_x + G_k(W^n) n_y] \, d\sigma \right\} \end{cases}$$

Step 2 ; Corrector :

$$(3.8)_2 \begin{cases} W^{n+1} \in (V_h)^d \text{ , and } \forall \phi \in (V_h)^d \text{ , } \forall k = 1, 2, \dots d \text{ ,} \\ \\ \iint_\Omega \mathcal{G}_o \left[\dfrac{W_k^{n+1} - W_k^n}{\Delta t}\right] \mathcal{G}_o \, \phi_k \, dxdy = \\ \\ \qquad \iint_\Omega^* \{\beta_1 [F_k(W^n) \dfrac{\partial \phi k}{\partial x} + G_k(W^n) \dfrac{\partial \phi k}{\partial y}] \\ \\ \qquad\quad + \beta_2 [F_k(\tilde{W}) \dfrac{\partial \phi k}{\partial x} + G_k(\tilde{W}) \dfrac{\partial \phi k}{\partial y}]\} \, dxdy \\ \\ \qquad - \int_{\partial\Omega}^* \phi_k [F_k(W^n) n_x + G_k(W^n) n_y] \, d\sigma \end{cases}$$

where

$$\beta_2 = \frac{1}{2\alpha} \quad , \quad \beta_1 = \frac{2\alpha-1}{2\alpha}$$

Ω is the domain of integration of (3.7).

According to LERAT and PEYRET's one dimensional study, we chose the optimal length of the first step :

$$\alpha = 1 + \frac{\sqrt{5}}{2} \quad ;$$

some experiments with Burger's equation showed that this choice is advantageous, even for the computation of stationary shocks.

Numerical integration is necessary to compute the nonlinear terms :

- A rough quadrature is possible for the boundary integral in $(3.8)_1$, because it will be multiplied by Δt^2 in the resulting scheme.

- A finer quadrature, exact for P_2 integrands, is used for integrals with stars in $(3.8)_2$.

The last integral of $(3.8)_2$ (boundary fluxes) is not time centered for simplicity ; this is only first-order accurate in time ; actually second-order spatial accuracy is conserved for steady state simulations. A slightly more expensive variant with a boundary predictor and time centered boundary fluxes have been experimented, which brought no noticeable improvements.

At last simplified LAPIDUS type artificial viscosity terms are added for shock resolution, which is a discretization of

$$\chi\{ \frac{\Delta x^2}{2} \frac{\partial}{\partial x} [|\frac{\partial W_k}{\partial x}| \frac{\partial W_k}{\partial x}] + \frac{\Delta y^2}{2} \frac{\partial}{\partial y} [|\frac{\partial W_k}{\partial y}| \frac{\partial W_k}{\partial y}] \}$$

with the classical choice $\chi = 0.8$.

3.3. Numerical Experiments

For transonic simulations, we had to construct inflow and outflow boundary conditions ; several extrapolation procedures have been experimented with failure in the obtention of a steady solution for non regular meshes.

Convergence has been obtained with the use of the following upwind scheme for boundary triangles :

For any triangle T such that one vertex at least is inflow or outflow, fluxes between two vertices i and j are computed as integral along segment CI_{ij} of functions $Fn_x + Gn_y$ (Figure 3.2) where C is the centroid of triangle T and I_{ij} the middle point of segment C_{ij}.

Then two cases are considered for the integration of $Fn_x + Gn_y$:

- First case : neither i nor j is on the inflow or outflow boundary : the flux through CI_{ij} is computed without using the values of dependant variables at the third vertex.

- Second case : vertex i is inflow (resp. outflow) and j is interior (or vise-versa) : if i is inflow, then it is upstream and j is downstream ; if i is outflow, it is downstream and j is upstream ; following LERAT and SIDES [13], fluxes are computed by using upstream values of the entropy deviation S

$$S = (p/p_\infty) \quad (\rho_\infty/\rho)^\gamma - 1 \quad ,$$

the enthalpy

$$H = \frac{\gamma p}{(1-\gamma)\rho} + \frac{1}{2}(u^2+v^2)$$

and the direction of the flow, and using the downstream value of the pressure p.

Summing up, all the four infinity conditions are imposed on inflow and outflow vertices, but only the convenient quantities (three inflow and one outflow) are taken in account by the upwind boundary scheme.

As in Section 1, the steady state simulations which

we present here have been computed with the consistent time integration.

The shock tube problem :

The problem and the triangulation are described in Section 1.3 ; results at time t=0.16 are presented in Figure 3.3.

GAMM channel with circular bump :

Physical conditions are defined in Section 1.3 and the triangulation is the same with 72 × 21 vertices (= degrees of freedom).

The convergence to the stationary solution is slower than the above upwind methods ; typically 7000 time steps (T ~ 40 seconds) were needed to get a root mean square value $\frac{\partial \rho}{\partial t}$ less than 2.10^{-5}.

Now in the results presented some improvements in cpu time have been obtained by using local courant numbers and by forcing the enthalpy $H = \frac{\gamma}{\gamma-1}\frac{p}{\rho} + \frac{1}{2}(u^2+v^2)$ at its value at infinity.

We present in Figure 3.4 to 3.8 the Mach, K_p, and entropy deviation distributions on the bottom, and isomach and isentropic lines.

With an artificial viscosity coefficient equal to 1., some oscillations remain before are after the shock. Results are generally comparable with simulations presented by LERAT and SIDES [13],[13'], and especially with simulations presented by LERAT and SIDES optimal S^{α}_{β} scheme (see LERAT [11], p. 97 Fig. 9b) as could be expected since the scheme presented in this section is quite similar to this latter finite difference scheme.

Flow past a cylinder :

A polar-type mesh is used, the radius of which is 25 chords with 64 intervals in the chordwise direction and 14 intervals in the normal direction. Distribution is presented in Figure 3.9 for the case Mach .45

Flow past a NACA0012

Experiments with a quite coarse mesh are important for an a priori evaluation of the 3-D version of the scheme ; the mesh presented in Figure 3.10 contains 600 points (300 for the half domain) and have been extensively used for full potential runs. Two non lifting for the Richtmyer Galerkin scheme are compared (Figures 3.10-3.15) with the GAMM workshop contributions. Although the Cp curve is not high enough, the shock is well positionned and the leading edge pressure peak is well captured with a maximum Cp of 1.20 for the first result, 1.23 for the second.

For the two cases, we present also the Mach and entropy distribution gust as the isomach and isentropic lines (figures 3.10-3.15 and 3.16-3.19).

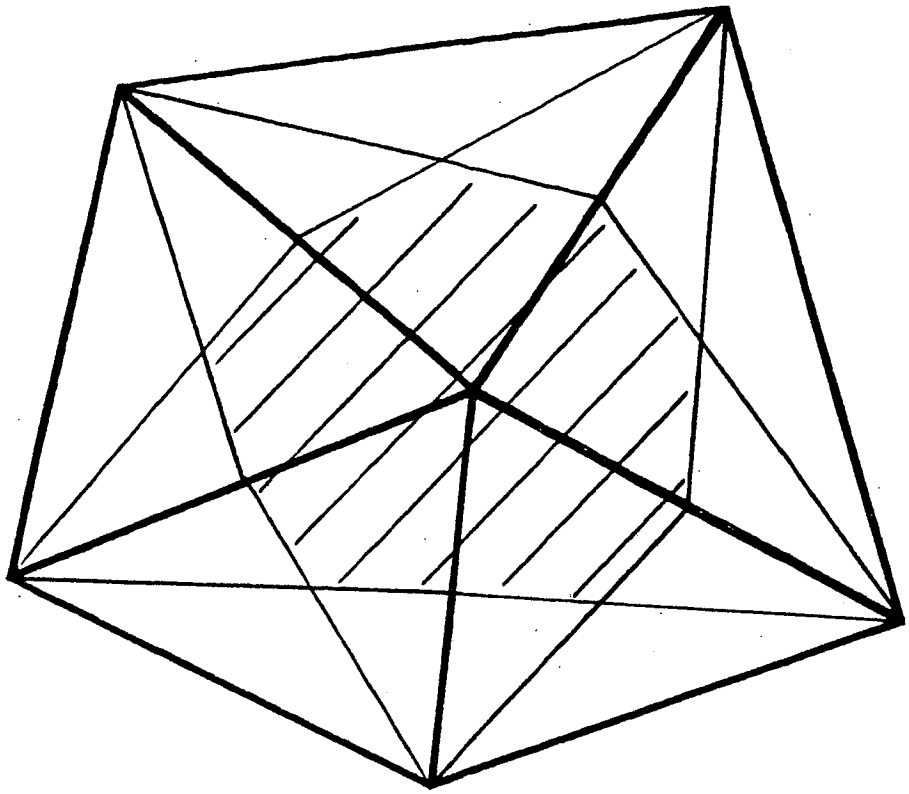

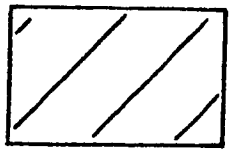

The integration zone $\hat{A}$ of a vertex A

Figure 3.1.

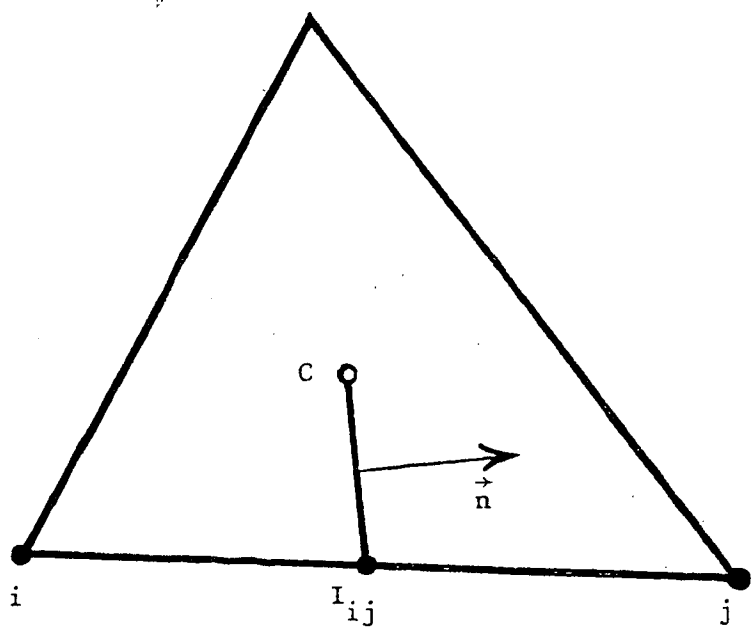

Figure 3.2. : Control volume type flux computation for boundary triangles

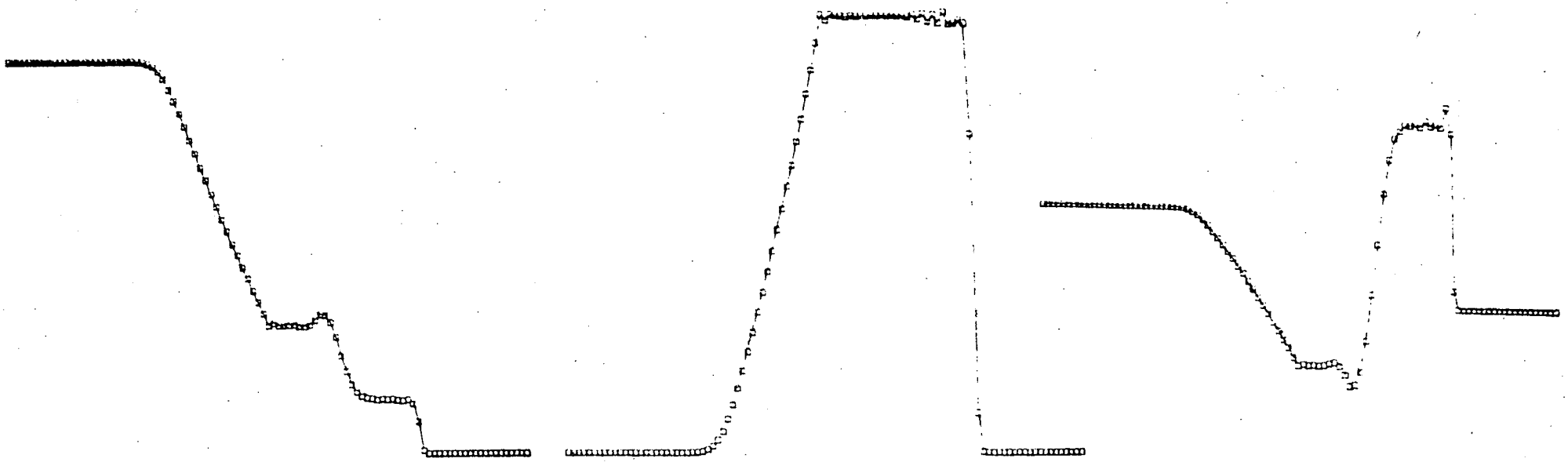

Figure 3.3 : The schock tube test for the 2-D Rychtmyer scheme (time=0.16).

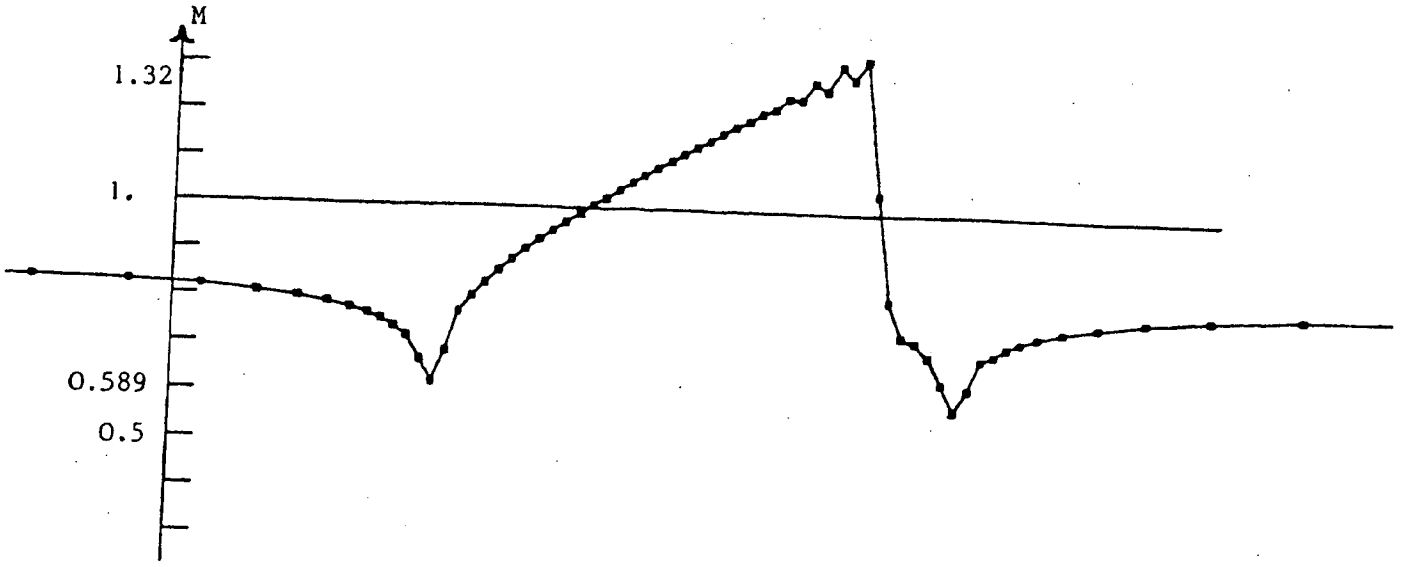

Figure 3.4 : GAMM channel with circular bump ; Mach distribution on the bottom (Richtmyer scheme)

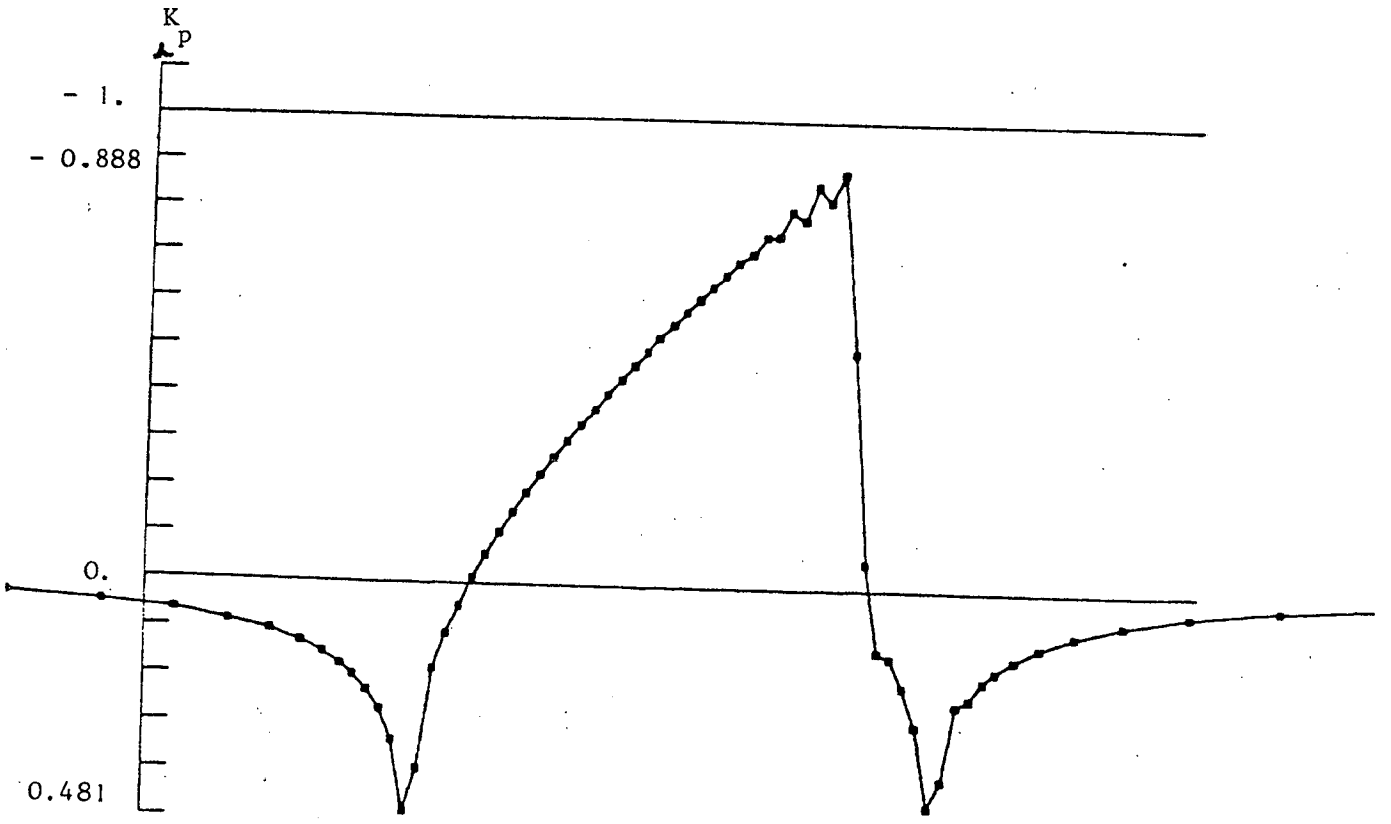

Figure 3.5 : GAMM channel with circular bump ; K_p distribution on the bottom (Richtmyer scheme)

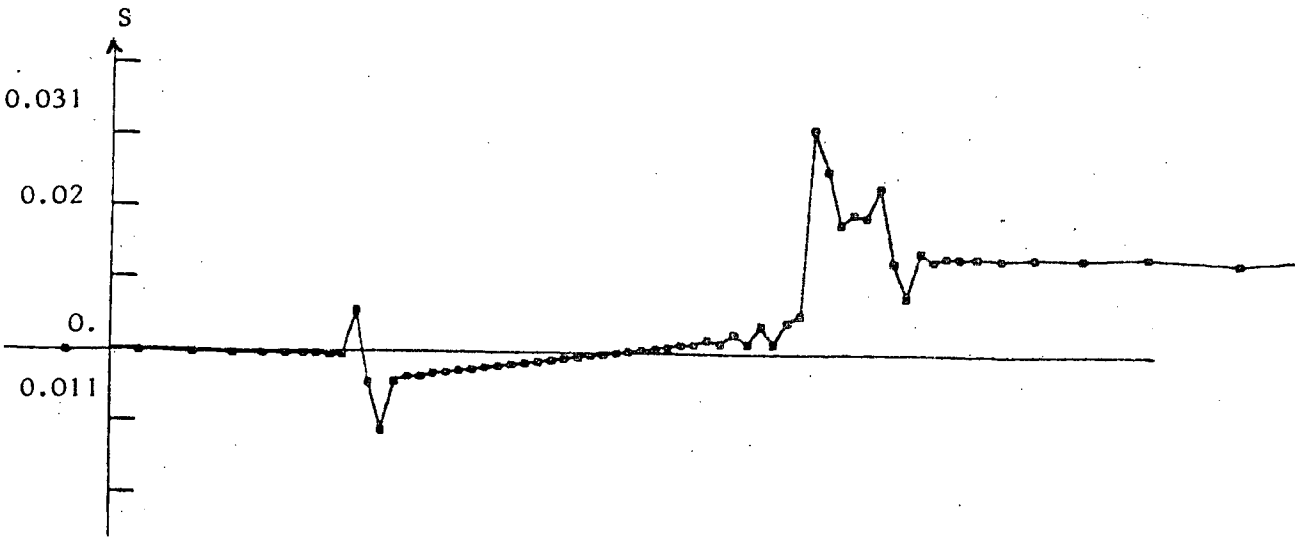

Figure 3.6 : GAMM channel with circular bump ; entropy distribution on the bottom (Richtmyer scheme)

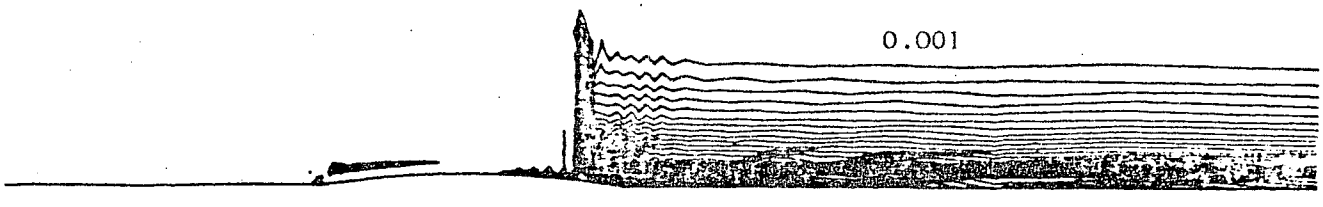

Figure 3.7 : GAMM channel with circular bump ; isentropic lines (increment $\Delta S = 0.001$) (Richtmyer scheme)

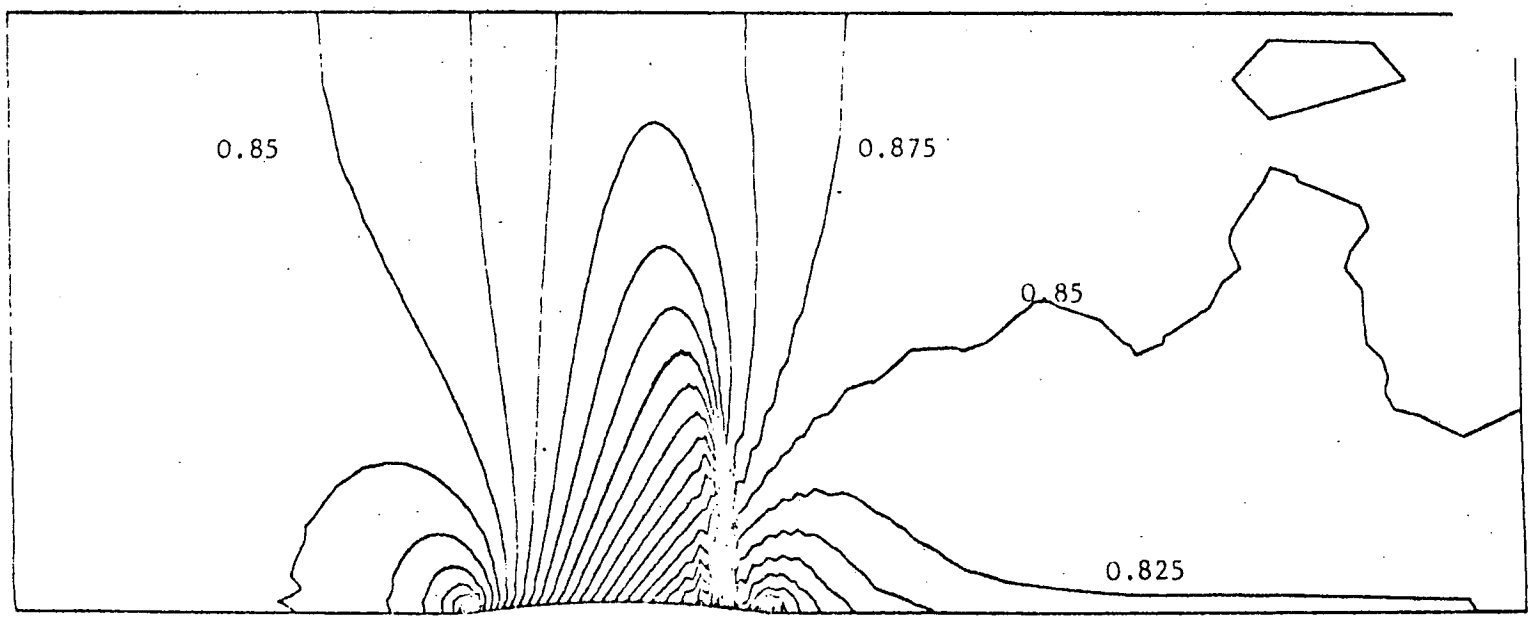

Figure 3.8 : GAMM channel with circular bump, isomach lines (Richtmyer scheme)

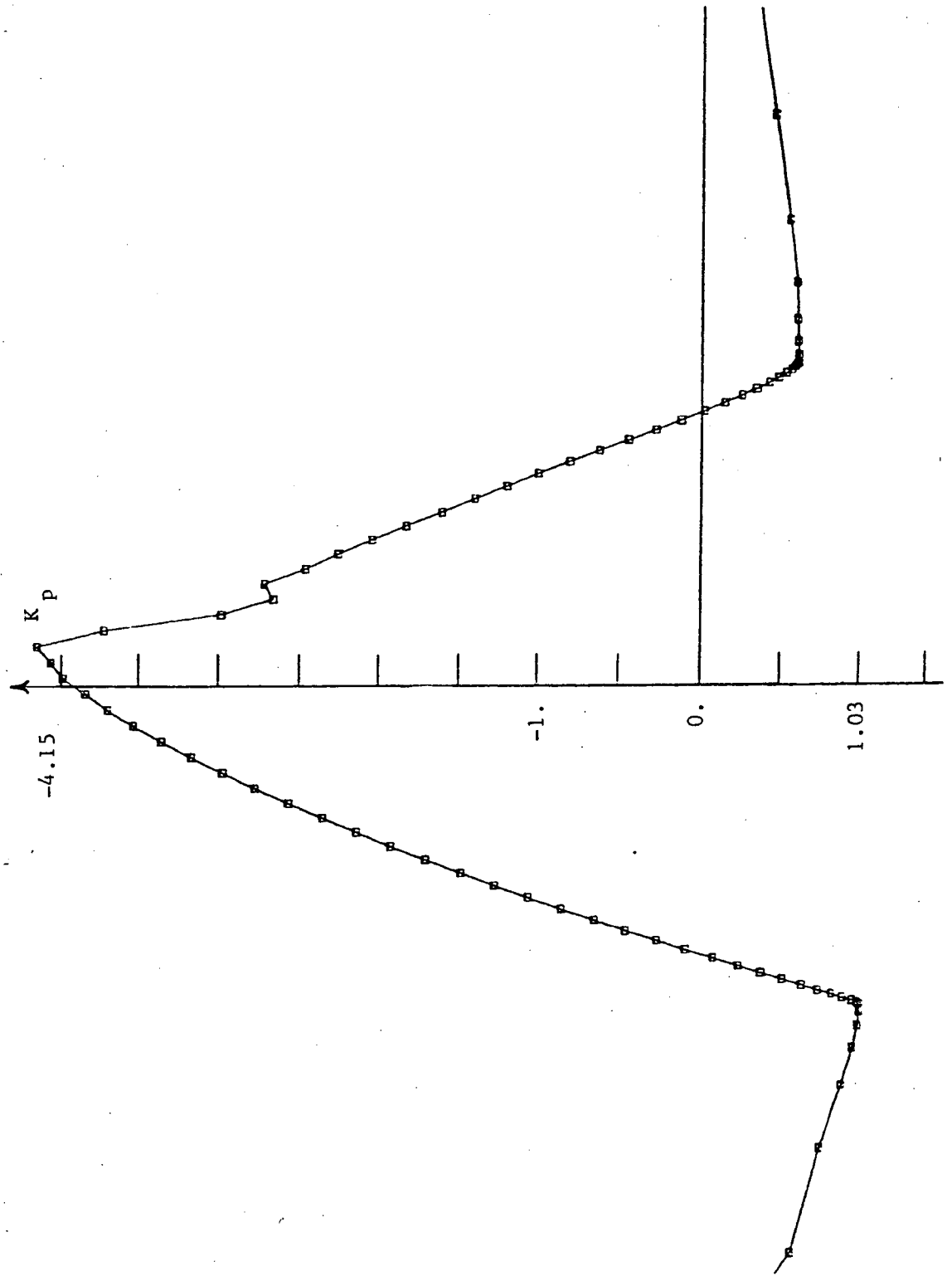

Figure 3.9 : External flow past a cylinder ; K_p distribution on profile and axis

(Richtmyer scheme)

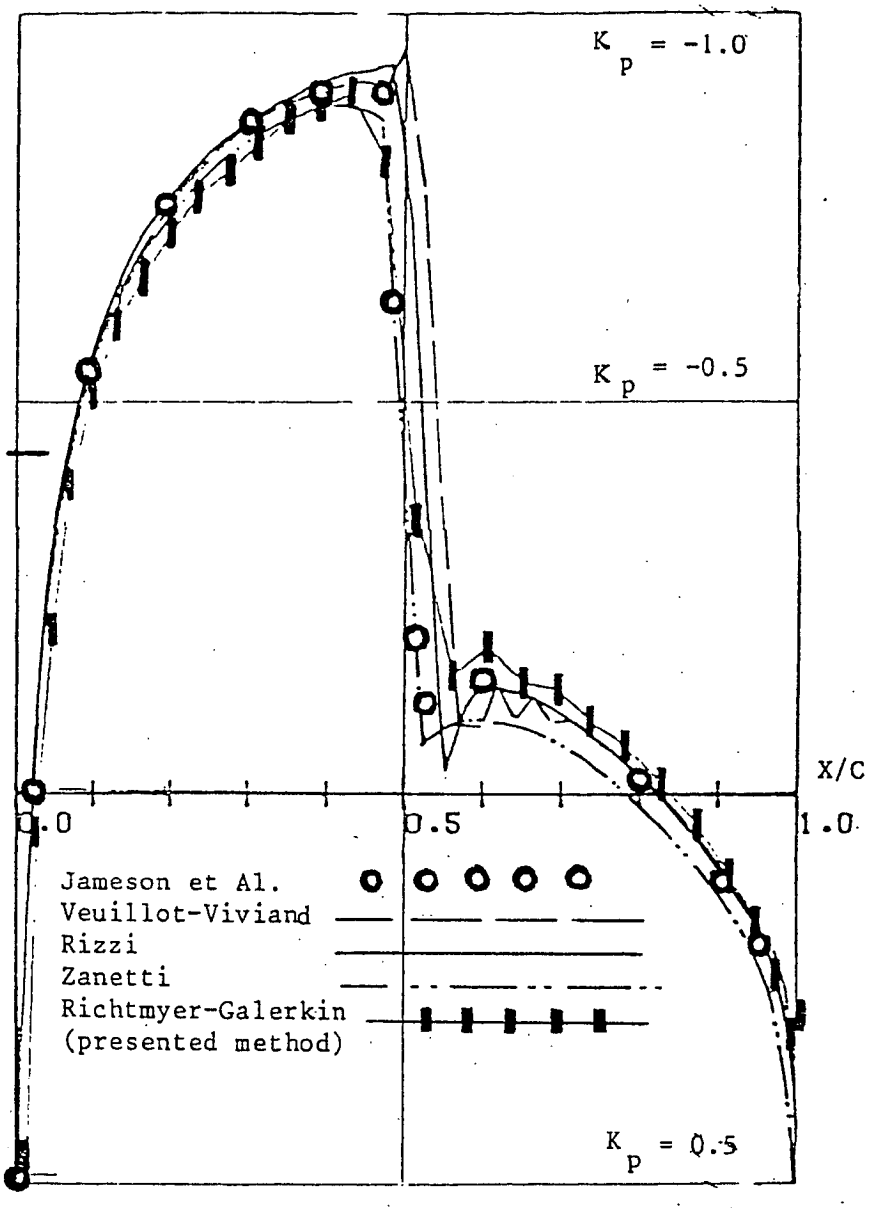

Figure 3.10. : K_p distribution for a flow past a NACA 0012 airfoil, M = 0.80, $\alpha = 0°$; 600 points mesh ; comparison with GAMM workshop Euler contributions [17].

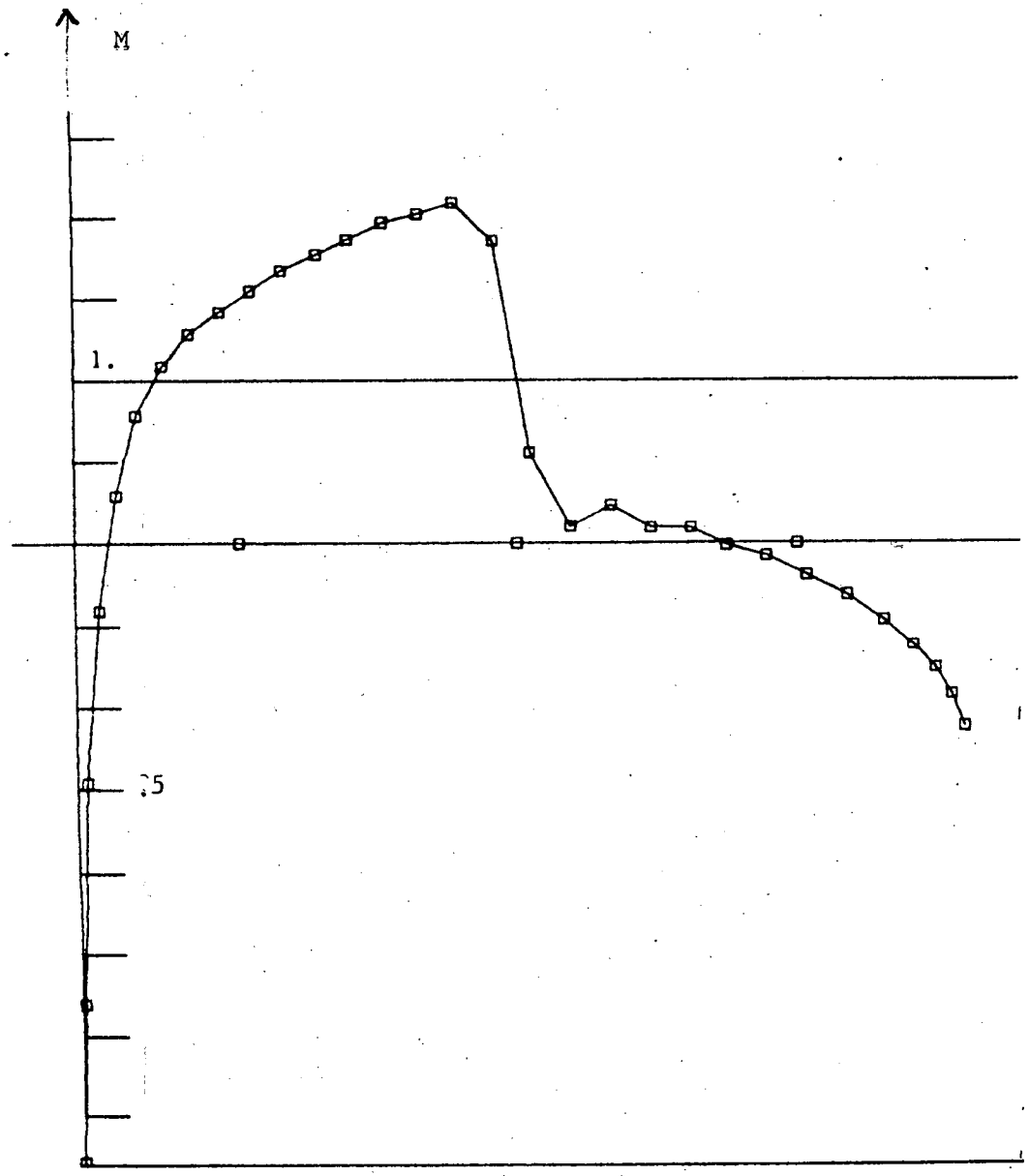

Figure 3.11 : NACA0012 Airfoil M=0.80 α=0°
Mach distribution.

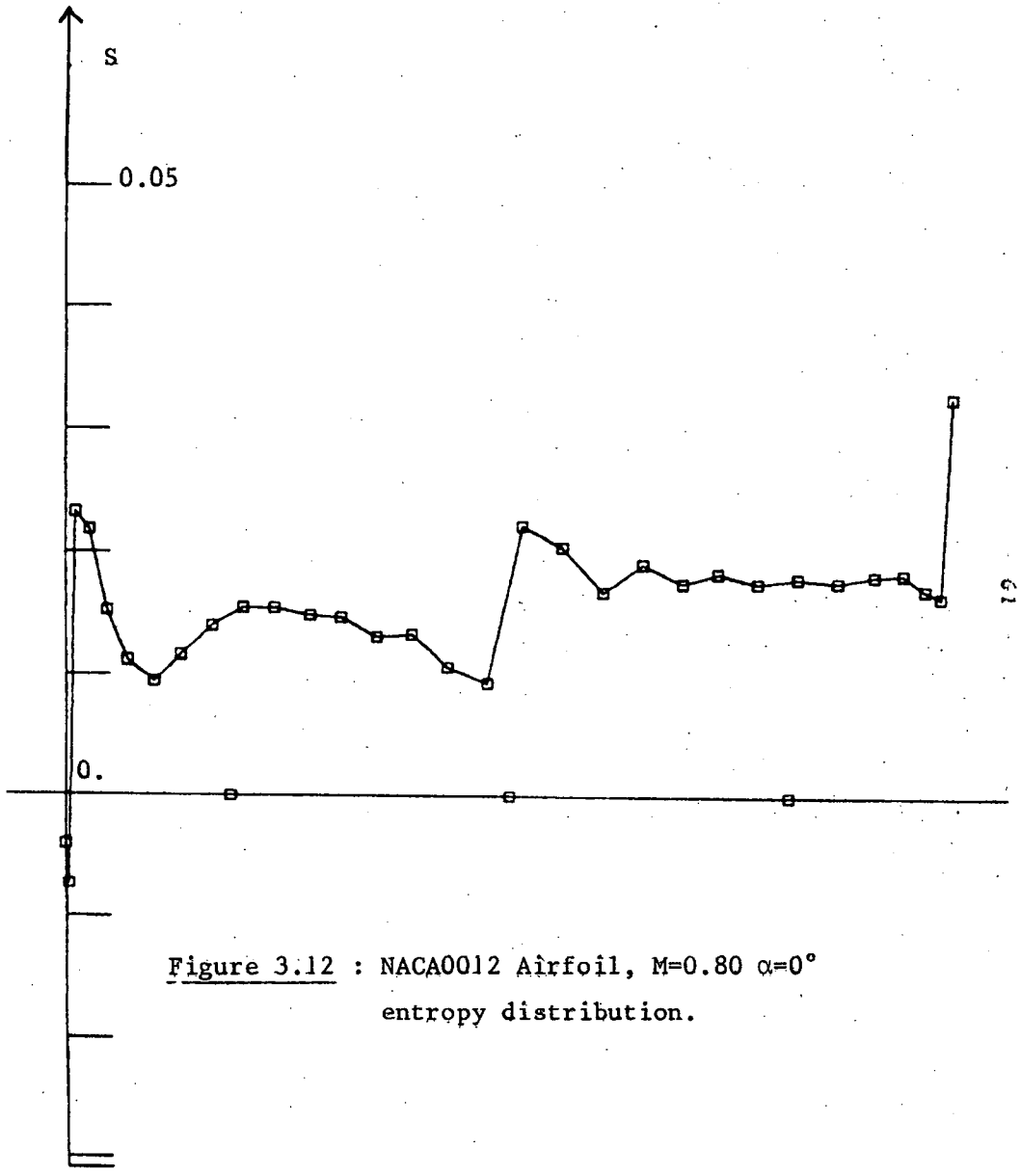

Figure 3.12 : NACA0012 Airfoil, M=0.80 α=0°
entropy distribution.

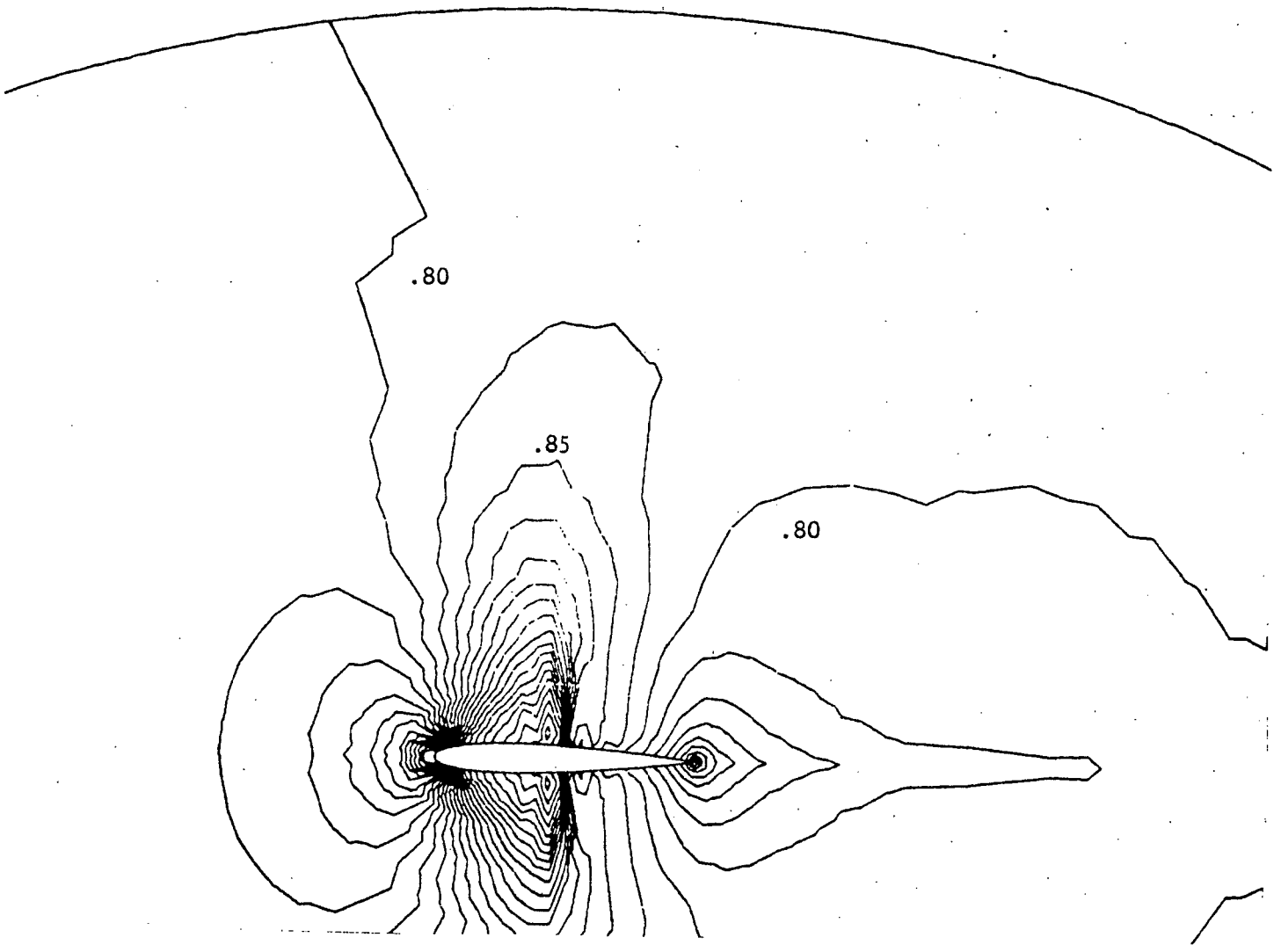

Figure 3.13 : NACA0012 Airfoil, M=0.80, α=0°
isomach lines.

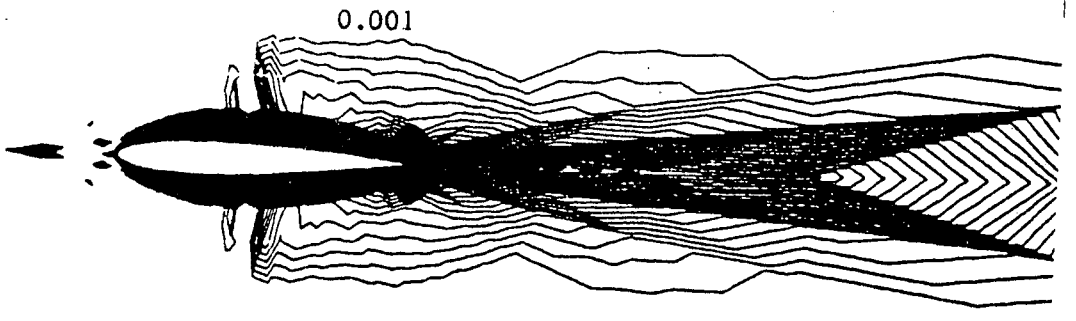

Figure 3.14 : NACA0012 Airfoil, M=0.80 α=0°
isentropic lines.

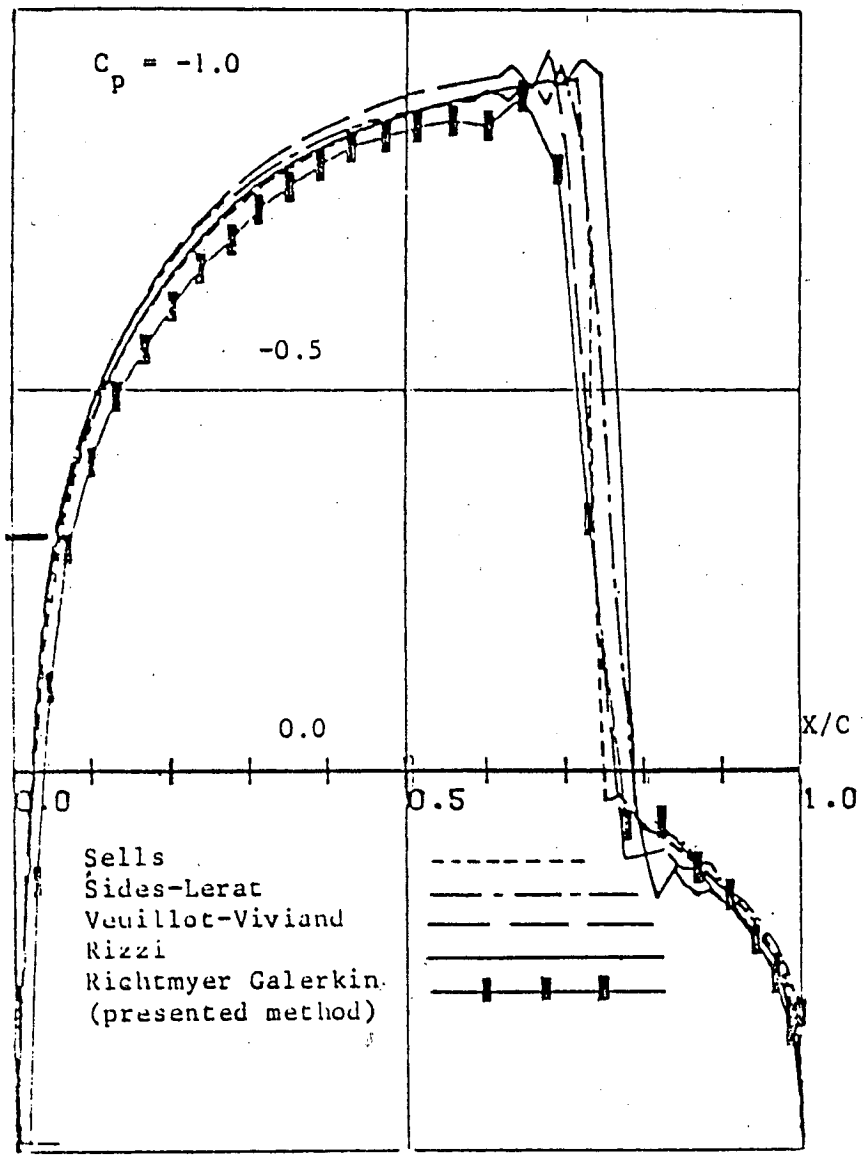

Figure 3.15. : K_p distribution for a flow past a NACA 0012 airfoil, M = 0.85, $\alpha = 0°$; 600 points mesh ; comparison with GAMM workshop Euler contributions [17].

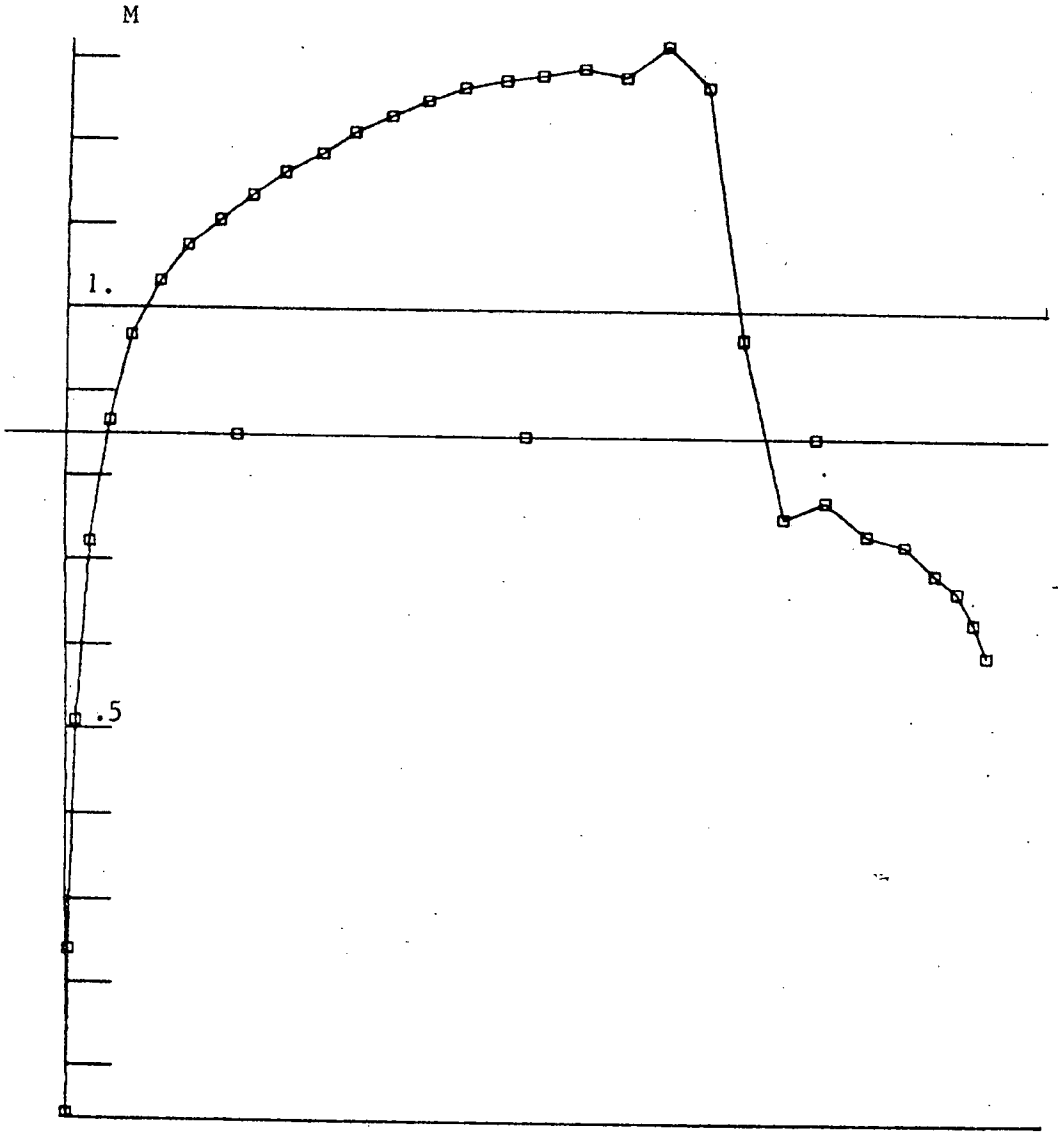

Figure 3.16 : NACA0012 M=0.85 α=0°
mach distribution.

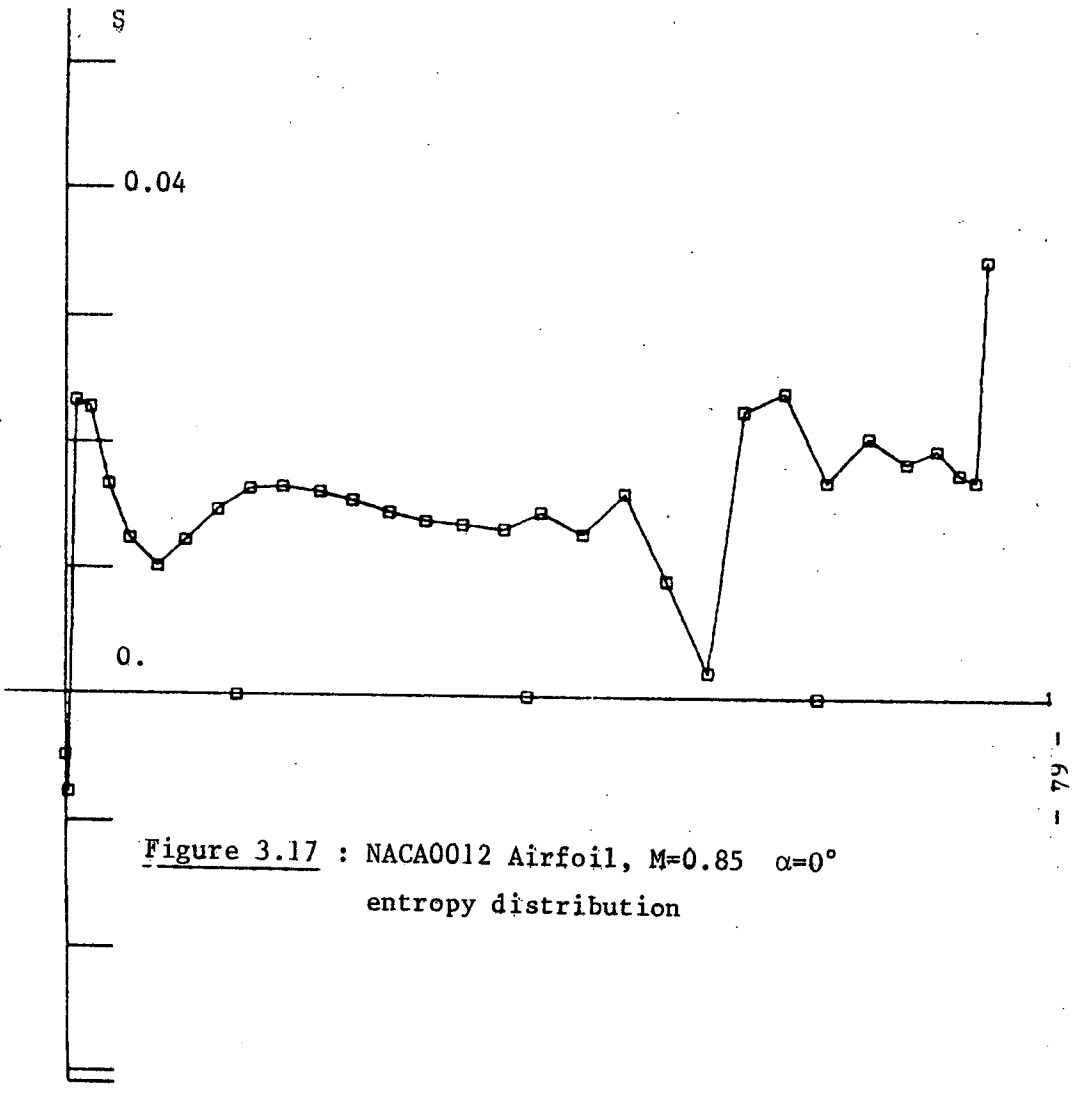

Figure 3.17 : NACA0012 Airfoil, M=0.85 α=0°
entropy distribution

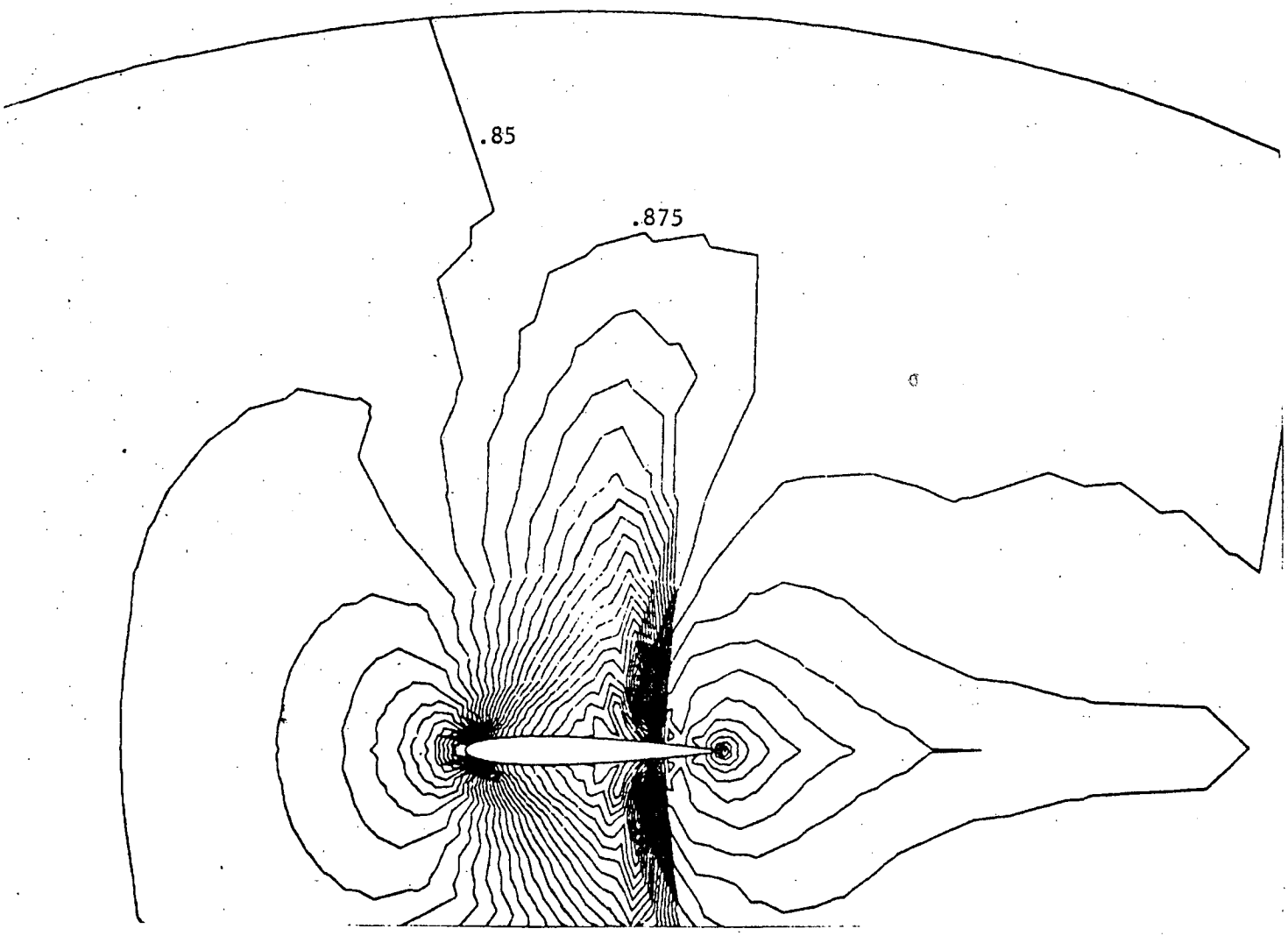

Figure 3.18 : NACA0012 Airfoil, M=0.85 $\alpha=0^{\circ}$
isomach lines.

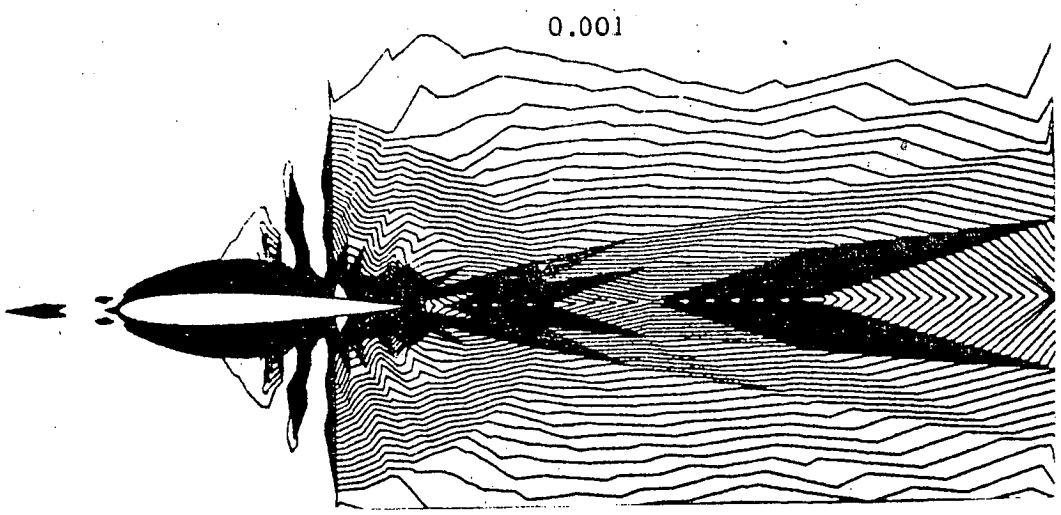

Figure 3.19 : NACA0012 Airfoil M=0.85 $\alpha=0^{\circ}$
isentropic lines.

4. RUNGE-KUTTA SCHEMES

4.1. Spatial variational discretization

The system of conservation laws is defined as in (1.1) and (1.2), and we want to derive a spatial approximation of the system ; if we refer to Friedrichs theory for stationary linear systems (see [8]), it may seem reasonable to look for a W variable in $H^1(\Omega)$ where Ω stands for the geometrical domain ; this is the same option as for the above Richtmyer scheme and, as for this latter scheme, we hope to solve via an artificial viscosity the contradiction between using a nearly continuous space and capturing shocks.

Then the conservative variational form of (1.1) is the following

$$(4.1)\begin{cases} W(t) \in [H^1(\Omega)]^4 \text{ , and } \forall v \in [H^1(\Omega)]^4 \\ \int_\Omega \{\frac{\partial W}{\partial t} v - F(W) \frac{\partial v}{\partial x} - G(W) \frac{\partial v}{\partial y}\} \, dxdy \\ + \int_{\partial\Omega} v[F(W)n_x + G(W)n_y] \, d\sigma = 0 \end{cases}$$

Given a triangulation $\mathcal{T}_h$ of Ω and Lagrangian finite element, we can construct finite dimensional space V_h included in $[H^1(\Omega)]^4$, and approximating (in the usual way) that space ; then the spatial semi-discretization of (4.1) is

$$(4.2)\begin{cases} W_h(t) \in V_h, \text{ and } \forall v \in V_h \\ \int_\Omega^* \{\frac{\partial W_h}{\partial t} v - F(W_h) \frac{\partial v}{\partial x} - G(W_h) \frac{\partial v}{\partial y}\} dxdy \\ + \int_{\partial\Omega}^* v[F(W_h)n_x + G(W_h)n_y] \, d\sigma = 0 \, . \end{cases}$$

where the $*$ denotes numerical integration and some boundary procedure.

4.2. Boundary conditions

Boundary conditions are plugged via the boundary integral $\int_{\partial\Omega}^{*}$ of (4.2) for the wall and profile conditions as well as for the conditions at infinity (instead of the upwinded control volume scheme used in the Richtmyer scheme).

For the integrals at infinity, values of W_h are replaced at each integration point by a value obtained from a choice of infinity and interior quantities in accordance to table 1, which gives a discretization of the conditions in Section 3.3 ; this discretization introduces no diffusion : no upwinding is used, neither extrapolation since with Lagrangean finite elements, the dependant variables are defined along the boundaries.

quantities / boundary	Entropy	Enthalpy	Velocity direction	pressure
inflow	infinity	infinity	infinity	interior
outflow	interior	interior	interior	infinity

TABLE 1 : Conditions at infinity

4.3. Time stepping

Let us denote by

(N_i) the canonical (local) basis of V_h

M a (consistent or not) mass matrix

$$M_{ij} = \int_{\Omega}^{*} N_i N_j \, dxdy$$

standing for the (exact or reduced) time derivative

Q the other (nonlinear) terms in (4.2) :

$$Q_j(W_h) = -\int_\Omega^* \{F(W_h)\frac{\partial N_j}{\partial x} + G(W_h)\frac{\partial N_j}{\partial y}\}\,dxdy + \int_{\partial\Omega}^* N_j\,[F(W_h)n_x + G(W_h)n_y]\,d\sigma$$

Then the system of ordinary differential equations is rewritten as follows :

$$\frac{\partial}{\partial t} M W_h + Q W_h = 0$$

or

$$\frac{\partial W_h}{\partial t} + P W_h = 0, \quad \text{with } P = M^{-1}Q \tag{4.3}$$

We follow SCHMIDT, JAMESON [18] and use the classical fourth order Runge-Kutta scheme

$$W^{(0)} = W_h(t^m) \; ; \quad \Delta t = t^{m+1} - t^m$$

$$\left\{\begin{array}{l}
\underline{\text{Step 1.}} \\
\qquad W^{(1)} = W^{(0)} - \frac{\Delta t}{2} P W^{(0)} \\
\underline{\text{Step 2.}} \\
\qquad W^{(2)} = W^{(0)} - \frac{\Delta t}{2} P W^{(1)} \\
\underline{\text{Step 3.}} \\
\qquad W^{(3)} = W^{(0)} - \Delta t\, P W^{(2)} \\
\qquad W^{(1)} = \frac{1}{3} W^{(1)} + \frac{2}{3} W^{(2)} + \frac{1}{6} W^{(3)} - \frac{1}{3} W^{(0)} \\
\underline{\text{Step 4.}} \\
\qquad W^{(2)} = W^{(3)} - \Delta t\, P W^{(3)} \\
\qquad W^{(2)} = \frac{1}{6} W^{(2)} + W^{(1)} \\
\qquad W(t^{m+1}) = W^{(2)}
\end{array}\right. \tag{4.4}$$

For the stability of such schemes, see for example [20] ; a typical Courant maximum number for this kind of problem is $2\sqrt{2}$ for centered second order discretization.

For simplicity a separate time step is used to introduce the same Lapidus-type numerical viscosity than for the Lax Wendroff scheme (see section 3.2).

4.4. Linear Elements

The V_h space is defined as in Section 3.1.1.

4.4.1. Specific implementation choices

Because we are mainly looking for stationary solutions, the same mass-lumping than Section 3 is used.

The quadrature formulas for the nonlinear flux are also identical to those of Section 3 (exact integration for quadratic integrands).

4.4.2. Shock tube simulation

With the same conditions as for the above schemes (except CFL = $0.9 \times 2\sqrt{2}$) we see (Fig. 4.1) that the present Runge-Kutta + FEM scheme is not as accurate (oscillations) as some of the above schemes (see the Richtmyer result, Fig. 3.3), for unsteady Euler simulations with shocks.

4.4.3. GAMM Channel with bump

The convergence towards the stationary solution have been clearly obtained only with a coarse mesh. Such a difficulty have been noted by SCHMIDT and JAMESON [18] for a finite volume approximation ; the solution proposed by these authors is the use of a fourth order dissipation ; we have not yet tested this viscosity which is quite expensive with finite elements.

The coarser mesh used is a 23×7 vertices one (264 triangles) ; see Fig. 4.2. The results obtained are presented in Fig. 4.3 to 4.6. In figure 4.7 the K_p distribution is compared with the Richtmyer result (same coarser mesh) and with LERAT and SIDES' curve (obtained with the finer GAMM mesh).

4.5. Quadratic elements

We considered only straight elements.

Space V_h is defined by

$$V_h = \{v \in H^1(\Omega),\ v \text{ is continuous and } \forall T \in \mathcal{T}_h\ v_{|T} \in P_2\}$$

where P_2 is the polynomial space generated by $[1,x,y,x^2,y^2,xy]$.
Degrees of freedom are values on vertices and at middle of sides.

4.5.1. Specific implementation choice

The interior (2 dimensional) quadrature formula for the nonlinear term is the classical one, defined with the six degrees of freedom (vertices and mid-side), exact for products of polynomial of degree less or equal to two.
The boundary quadrature formula is the usual one dimensional three points Gauss formula, exact for polynomial of degree less or equal to five.

Let us discuss now the choice of the mass matrix : two possibilities have been explored :

- The consistent mass matrix, which is factored once for all times.
- The above P_1 diagonal mass matrix : time consistency is lost ; the unsteady solution if highly oscillating and time steps have to be reduced (empirically 0.4. CFL).

Let us describe the numerical viscosity that we used : we chose exactly the same P_1 discretized artificial viscosity than for the P_1 versions (Sections 3.2 and 4.4) ; our motivations in that choice are the following :

- we consider this viscosity as a Schuman-type filter, and consistency with a continuous model is moderately important as far as some fundamental properties (conservation, accuracy...) are available ; this artificial device does not need to be discretized with accuracy (viz. using quadratic approximation) since the main error comes from using this device and not from the roughness of its approximation.

- our main interest is to compare the P_1 and P_2 (linear and quadratic) approximations of the hyperbolic part so it is convenient to use the same filter.

One disadvantage is that this filter introduces a limitation to second order accuracy.

Some comments about the triangulations : significant comparisons can be done between linear and quadratic elements only if the same number of points at the same places are used for the comparison.

4.5.2. Shock tube simulation

We use a 2-D code like in the above experiments, but now, the 101 × 3 mesh contains only one range of 50 triangles (instead of two ranges of 100 = 200 triangles for the P_1 counterpart) and all the diagonals between the triangles are parallel, (see Fig. 4.14) so that the discretization is strongly dependant of the y-direction (while symmetry between {y=0} and {y=1} was available for the P_1 discretizations). To show the consequences for the results, we present on the

same Figure 4.9 the {y=0} and {y=1} distributions ([1])

We must emphasize that the adjustment of the filter seemed more difficult than with linear approximations and the parameter used was $\chi = 2.$, i.e. more than twice the usual one in the above sections. In despite of this, we think that we got in a manner the best result of the present paper for this test, with only four points ([2]) in the contact discontinuity. One conclusion is that, with a fine enough mesh and for the nonstationary case, shock and especially contact discontinuities may be better resolved with higher order finite elements.

4.5.3. GAMM Channel with bump

The coarser mesh (23 × 7 points) is used, which gives now only 66 triangles. Because straight (not curved) elements are used, the bump is not well approximated, and singularities are introduced by the angles of the boundary, and interact with the approximation, generating oscillations. With this coarse mesh, the influence of the artificial viscosity is important and we chose the usual coefficient : $\chi = 0.8$.

The consistant mass matrix version has been used for those cases ; same results, with about the same cost are obtained with the diagonal mass matrix version, the convergence of which is more delicate (so that this version is only memory saving).

([1]) The consistent mass matrix version is used since the diagonal mass matrix one is not time-consistent.

([2]) For each {y=0} and {y=1} distribution.

For efficiency, the derivatives of the basis functions were computed once for all and in this condition, the ratio of C.P.U. cost between 1 iteration of the linear code and 1 iteration of the quadratic one was for those experiments of about .3 (convergence speeds were similar).

For the above transonic test case (Figure 4.9), no noticeable improvement has been observed. A subsonic case (presented in Figures 4.10, 4.11, to be compared with the P_1 runs in Figures 4.12, 4.13) shows that the bad fitting of the profile induce a spurious separation after the leading edge ; however the entropy distribution shows some advantage for the P_2 approximation.

We can also explain these quite disapointing results as follows : The linear approximations are already quite accurate, except near singularities (viz. shock and stagnation points), which are not well captured. These loss of accuracy are due to the fact that the artificial viscosity produces the main part of the error and so is too large. Now the viscosity is also clearly not enough, especially for the quadratic approximation.

Our first conclusion is that an efficient filter remains to be found. But this very short study is of course not enough to dissuade from the use of these higher order elements ; in particular if would be interesting to have an further evaluation with curved elements on a nonsingular test case.

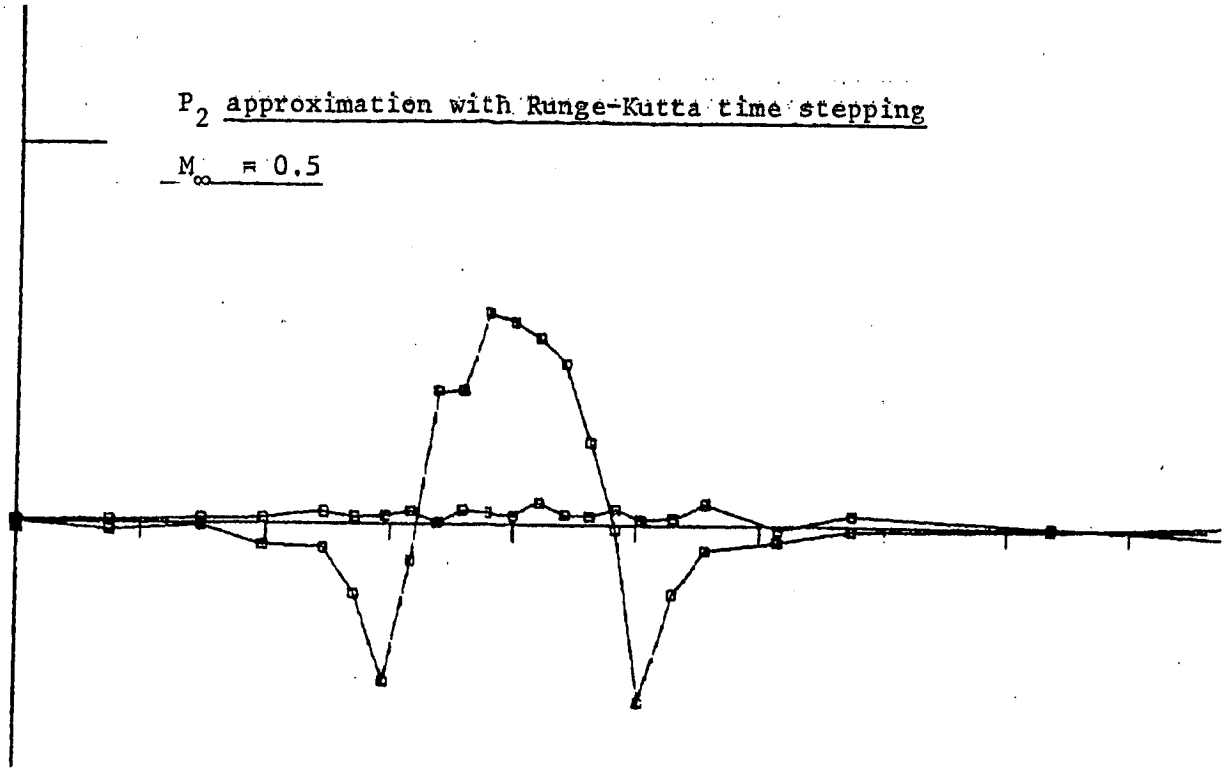

Figure 4.10. C_p distribution

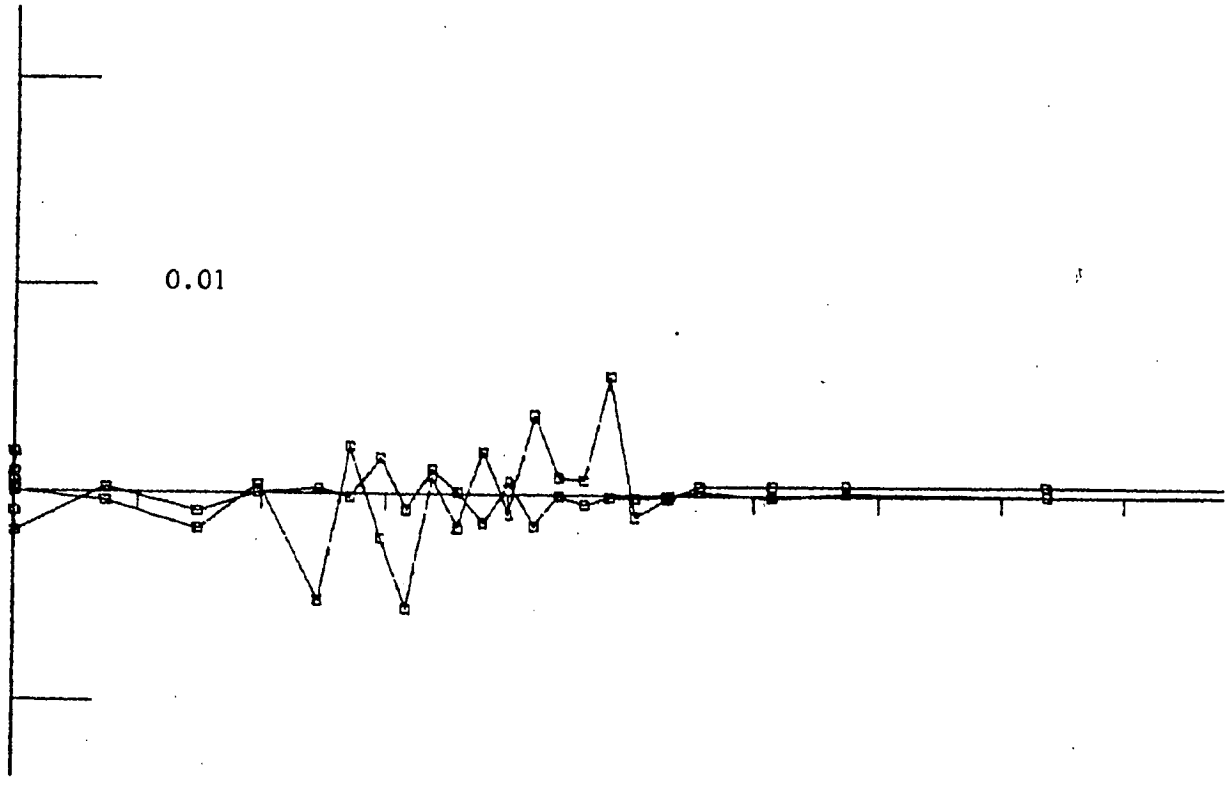

Figure 4.11. Entropy deviation

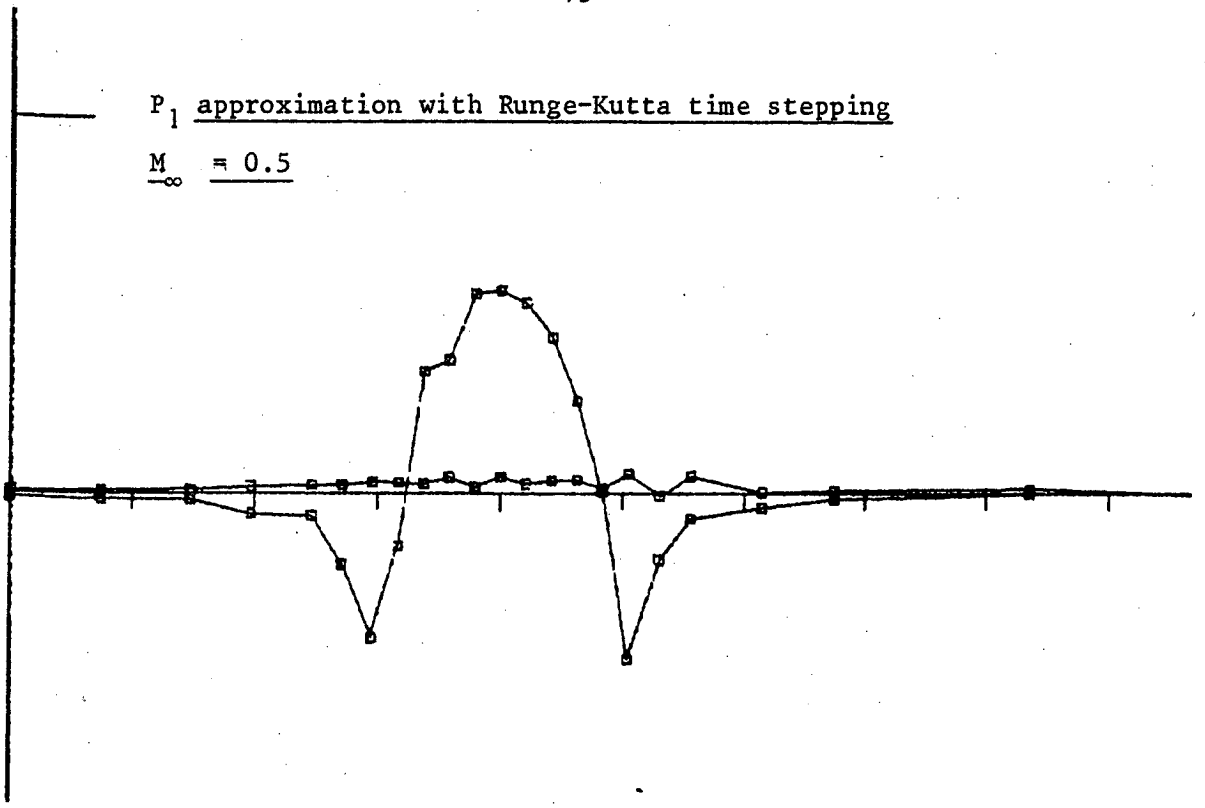

Figure 4.12. C_p distribution

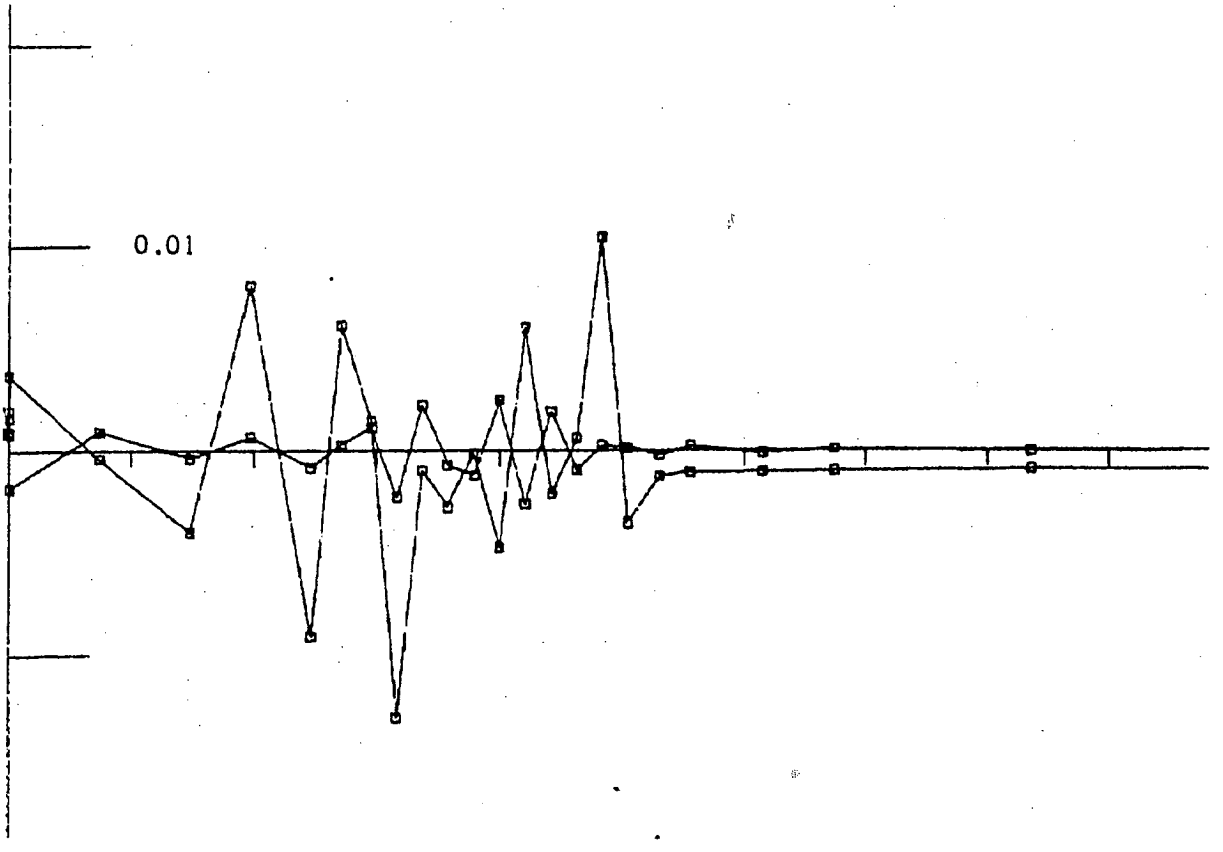

Figure 4.13. Entropy deviation

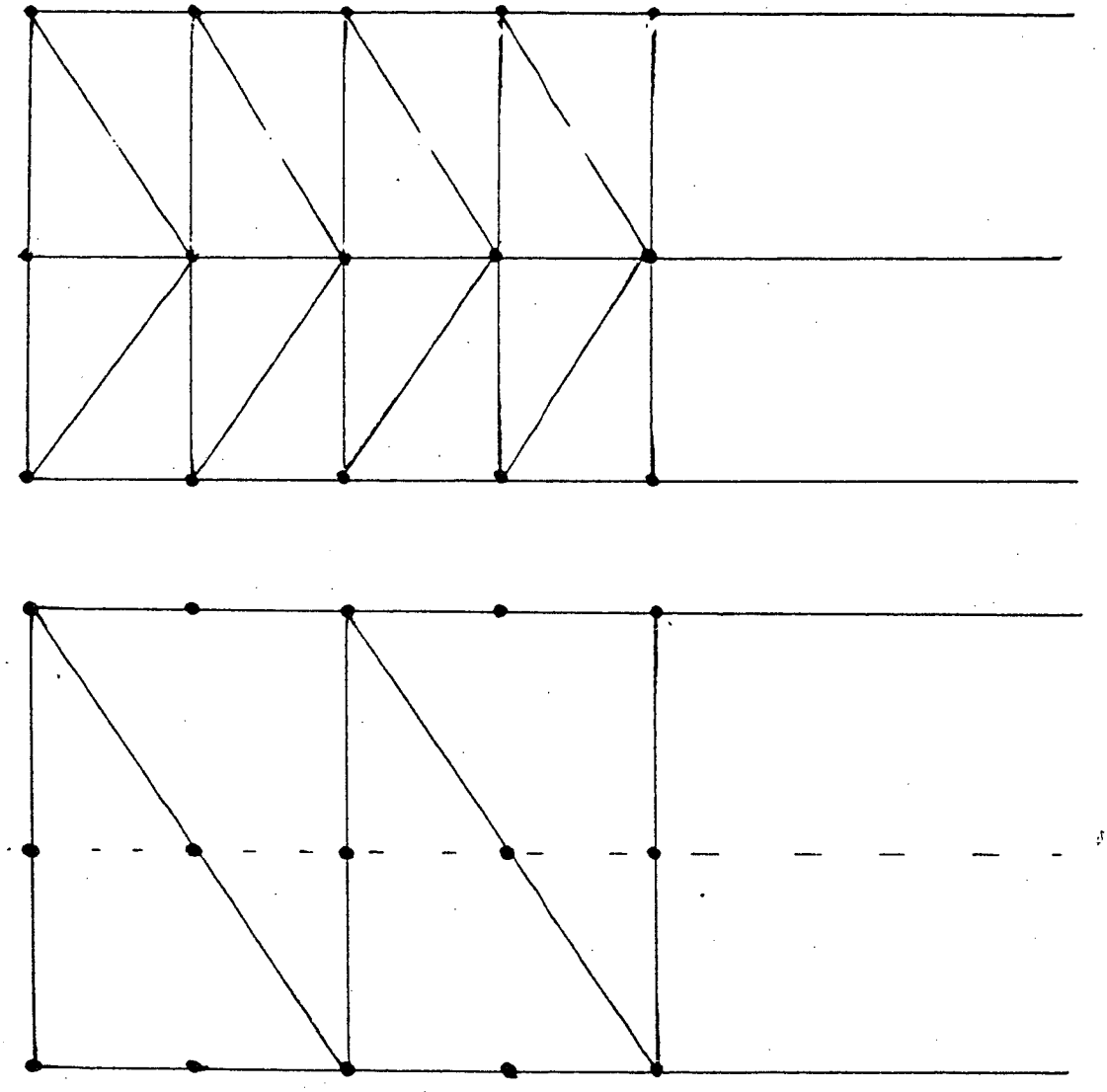

Figure 4.14. : P_1/P_2 comparison for the shock tube test :

(a) P_1 (101 × 3) triangulation (200 triangles)

(b) P_2 (101 × 3) triangulation (50 triangles).

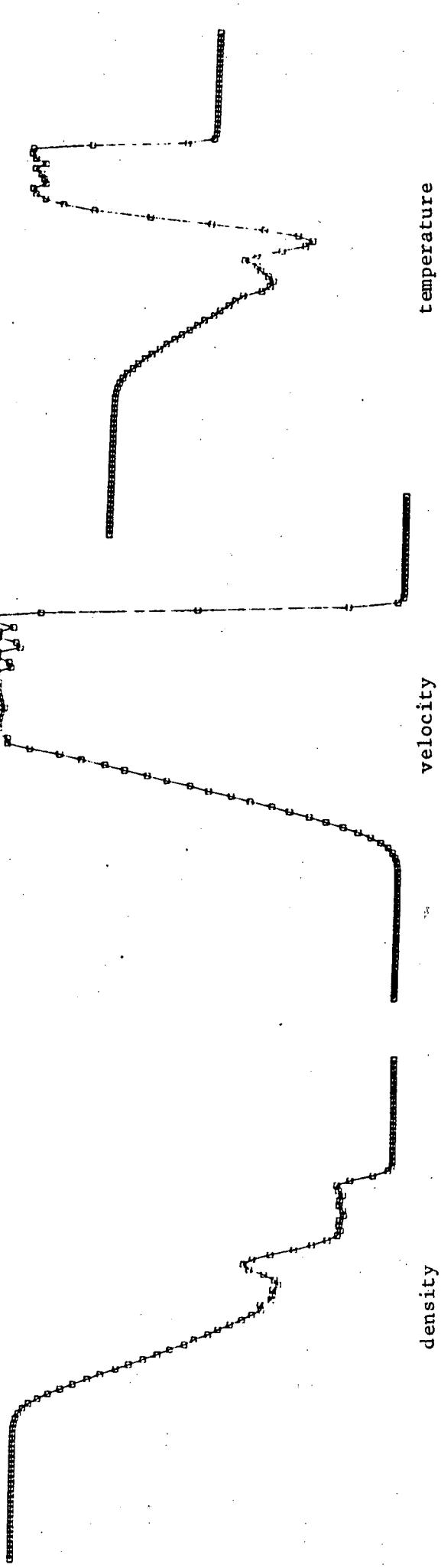

Figure 4.1. : The shock tube test for the 2-D Runge-Kutta P_1 scheme with mass lumping.

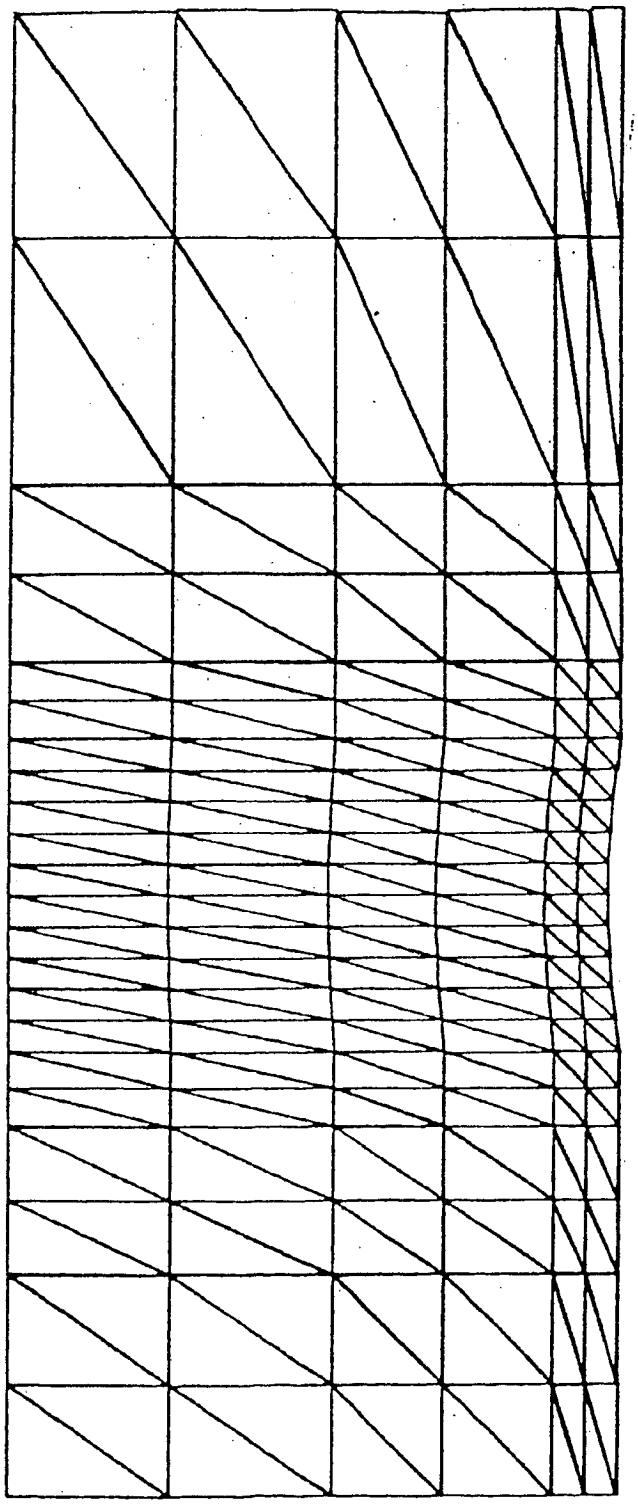

Figure 4.2. : Coarser triangulation around the GAMM channel with circular bump.

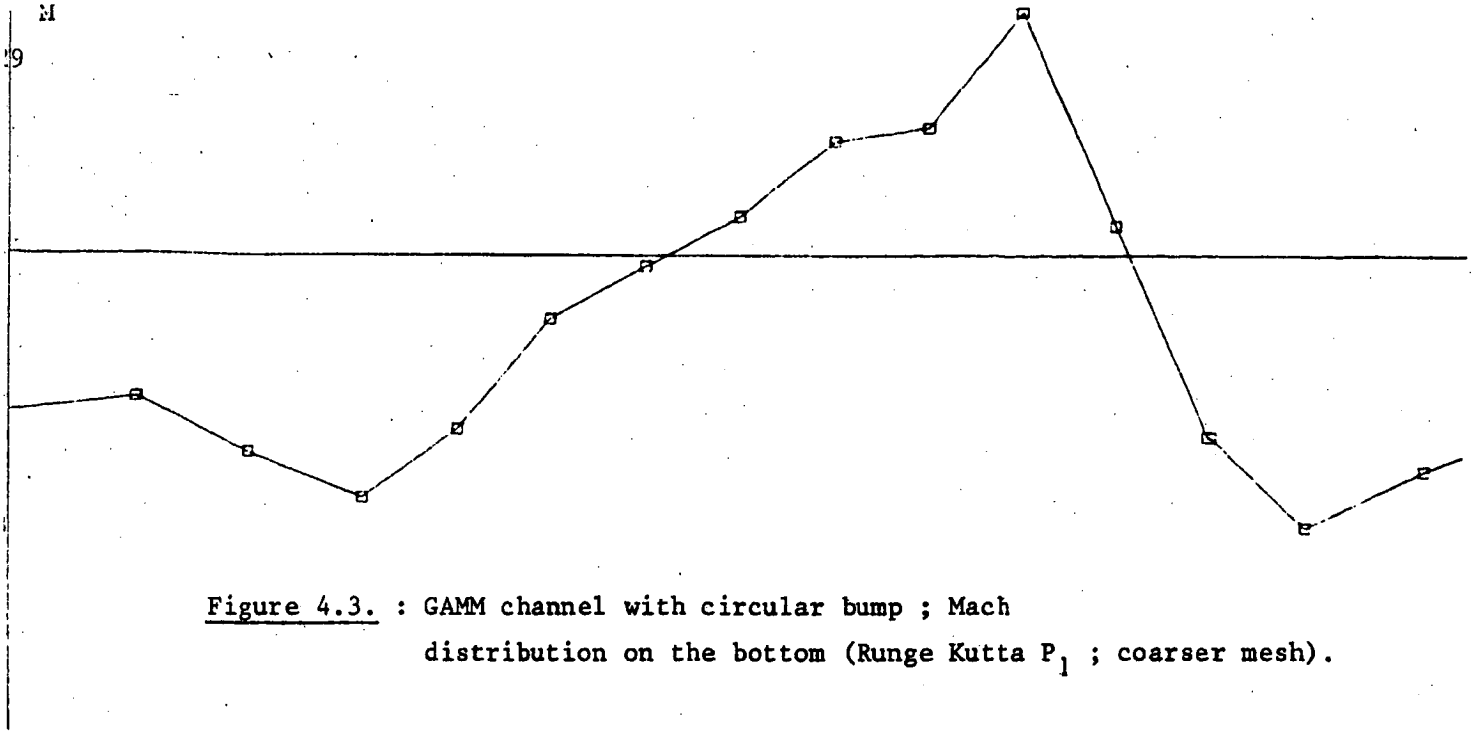

Figure 4.3. : GAMM channel with circular bump ; Mach distribution on the bottom (Runge Kutta P_1 ; coarser mesh).

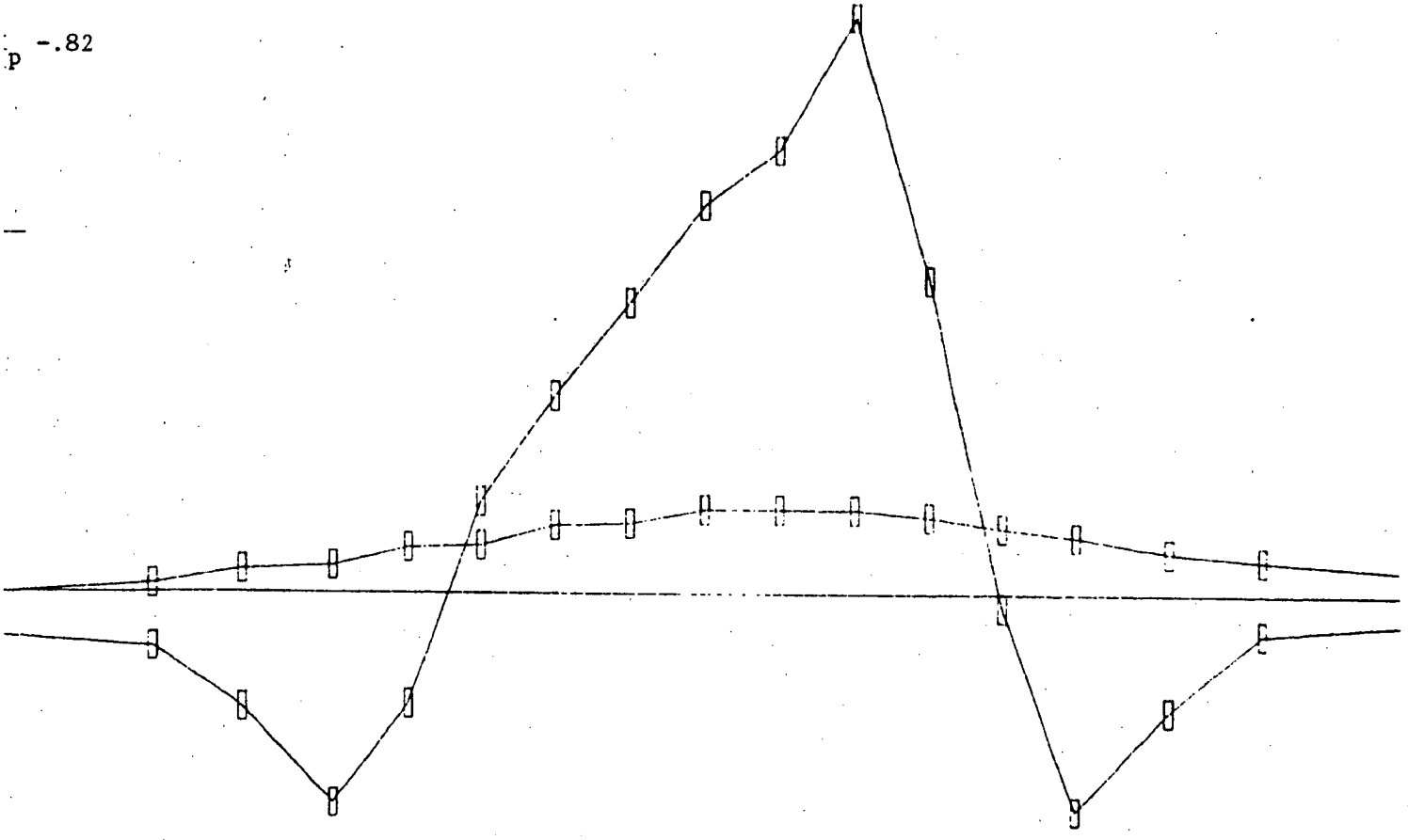

Figure 4.4. : GAMM channel with circular bump ; K_p distribution on the bottom (Runge Kutta P_1 ; coarser mesh).

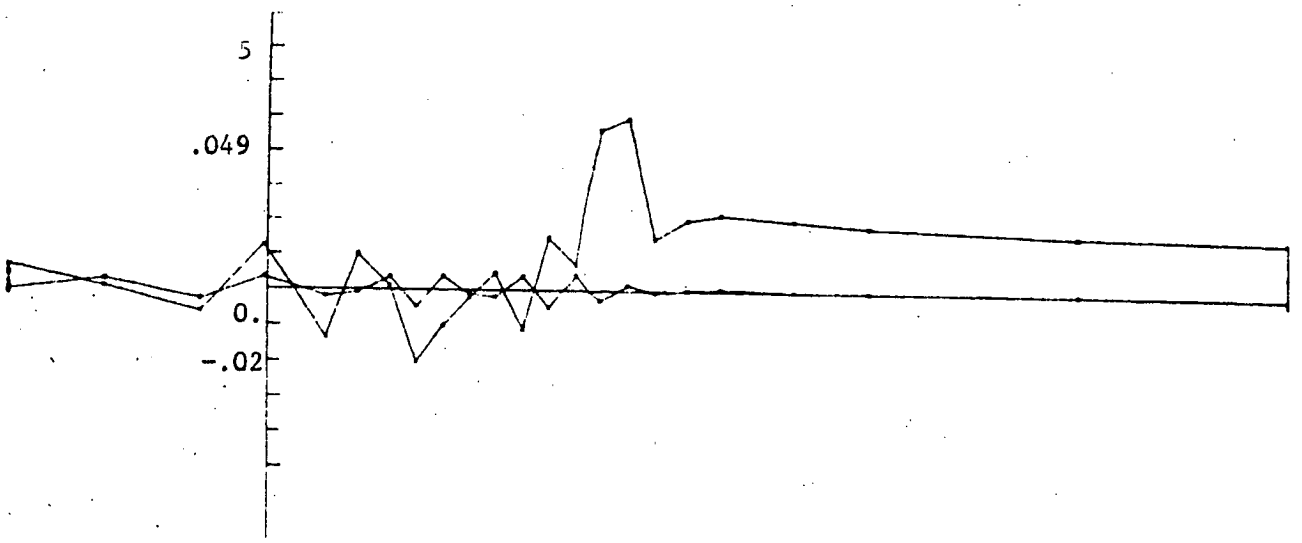

Figure 4.5. : GAMM channel with circular bump ; entropy distribution on the bottom (Runge Kutta P_1, coarser mesh).

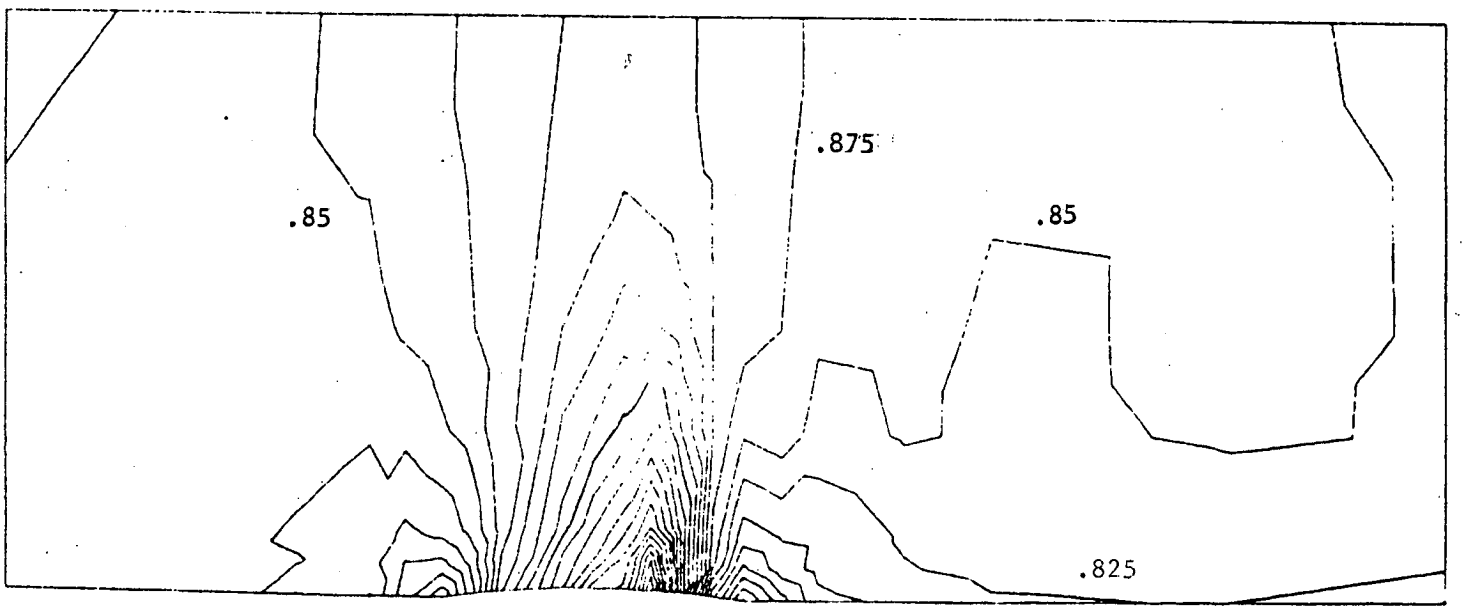

Figure 4.6. : GAMM channel with circular bump ; isomach lines (Runge Kutta P_1, coarser mesh).

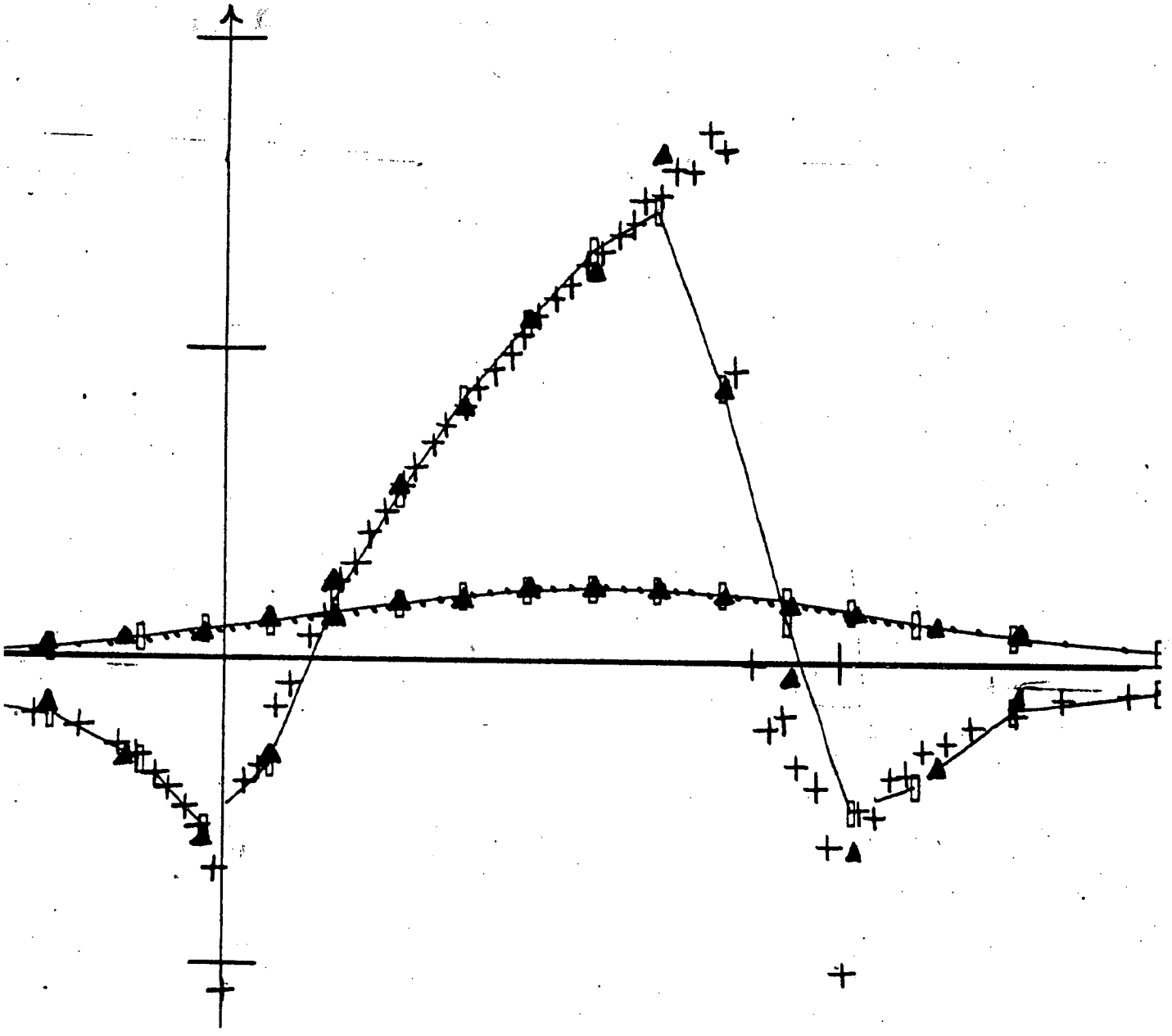

Figure 4.7. : K_p distribution for a flow past a circular bump ; comparisons with LERAT-SIDES [13] scheme and with Richtmyer scheme (section 3).

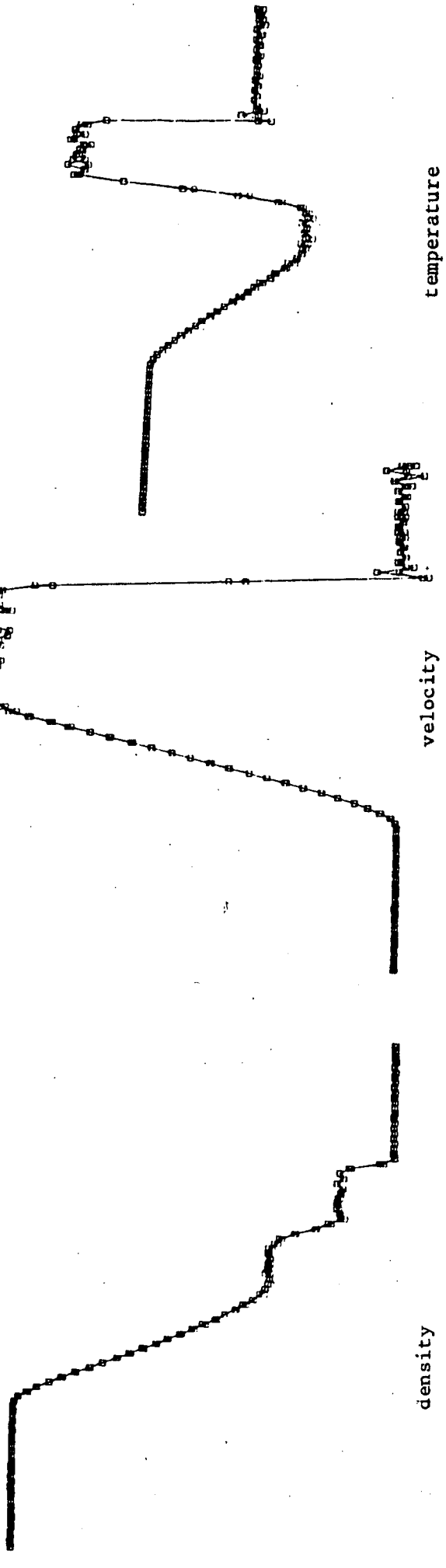

Figure 4.8. : The shock tube test for the 2-D Runge-Kutta P_2 scheme with a consistent mass matrix.

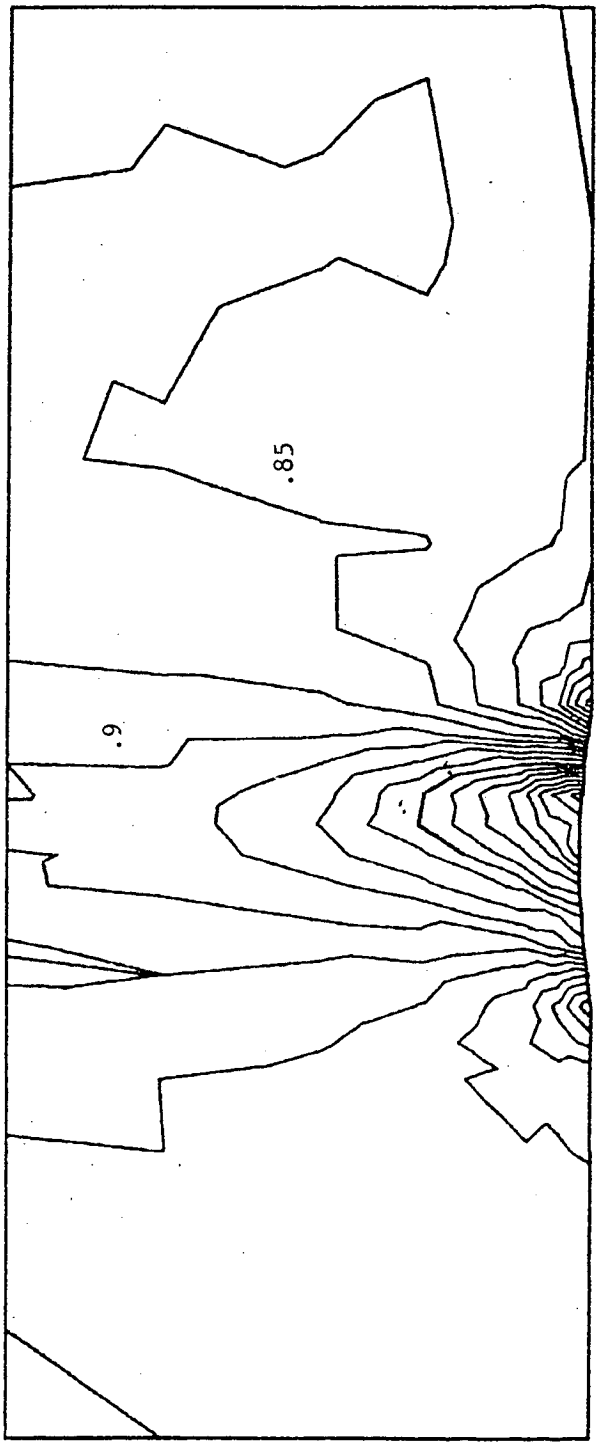

Figure 4.9. : GAMM Channel with circular bump ; isomach lines (Runge Kutta P_2).

5. CONCLUSION

Several explicit schemes for F.E.M. arbitrary triangulations have been presented.

The two first order schemes with convective-type upwinding are very easy to use ; the one-step scheme is fastly convergent but quite diffusive.

Stationary simulations with both schemes show shocks captured without oscillations.

The characteristic or Godunov-type scheme is much less diffusive than the convective upwind schemes ; shocks are captured almost without oscillations and are not smeared.

The Richtmyer scheme seems as precise as Finite Differences or Finite Volumes second order schemes. LERAT-type implicit extension (see [11] [14]) seems possible and interesting since the scheme is only a seven point one.

The Runge-Kutta schemes are mainly interesting for stationary simulations. The P_2 experiment shows that higher order elements are efficient for the evolutive case as soon as a good enough Schuman-type Filter (or artificial viscosity) is employed. But, for complex geometries where a minimal number of points has to be used, the advantage of the P_2 approximation is not clearly stated.

A lot of things remains to be done, some of them are already in progress :

- further experiments : profile with incidence
- faster solvers :
  - . pseudo steady explicit methods
  - . implicit methods
- 3-D extension [5].

REFERENCES

[1] F. ANGRAND, V. BOULARD, A. DERVIEUX, J. PERIAUX, G. VIJAYASUNDARAM, Transonic Euler simulations by means of F.E.M. explicit schemes, 6th AIAA Computational Fluids Dynamics Conference, Danvers (U.S.A.), July 13-15, 1983, paper 83-1924

[2] F. ANGRAND, A. DERVIEUX, Some explicit triangular finite elements schemes for the Euler equations, submitted to I.J. for Num. Methods in Fluids (1983).

[3] K. BABA, M. TABATA, On a conservative upwind finite element scheme for convective diffusion equations, R.A.I.R.O., Numerical Analysis, 15, n° 1, 3-25 (1981).

[4] M. BORREL, Ph. MORICE, A Lagrangian-Eulerian approach to the computation of unsteady transonic flows, 4th GAMM Conference (Paris 7-9 Oct. 1981), Numerical Methods in Fluid Dynamics, Vieweg and Sohn, Braunschweig/Wiesbaden (to appear).

[5] V. BOULARD, 3rd Cycle Thesis, in preparation.

[6] M.O. BRISTEAU, R. GLOWINSKI, J. PERIAUX, P. PERRIER, O. PIRONNEAU, G. POIRIER, Transonic flow simulations by Finite Elements and least square methods, in R.H. Gallagher (ed.), Finite Elements in Fluids, Vol. 4, Wiley, Chichester 1982-1983.

[7] J.C. DESGRAZ, P.M. LASCAUX, Stabilité de la discrétisation des équations de l'hydrodynamique Lagrangienne 2-D, in Computing Methods in Applied Sciences, R. Glowinski and J.L. Lions Ed., Lecture Notes in Physics 58, 510-529, Springer, Berlin (1976).

[8] K.O. FRIEDRICHS, Symmetric Positive linear Differential Equations, Comm. on Pure and Applied Math., 11, 333-418 (1958).

[9] T.J.R. HUGHES, T.E. TEZDUYAR, A.N. BROOKS, A Petrov-Galerkin finite element formulation for systems of conservation laws with special reference to the compressible Euler equations, Proceeding of the IMA Conference on Numerical Methods in Fluid Dynamics, 29-31 Mars 1982, Université de Reading, Angleterre, à paraître (Academic Press).

[10] A. JAMESON, W. SCHMIDT, E. TURKEL, Steady state solution of the Euler equations for transonic flow, AIAA Paper 81-1259, 1981.

[11] A. LERAT, Sur le calcul des solutions faibles des systèmes hyperboliques de lois de conservation à l'aide de schémas aux différences, Thesis, Paris (1981).

[12] A. LERAT, R. PEYRET, Sur le choix de schémas aux différences du second ordre fournissant des profils de chocs sans oscillation, Comptes rendus Acad. Sc., Paris, Série A, 277, 363-366 (1973).

[13] A. LERAT, J. SIDES, A new finite volume method for the Euler equations with applications to transonic flows, IMA Conference on Numerical Methods in Aeronautical Fluid Dynamics, University of Reading (March 1981), to appear in Academic Press.

[13] A. LERAT, J. SIDES, Contribution to [17] .

[14] A. LERAT, J. SIDES, V. DARU, An implicit Finite-Volume method for solving the Euler equations, in E. Krause (Ed.), (Proceedings of the) Eight International Conference on Numerical Methods in Fluid Dynamics (Aachen, 1982), Lecture Notes in Physics, 170, Springer, 1982, pp. 343-349.

[15] T. NAGAYAMA, T. ADACHI, Numerical analysis of flow through turbine cascade by the Modified FLIC method, Comm. to Tokyo Joint Gas Turbine Congress, May 22-27, 1977, Tokyo (Nagasaki Technical Institute, Mitsubishi Heavy Industries,LTD, Nagasaki, Japan).

[16] R.D. RICHTMYER, K.W. MORTON, Difference Methods for Initial-Value Problems, Wiley, New-York (1967).

[17] A. RIZZI, H. VIVIAND (Eds.), Numerical methods for the computation of inviscid transonic flows with shock waves, Wieweg and Sohn, Braunschweig/Wiesbaden, 1981.

[18] W. SCHMIDT, A. JAMESON, Recent developments in Finite-Volume time-dependent techniques for two and three dimensional transonic flows, Von Karman Institute for Fluid Dynamics, Lecture Series 1982-04, Computational Fluid Dynamics, March 29-April 2, 1982.

[19] G.A. SOD, A survey of several finite difference methods for systems of nonlinear hyperbolic conservation Laws, J. Comp. Phys., 27, 1-31 (1978).

[20] H.J. STETTER, Improved Absolute Stability of Predictor-Corrector Schemes, Computing, 3, 286-296, 1968.

[21] T. USHIJIMA, Error estimates for the Lumped mass approximation, Memoirs of Numerical Mathematics, n° 6, 65-82 (1979).

[22] B. VAN LEER, Towards the ultimate conservative difference scheme III, upstream centered Finite Difference schemes for ideal compressible flow, J. of Comp. Phys., 23, 263-275, 1975.

[23] G. VIJAYASUNDARAM, Résolution numérique des équations d'Euler pour des écoulements transsoniques avec un schéma de Godunov en Eléments Finis, Thesis, University Paris VI, 1983.

[24] O. ZIENKIEWICZ, The Finite Element Method in Engineering, Mc Graw Hill (1971).

Imprimé en France
par
l'Institut National de Recherche en Informatique et en Automatique